AFRL-IF-RS-TR-2001-279
Final Technical Report
January 2002


# PROTEIN-BASED THREE-DIMENSIONAL MEMORIES

Syracuse University


*APPROVED FOR PUBLIC RELEASE; DISTRIBUTION UNLIMITED.*


**AIR FORCE RESEARCH LABORATORY**
**INFORMATION DIRECTORATE**
**ROME RESEARCH SITE**
**ROME, NEW YORK**


**20020308 074**

This report has been reviewed by the Air Force Research Laboratory, Information Directorate, Public Affairs Office (IFOIPA) and is releasable to the National Technical Information Service (NTIS). At NTIS it will be releasable to the general public, including foreign nations.

AFRL-IF-RS-TR-2001-279 has been reviewed and is approved for publication.

APPROVED: EDWARD J. DANISZEWSKI
Project Engineer

FOR THE DIRECTOR: JOSEPH CAMERA
Information & Intelligence Exploitation Division
Information Directorate

# REPORT DOCUMENTATION PAGE

Public reporting burden for this collection of information is estimated to average 1 hour per response, including the time for reviewing instructions, searching existing data sources, gathering and maintaining the data needed, and completing and reviewing the collection of information. Send comments regarding this burden estimate or any other aspect of this collection of information, including suggestions for reducing this burden, to Washington Headquarters Services, Directorate for Information Operations and Reports, 1215 Jefferson Davis Highway, Suite 1204, Arlington, VA 22202-4302, and to the Office of Management and Budget, Paperwork Reduction Project (0704-0188), Washington, DC 20503.

| 1. AGENCY USE ONLY *(Leave blank)* | 2. REPORT DATE | 3. REPORT TYPE AND DATES COVERED |
|---|---|---|
| | Jan 02 | Final  Jun 98 - Jun 00 |

**4. TITLE AND SUBTITLE**

PROTEIN-BASED THREE-DIMENSIONAL MEMORIES

**5. FUNDING NUMBERS**
C  - F30602-98-C-0105
PE  - 62702F
PR  - 4954
TA  - J8
WU  - 03

**6. AUTHOR(S)**

Jeffrey A. Stuart

**7. PERFORMING ORGANIZATION NAME(S) AND ADDRESS(ES)**
Syracuse University
Office of Sponsored Programs
113 Bowne Hall
Syracuse NY 13244-1200

**8. PERFORMING ORGANIZATION REPORT NUMBER**

**9. SPONSORING/MONITORING AGENCY NAME(S) AND ADDRESS(ES)**

AFRL/IFED
32 Brooks Road
Rome NY 13441-4114

**10. SPONSORING/MONITORING AGENCY REPORT NUMBER**

AFRL-IF-RS-TR-2001-279

**11. SUPPLEMENTARY NOTES**

AFRL Project Engineer:  Edward J. Daniszewski, IFED, 315-330-4466

**12a. DISTRIBUTION AVAILABILITY STATEMENT**

Approved for public release; distribution unlimited.

**12b. DISTRIBUTION CODE**

**13. ABSTRACT** *(Maximum 200 words)*
Significant progress has been made in the remaining tasks, specifically materials development, protein optimization, computer interface development, and prototype development.  The primary goal of the materials effort was to develop a polymer matrix for encapsulation of the protein, characterized by optical clarity, long-term stability, protein compatibility, and resistance to gel dehydration and contraction.  Handled via subcontract to Wayne Wang of Carleton University in Ottawa, Canada, a poly(acrylamide) based hydrogel has been developed that fits the majority of these characteristics.  Light scattering was achieved primarily by the addition of refractive index-matching agents, with sucrose achieving the best reduction.  A newly developed high-density acrylamide matrix demonstrates the largest reduction of light scattering, by roughly one order of magnitude over previous gels.  Optimization of the protein response was approached primarily through site-directed mutagenesis (SDM), with the goal of increasing the efficiency with which the branched photocycle can be assessed; two avenues were explored to this end, including enhancement of the O-state yield and the quantum yield of the O-->P transition.  The former avenue increases the amount of P-state formed through simple mass transfer--a higher yield of O will result in more P formation, despite the O-->P quantum efficiency.  The latter approach seeks to directly increase the  O-->P quantum efficiency.

| 14. SUBJECT TERMS | 15. NUMBER OF PAGES |
|---|---|
| Bacteriorhodopsin, Genetic Engineering | 156 |
| | **16. PRICE CODE** |

| 17. SECURITY CLASSIFICATION OF REPORT | 18. SECURITY CLASSIFICATION OF THIS PAGE | 19. SECURITY CLASSIFICATION OF ABSTRACT | 20. LIMITATION OF ABSTRACT |
|---|---|---|---|
| UNCLASSIFIED | UNCLASSIFIED | UNCLASSIFIED | UL |

# Table of Contents

# Table of Figures

# 1.0. Abstract

The progress in the development of the bacteriorhodopsin-based three dimensional memory from May 1999 through September 2000 of Air Force Contract No. F30602-98-C-0105 is described. The last 16 months of the contract saw changes in both direction and emphasis of the research and development effort. Perhaps the most salient discovery during this period was that the efficiency with which the branched photocycle can be accessed in bacteriorhodopsin is lower than earlier believed. The impact of this realization on the scope of the overall contract was substantial, resulting in a refocussing of the effort from a device-based orientation to one of materials optimization. Despite this fact, however, with the exception of tasks 3 and 4, the majority of the original tasks outlined in the contract Statement of Work were for the most part completed. Tasks 3 and 4 concerned the implementation of multitasking techniques and Fourier methodologies to the optical layout, and were too ambitious when considering the unanticipated efficiency problems with the branched photocycle.

Significant progress has been made in the remaining tasks, specifically materials development, protein optimization, computer interface development, and prototype development. The primary goal of the materials effort was to develop a polymer matrix for encapsulation of the protein, characterized by optical clarity, long-term stability, protein compatibility, and resistance to gel dehydration and contraction. Handled *via* subcontract to Wayne Wang of Carleton University in Ottawa, Canada, a poly(acrylamide) based hydrogel has been developed that fits the majority of these characteristics. Light scattering was achieved primarily by the addition of refractive index-matching agents, with sucrose achieving the best reduction. A newly-developed high density acrylamide matrix demonstrates the largest reduction of light scattering, by roughly one order of magnitude over previous gels. Optimization of the protein response was approached primarily through site-directed mutagenesis (SDM), with the goal of increasing the efficiency with which the branched photocycle can be accessed; two avenues were explored to this end, including enhancement of the O-state yeild and the quantum yeild of the O→P transition. The former avenue increases the amount of P-state formed through simple mass transfer—a higher yeild of O will result in more P formation, despite the O→P quantum efficiency. The latter approach seeks to directly increase the O→P quantum efficiency. To date, several orders of magnitude enhancement have been achieved in the O-state yeild though SDM, although no progress has been made as of yet with the quantum yeild. Both Apple MacIntosh and IBM PC computer interfaces have been developed to enable complete computer control for all the prototypes. All facets of prototype operation are interface-controlled, including timing, write & read-cycle duration, memory cuvette temperature, and cuvette location. The prototypes developed during this contract demonstrated both proof-of-principle and materials screening capabilities. The ability to screen different BR-based memory media has proven to be extremely valuable, enabling performance-based optimization of the memory media as a result of feed-back provided by runs in actual memory devices. Critical Link of Syracuse NY is in the process of developing a more sophisticated prototype capable of stand-alone operation.

## 2.0 Introduction

Present computer memory architectures largely are confined to two dimensions, typically in the form of a disk. The storage density of such devices is ultimately constrained by the physical limitations of the materials, i. e., both the size of the actual bit and the ability to mechanically access that bit is limited by both the material used as a recording medium and the size of the device used to detect it. An approach to increasing storage density that holds a lot of promise is moving into three dimensions, in the form of volumetric optical molecular architectures. In their present form, conventional silicon-based technologies are incapable of making that transition. The need for new materials and architectures is becoming increasingly apparent.

Bacteriorhodopsin (BR) is a 26 kD photosynthetic protein isolated from the bacterium *Halobacterium halobium*, a common halophilic resident of salt marshes (**Figure 2.1**). The protein occurs in the membrane of the organism, arranged in a two-dimensional semi-crystalline array of trimers. When oxygen is scarce, the protein is used by the organism in a photosynthetic role, by functioning as a light to chemical energy transducer. The chromophore responsible for absorption of light by the protein is all-*trans* retinal, which is bound via a protonated Schiff base to Lys-216. Light induces an all-*trans* to 13-*cis* isomerization in the chromophore, followed by a series of thermal protein intermediates characterized by different absorption spectra, vectoral proton transport, and ultimately the reisomerization of the chromophore with consequent re-generation of the protein's resting state. The last of the thermal intermediates is the O-state, which absorbs maximally at 640 nm. Exposure of this state to 640 nm light results in a small segment of the protein population being driven into the branched portion of the photocycle, first characterized in 1993 [1], and containing two



**Figure 2.1**: Bacteriorhodopsin is a membrane-bound protein with seven alpha-helical segments. When it absorbs light, it pumps a proton, which the bacterium uses as a source of energy. We use the protein to store information by using light to induce a change in the geometry of the chromophore (orange atoms). The overall dimensions are roughly 40 Ångstroms x 40 Ångstroms x 50 Ångstroms, making it a nanoscale data storage device.

intermediates, P and its thermal product Q. The chromophore in both intermediates has a 9-cis configuration. The Q-state is very long-lived, and is proving to be a promising candidate for long-term data storage.

2

The ultimate goal of this project is the creation of a new industry based on a novel product (the bacteriorhodopsin-based volumetric optical memory); therefore, the development and refinement of all aspects of this technology is of the utmost importance. A production strategy is necessary to create a new product capable of spawning an independent industry. Additionally, the industry should have the technical foundations and merit necessary to enable continuous research, development, and refinement, thereby securing its place as a competitive technological leader. The new opportunities presented by such an effort have the potential of bringing increased industry involvement, as well as employment. It is for these reasons that we plan to not only explore new architectures for our device, but also the different techniques necessary for the manufacture of a commercial product. In order to do this, it will be necessary to take into consideration the limitations imposed by the manufacturing process. It will therefore be necessary to explore component design and fabrication with an emphasis on mass production and the implementation of low cost solutions.

The current contract between Syracuse University and the United States Air Force, No. F30602-98-C-0105, is dedicated to the development of a volumetric optical memory based on the branched photocycle of the photosynthetic protein bacteriorhodopsin. The purpose of this engineering change proposal is to provide a research plan to justify the addition of two years of funding to this project. The proposal will be divided into four main areas, including an overview of the memory, a summary of the progress made to date in the current contract (section 4), a proposal describing the work to be accomplished with the additional time and funding, and a revised statement of work.

## 2.1. Overview of Bacteriorhodopsin-Based Volumetric Optical Memory.

The proposal for the original contract, Protein-based Three-dimensional Memories (No. F30602-98-C-0105) has a detailed description of both the theory behind the BR-based volumetric memory, and advantages over other volumetric optical architectures described in the literature (e.g., cyclicity, one-photon vs. two-photon issues, non-destructive writing and reading operations, etc.). The reader is referred to that document for further detail. However, a brief overview is included here for the sake of convenience.

In 1993, researchers in Germany described photoproducts that were produced upon illumination of the O-state [1]. Instead of converting to either BR or another main photocycle intermediate, a branching side reaction was found that contained two novel intermediates. These photoproducts, denoted as P and Q, were blue-shifted in absorbance with respect to most of the other photocycle intermediates, and were characterized as having a 9-*cis* chromophore. In addition, the Q-state displayed enhanced stability. The O-state acts as the entry point to the branched photocycle. Upon absorption of red light (~640 nm), an isomerization of the all-*trans* retinal chromophore occurs at the $C_9$-$C_{10}$ double bond, forming the P-state (490 nm). The resulting chromophore configuration is not stable in the binding site, presumably due to steric interactions, ultimately breaking the bond between the chromophore and the protein. Concurrent with the cleavage of this bond is the formation of the Q-state (380 nm), which has a stability on the order of years.

For the purposes of the branched-photocycle architecture, the bR state is assigned as a binary unit ZERO, and the P- and Q-states are collectively assigned as a binary unit ONE (**Figure 2.2**). Problems associated with previous architectures (two-photon-based systems) are easily circumvented by the unique nature of the branched-photocycle, in that it produces intermediates that are unaffected by the wavelengths of light used in write and read operations (i.e., unwanted photochemistry is rigorously avoided). Two photons are still required to write data, but they are absorbed by the protein sequentially, rather than simultaneously as in the two photon architecture.

The basis of the sequential one-photon branched photocycle architecture is illustrated in **Figures 2.2** and **2.3**. In order to access the branched portion of the photocycle, and thereby change a binary ZERO to a binary ONE, two conditions must be fulfilled: the bR photocycle must be initiated with a photon of green light, followed by a photon of red light at the appropriate time interval to drive O to the P-state. If, and only if, these two criteria are fulfilled, will data be written in the cube. The first process is referred to as paging, and involves initiating the BR photocycle with a photon of green light. The term "paging" refers to the process of using a green laser to select a slice within the cube where the protein is

### The Branched-Photocycle Architecture

**Figure 2.2:** The native photocycle includes the resting state (bR) and the intermediates K, L, M, N, and O. The last intermediate in the photocycle, O, will convert to a blue-shifted photoproduct, P, if it absorbs red light. The P state relaxes to form Q, a long-lived (>5 years) intermediate. Let bR represent bit 0 and P and Q represent bit 1. Data can be written into any location within a solid polymer matrix containing the protein by using a combination of paging (the green arrow) followed two milliseconds later by orthogonal writing (the red arrow). The protein operates like an optical AND gate— that is, data are written if, and only if, both of the input conditions are satisfied.

activated. The protein within this page starts to cycle through the photocycle intermediates, until the majority of the protein exists within the O-state after about 2 ms. At this time, the red data laser is fired, which drives the O-state into the branched photocycle, forming the P and Q intermediates. In this way, the protein acts as an optical AND gate: if only the green paging laser is fired, photochemistry is initiated and the net effect is that the protein cycles through the intermediates and returns to its resting state, resulting in the re-writing of a binary ZERO. If only the red data laser is fired, no action is stimulated in the protein because the wavelength of the data laser is not within the bR absorption band (net result = no change). However, if the green paging laser is fired, followed by the red data laser at the appropriate interval (after the paging laser has been turned off), protein that exists in the O-state is driven into the branched photocycle, the P- , and then Q-states are formed, and the formation of a binary ONE results. The combination of orthogonal laser excitation (enabling facile access to any volumetric element in three dimensions, as defined by the cross section of the two laser beams) and the energetically and temporally separated states of the branched photocycle, provides a realistic basis for the storage of information in three dimensions.
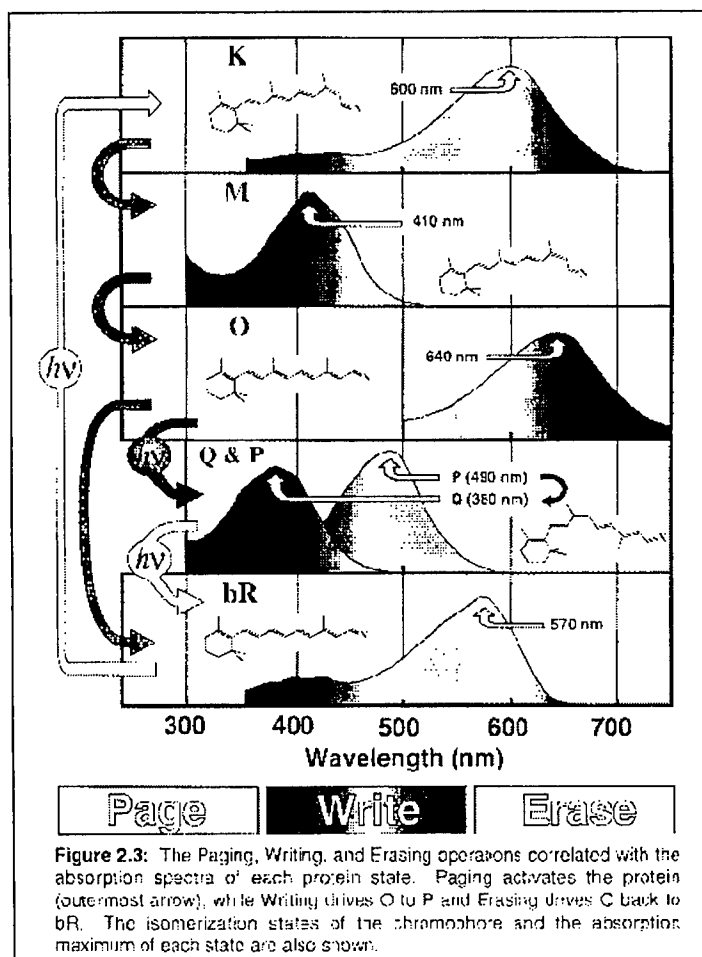
**Figure 2.3:** The Paging, Writing, and Erasing operations correlated with the absorption spectra of each protein state. Paging activates the protein (outermost arrow), while Writing drives O to P and Erasing drives C back to bR. The isomerization states of the chromophore and the absorption maximum of each state are also shown.

**Writing:** **Figure 2.4** illustrates both the parallel write and read operations for the sequential one-photon branched photocycle architecture. The process of orthogonal paging is shown in insert (a): volumetric elements within the cube are defined by the cross-sectional volume defined by the paging and data lasers. Note that these two lasers are not fired simultaneously, as illustrated in **Figure 2.4** (right- and left-hand columns). The vertical axis denotes time relative to the firing of the initial paging laser. To initiate the writing process, the paging lasers are fired to activate the protein. Photochemistry is initiated and after approximately 1 millisecond, the bulk of the protein excited during paging has cycled into the M-state. After an additional ms (2 ms relative to paging) the protein exists in the O-state, and the data laser is fired. The latter is modulated by some sort of spatial light modulator that defines exactly what volumetric elements will be irradiated in the paged region. Within these volumes, the branched photocycle is initiated photochemically by driving the O-state into the P-state. Finally, P decays to Q over several hours ($\tau_P$), completing the writing process. The full writing sequence (to the P-state) is complete in roughly 10 ms, the time necessary for the protein to complete the photocycle.

**Reading:** The reading process is unique in that it only examines those elements of data that exist as binary ZEROS. The operation starts out identically to that used to write data (**Figure 2.4**, right-hand column). The paging laser is used to select the page of interest, and after a few milliseconds, the majority of the protein excited by the paging operation exist in the O-state, just as in the writing process. Once again, the data laser is fired, but this time at a much lesser intensity. The amount of light allowed through the spatial light modulator is adjusted to be absorbed completely by the protein in the selected page (0.01% of full intensity). No appreciable photochemistry is stimulated by the low intensity laser light (the O → P transition is not very efficient), and those volumetric elements existing in the P- and/or Q-states are invisible to the wavelength used. Therefore, regions of the cube that exist as binary ones transmit the low-intensity light, because it can't be absorbed by P ($\lambda_{max}$=480 nm) or Q ($\lambda_{max}$=380 nm). The transmitted light is imaged onto a CCD or CID detector. If the page is imaged prior to, and then

5

**Figure 2.4:** The parallel write and read sequences (time progressing from bottom to top). The write sequence (left column) is as follows: (1) turn on the paging laser to activate the bR photocycle within selected page. (2) after ~2 ms, activate 690nm data Laser and select data elements with SLM to convert O to P. The read sequence (right column) is as follows: (1) page, (2) after ~2 ms, read entire page as an image on the CCD array detector. The basic optical architecture is shown in insert (a).

again during the firing of the data laser, a differential read can be done which has the added benefit of enhanced sensitivity. In this way, the read process essentially examines only the binary ZEROS, while leaving the ONES unperturbed, resulting in a reading operation that is totally nondestructive. Because the O-state has an absorptivity better than 1000 times larger than that of the remaining volume elements combined, a very weak read beam can generate a large differential signal. Erasing operations are currently implemented with a standard Xenon lamp to provide the blue light necessary to drive Q back to BR; because blue diode lasers do not yet commercially exist, at this time data can only be erased via a global operation. Figure 2.5 shows a schematic of the modular prototype developed during the first year of the project.

Before commercialization can be seriously considered, several issues must still be addressed. As will be discussed below, the most serious factor that precludes commercialization at this point is the protein itself, which has proven not to be efficient enough to be competitive with conventional technologies. As part of the parallel research effort from AFRL, we are exploring ways through genetic engineering to address these problems, especially through a relatively new technique known as Directed Evolution. This is a method in molecular biology that offers a means by which genetic engineering can be used as a tool to produce highly optimized proteins for specific applications. As part of the research effort described herein, a sizeable effort in standard molecular biology techniques, predominantly site-directed mutagenesis (SDM), was used to produce improved bacteriorhodopsin variants. Considerable progress toward an optimized material has been made, as illustrated below. The rationale in determining the direction of SDM on BR was to produce mutant proteins that exhibit enhanced yields of the O-state, the gateway to the branched photocycle architecture. More O should translate into enhanced yields of P&Q—progress described below has resulted in an improvement of the O-state yield by several orders of magnitude. The protein has also proven to be extremely sensitive to the chemical environment, with enhanced O-state formation at lower pH values and enhanced P&Q formation at higher temperatures. More recent results from the parallel research effort (also sponsored by AFRL) indicate despite the fact that O-state formation is favored at lower pH, formation of the P-state follows the opposite trend. Therefore a balance has to be found between the two factors—this is currently an ongoing portion of the research effort.

What follows below is the progress that has been made since the annual report was submitted, and covers the period between May 1999 through September 2000. The annual report submitted in May 1999 is included as an appendix. As will be evident, the direction of the research effort had to be shifted to address issues in protein efficiency; despite this change, during the course of the project the branched photocycle architecture was verified and demonstrated in an in-house developed prototype. However, a consequence of this shift was that some of the goals in the original statement of work (SOW) were not addressed—not due to negligence, but as a result of the reevaluation of project priorities. The two tasks that suffered most were SOW 4.2, Optical considerations including development of Fourier



**Figure 2.5:** Schematic representation of the bacteriorhodopsin branched-photocycle 3D memory prototype, illustrating all routine data operations. See text for explanation. QHL = quartz halogen lamp, PA = page aperture, DBS = dichroic beam splitter, PBLN = prismatic beam line narrower, DC = data cuvette, BEO = beam expanding optics, SLM = spatial light modulator, BCO = beam condensing optics, DCKH = data cuvettet kinimatic holder, PTC = peltier

transform methodologies to simplify optical design, and SOW 4.3, Implementation of multiplexing techniques including polarization and gray scale technologies. Both of the aforementioned tasks were targeted to increase storage density in the protein memory matrix; in light of the reduced efficiency of the protein, storage density was determined to be of minor importance until such time that improved materials become available. Other tasks were largely unaffected and largely completed, with advances made in the following areas:

- Development of polymer matrices for protein encapsulation and stabilization, exhibiting reduced light scattering and long term stability (i.e., reduced tendency to contract).

- Development of mutant proteins with enhanced ability to operate as a light activated storage media.

- Kinetic evaluation of mutant proteins with respect to efficiency of O-state production, access to the branched photocycle, and photochromic efficiency.

- Development of an electronic interface between the computer and memory to facilitate invisible background operation of the memory device.
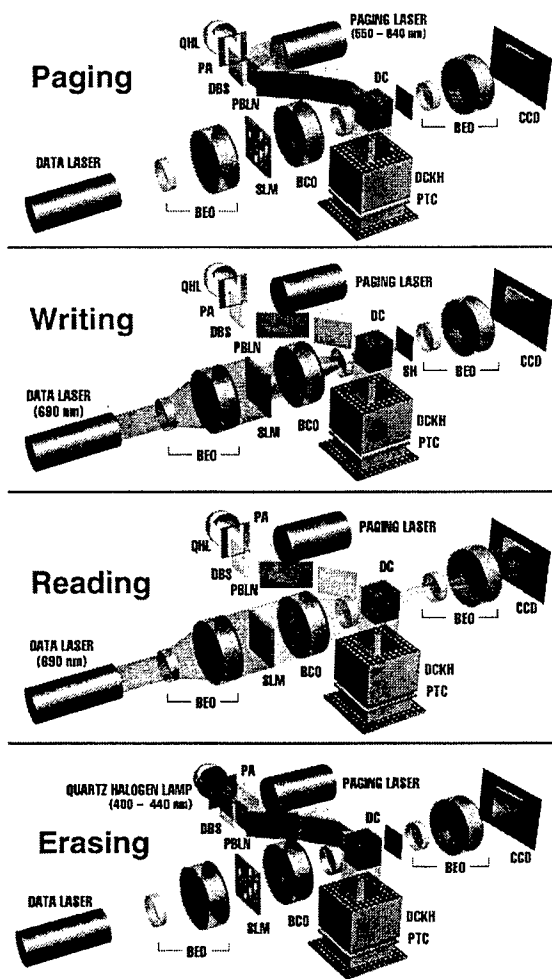
7

- Construction and demonstration of fully functional miniaturized memory prototypes.

All of these accomplishments will be described in detail below.

## 3.0. Progress Detailed by Task

In this section progress will be detailed in a format loosely based on the tasks described in the original Statement of Work.

## 3.1. Materials

The materials work performed during this contract had two basis goals: (1) Optimization of the polymer host matrix which encapsulates the protein and (2) Optimization of the protein, itself, with respect to efficiency by which the branched photocycle is accessed. The first goal was handled both in-house and under subcontract to Wayne Wang at Carleton University. Research and progress toward the second goal was performed both at Syracuse University and the University of Connecticut.

### 3.1.1. Optimization of the Protein

Perhaps the most critical factor of materials optimization is the work done to optimize bacteriorhodopsin itself. One of the most difficult "lessons learned" about this project has been that BR failed to live up to its initial potential as a memory storage element. The branched photocycle is real and it can be used to store information in three dimensions, as illustrated later in the report. However, the efficiency with which the branched photocycle can be accessed is extremely low; low enough that it was quickly realized that the wild-type protein would not suffice as an active element of a three-dimensional optical memory (at least not in a commercially-viable sense).

Several approaches have been taken to remedy this problem, mainly in the form of optimization of the chemical environment (i.e., pH, salinity, chemical additives) and/or actual genetic manipulation of the protein. Both approaches have been taken during this contract, but the latter—genetic manipulation—is by far the most powerful. Progress between the months of 6/99-9/00 will be discuss in this section.

### 3.1.1.2. Introduction to Site Directed Mutagenesis

Site-directed mutagenesis (SDM) involves mutation of one or more residues by changing a particular DNA base pair. The net result is the change of one amino acid. This can be done very easily in the laboratory using a commercially available mutagenesis kit from Stratagene called "Quick-Change." By using information available in the genetic code, short DNA sequences called primers are constructed which contain a centrally located mutation of interest flanked by 10-15 base pairs of sequence homology on either side. These mutagenic primers are annealed to the parental bacteriorhodopsin

protein gene (bop). An enzyme then digests away (removes) the parental template, leaving only recombinant, or mutant, DNA. These mutant DNA pieces are then transformed into the native organism for expression of protein.

Site-directed mutagenesis provides a very powerful means of controlling amino acid changes in the protein. In addition, SDM is ideal for structure/function studies of proton pumping in bacteriorhodopsin. The researcher can selectively mutate one amino acid at a time and study the resultant proteins. This makes SDM a effective technique for examining the potential of bacteriorhodopsin in device applications. This process is summarized in **Figure 3.1.1.1.**
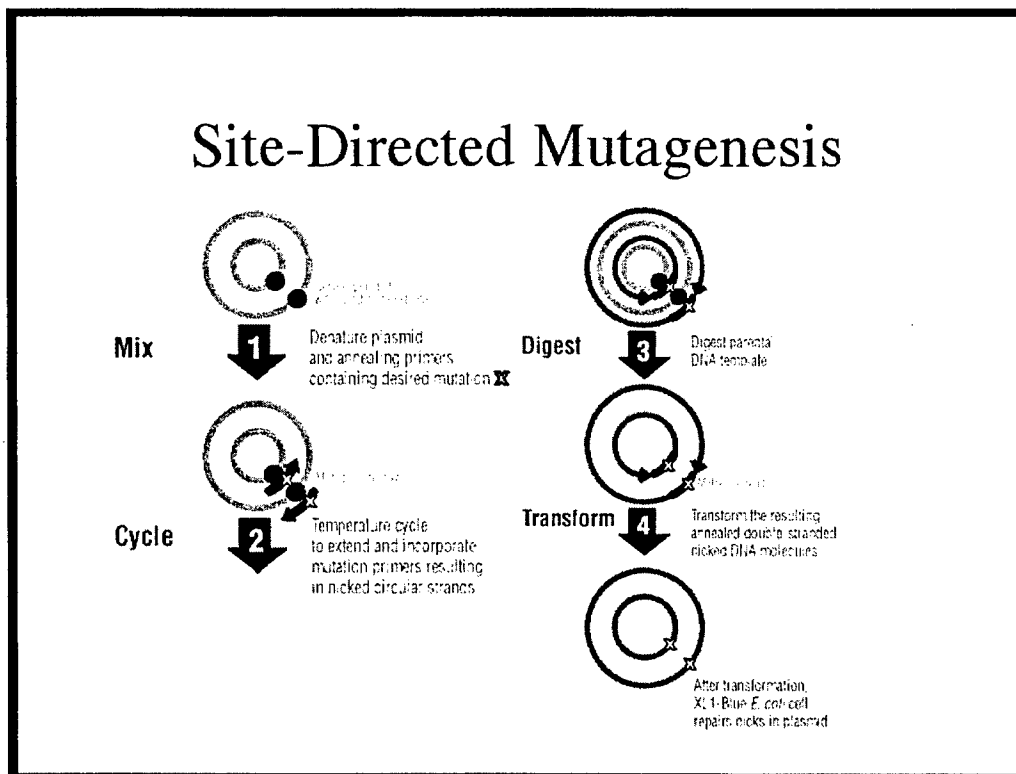


**Figure 3.1.1.1.** Basic steps in a standard Site Directed Mutagenesis procedure.

### 3.1.1.3. Goals for Application of SDM to Bacteriorhodopsin

As applied to bacteriorhodopsin, SDM has proven over the last decade to be an extremely powerful tool for determining structure-function relationships. Indeed the state-of-the-art has arrived at a point where the functions of many of the amino acids involved in the proton pump mechanism are thought to be fairly well understood. For example, mutations at D85 (aspartic acid residue no. 85 in the primary amino acid sequence of BR) are known to influence the nature and lifetime of the M-state. Likewise, mutations at E194 and E204 (E=glutamic acid) are known to affect the O-state. The latter class of mutations, i.e., those that influence the O-state, are of considerable interest to the development of the branched-photocycle memory due to the fact that the O-state serves as the gateway to the P- & Q-states. As detailed previously, the transition from O to P is fairly weak, with quantum yield determinations ranging from $10^{-4}$ to $10^{-2}$. The

most likely explanation for this weak transition is the formation of a 9-*cis* chromophore in a binding site that has evolved to accommodate either an all-*trans* or 13-*cis* chromophore. Indeed, once the 9-cis chromophore has been formed (P-state), it is unstable enough in the binding site that the Schiff base bond to the protein is hydrolyzed so that the chromophore can re-adjust into a more favorable orientation.

The obvious goal for genetic engineering of bacteriorhodopsin from the perspective of the branched photocycle is to target amino acids that affect the O-state in a way that will either enhance the formation of the P-state by increasing the quantum yield for its formation, or by increasing the amount of O-state available to be driven into the branched photocycle. Either way, the net result is an increased efficiency with which information can be written. The unfortunate aspect of genetic engineering as a general technique is that the effects of a specific mutation or set of mutations can be extremely hard to predict. A good example of this is the mutant F208N, where the phenylalanine (F) at position 208 is replaced by an arginine. F208 has never been reported to have a well-defined role in bacteriorhodopsin as part of the proton pump, yet by introducing the mutation, a protein results with a highly extended O-state and enhanced writing efficiency in the branched-photocycle memory architecture.

The unfortunate caveat in SDM is that the results are not always predictable. A new technique currently under exploration is directed evolution, a method which takes advantage of the very fact that SDM often leads to unpredictable results. The thrust of DE is to introduce a random mutagenic factor that will produce a number of genetically unique bacteriorhodopsin variants. The one with the most desirable properties can then be used as a parent to produce another round of genetically-engineered progeny. The new strains are then screened for whatever target property is of interest, and the process can start all over again with the best candidate. Key to any successful implementation of directed evolution is the ability to screen for selected properties. For simple properties such as thermal stability or enzymatic activity, the screening process is trivial. For a complex transition such as the generation of P & Q, screening becomes considerably more difficult. In conjunction with experimental *in vivo* screening techniques, directed evolution is currently being used to hone in on highly customized mutants for memory applications. However, to date there are no significant results to report.

### 3.1.1.4. Generation of Bacteriorhodopsin Mutant Proteins

Early mutants of bacteriorhodopsin were done almost exclusively in *E. coli*. Results gained from BR genetic analogs made in this way turned out to be suspect, however, due to problems with post-translational processing mechanisms not present in *E. coli*, and due to the fact that the protein was not inserted into a cell membrane, as is the case for the wild-type protein. Most BR analogs are now made directly in *H. salinarum*. The basis for making mutants in *H. salinarum* is covered in the last annual report, which is attached here as an appendix. The treatment below will deal primarily with the problems and progress encountered during the final 16 months of the project. There were only two major problems encountered in generating mutants in bacteriorhodopsin during the last 18 months of the contract, as outlined below.

10

### 3.1.1.4.1. Generation of Sequencing Primers

Sequencing primers are used for the purpose of quality control; a well-constructed sequencing primer will allow for quick and efficient sequencing of mutant gene products and final analysis of DNA sequences before they are transformed into *salinarum*. Sequencing primers were designed in the following manner: internal base pair primers were used to extend the nucleotides beyond the bop gene sequences (bop ≡ bacterio-opsin, referring to the protein without the retinal chromophore). The sequences immediately flanking the 3' and 5' ends of the gene were used to construct two primers. When sequenced with these primers, the gene should be completely included between these primers, and all sequences in the bop gene should be readable in both directions. Previously, no primers existed for the sequencing of the wild-type and mutant proteins in the bop gene vector pMR4 (an expression vector for bacteriorhodopsin mutants provided by Prof. Mark Braiman, Syracuse University). After sequencing one of the mutants with the primers for E204Q, upstream and downstream sequences were analyzed, and primers were constructed. Analysis at Cornell University indicated that the primers were properly constructed; the BR gene could now be sequenced in four places: 1) leading strand, start of the gene going in the 3' direction, 2) lagging strand, end of the gene going in the 5' direction, 3) leading strand, middle of the gene going in the 3' direction, and 4) lagging strand, middle of the gene going in the 5' direction. These primers show considerable overlap, and are sufficient for sequencing the entire gene in at least one direction, and in most cases, two directions. Overlapping and consistent sequences provide the most reliable data for ensuring a nucleotide sequence. The four primers that have been constructed work well for the sequences tested.

### 3.1.1.4.2. Extra Leader Sequence

Early on it was revealed by DNA sequencing of mutant sequences that there was an extra leader sequence in the mutant DNA code. The leader sequence is a stretch of DNA that, for bacteriorhodopsin, codes for a 13 amino acid segment on the N-terminous that is used for post-translational processing (conceivably for insertion of the protein into the membrane)—as part of the same post translational processing, the segment is ultimately cleaved off of the protein. The extra leader sequence in the mutant DNA meant that a second 13 amino acid sequences was being coded for on the protein's N-terminous.

The potential problem with having an extra 13 amino acid segment attached to the protein is that protein expression might be affected. Indeed, there is information present in the literature that elimination of the leader sequence results in misexpression of the protein. This may be due to a number of reasons ranging from mislocalization of the messenger RNA, to a decrease in stability of the messenger RNA, to misinsertion of the protein in the membrane. Although a sequence with no leader can still express the protein, it has been shown that this level is decreased as compared to having the proper one leader sequence. However, little is known about the ramifications of having two leader sequences. It is believed that the sequence mediates the insertion or direction of the bacteriorhodopsin protein to the proper location in the membrane (i.e. the leader may function as a molecular chaperone). Therefore, it does not seem unreasonable to

conclude that the addition of an extra leader will affect expression of the protein. Data on the mutants have shown that the expression in some of the mutants is far below what is to be expected. Although the expression levels of mutants are generally lower that wild-type (in-house experience), the mutants which had been constructed up to this point had shown exceedingly low levels of expression. Elimination of the extra leader was expected to enhance expression of mutant bacteriorhodopsin analogs.

The approach chosen to eliminate the extra leader was to introduce a restriction site into the plasmid. The DNA would then be cut, the leader removed, and the DNA religated to form a protein with only one leader sequence. However, since the introduction of this restriction site modified the non-coding sequence immediately following the start of the gene, another set of primers had to be ordered to reintroduce the wild-type sequence. Once the altered vector had been repaired, mutations were then constructed on the expression vector containing the gene with only one leader sequence. This will result in a wild-type plasmid with only one leader. The steps performed to make the desired change are as follows:

- Via site-directed mutagenesis, introduce a novel restriction site—VspI. VspI is a restriction endonuclease introduces a novel restriction site into the plasmid.

- The plasmid was then digested with NdeI and VspI, resulting in two components : the plasmid, and a 39 base pair excision which corresponds to the extra leader sequence.

- The mixture was run on a gel to isolate the plasmid with the leader removed.

- The plasmid was religated with the leader removed.

- Using site-directed mutagenesis, the wild-type sequence was reintroduced.

- The resulting plasmid was introduced into *E. coli* to produce mass quantities of the repaired DNA.

- Thermocycling reactions were used to make mutants which have the correct number of leader sequences.

DNA sequencing at Cornell University confirmed that the sequence of the repaired expression vector pMR4 had been corrected. The extra leader sequence that was hypothesized to be responsible for affecting the expression levels of bacteriorhodopsin in transformed cells was removed.

The first four mutants (E194Q, E204Q, R82A, and R82C) to be made with the repaired expression vector (pMR4) were plated on agar plates and within two weeks differences in cell morphology and growth rate in *salinarum* cells containing the new expression vector were noted. Cells possessing the new vector grew faster than those cells containing the old expression vector; after two weeks there were approximately 10-

100X more cells. Wild-type cells showed a distinct difference in color from E194Q, E204Q, R82A, and R82C. Enhanced proteins yields also confirmed that the removal of the extra leader sequence had the anticipated result.

### 3.1.1.4.3. BR Mutants Generated

DNA for a total of more than 45 mutants of bacteriorhodopsin was constructed during the course of this contract. Of those, a number of them proved not to be viable (i.e., the strain would not grow well or could not produce protein), while others remain to be fully analyzed. Of the total, 6 mutants resulted in actual protein with potential for the volumetric memory and were analyzed with respect to writing efficiency; those proteins were F208N, E194Q, E194C, E204Q, E204C, E194Q/E204Q, and E194C/E204C. The remainder of this section will focus on the results obtained for this set of mutants. All of these mutants involve mutation of key residues involved in the transfer of the proton during the cytoplasmic half-reaction of bacteriorhodopsin. In particular, E194, E204, and F208 have been shown to increase the O state lifetime by slowing proton mobility. E194 and E204 were mutated to lysine, asparagine, and arginine because these amino acids carry a positive charge, in contrast to the negative glutamate present in wild type. The double mutant E194C/E204C was constructed with the goal of introducing a disulfide bond; such an introduction to amino acids heavily involved with proton release is expected to strongly affect the O-state lifetime. As a memory element, extremely prolonged O-states are not desirable, but such mutants will be extremely helpful in mechanistic studies, especially for the formation of P & Q.

### 3.1.1.5. Spectroscopy of BR Mutants

All of the mutants were examined with respect to photocycle kinetics and O-state lifetime. The experiments were done on an OLIS RSM-1000 time domain spectrometer and two Coherent Infinity-XPO tunable laser systems as pump and probe beams. Spectra



Time [cs (s/100)]

chi^2= 0.2842485

13
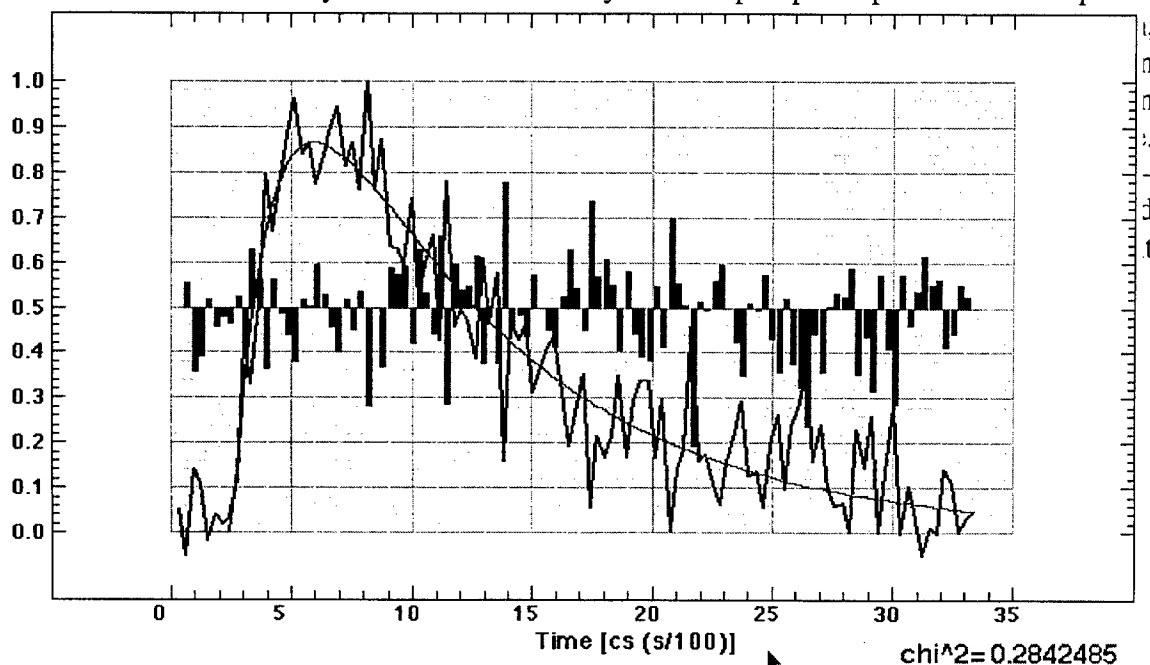
Figure 3.1.1.4. Wild-type monitored at 670 nm after being pulsed with a 568 nm laser.



```
WT.670
a0= 2.8827554
T0= 0.9943946 cs
Tau_formation= 0.5530857 cs
Tau_decay= 0.8686153 cs
Integral= 0.0152987 s
```
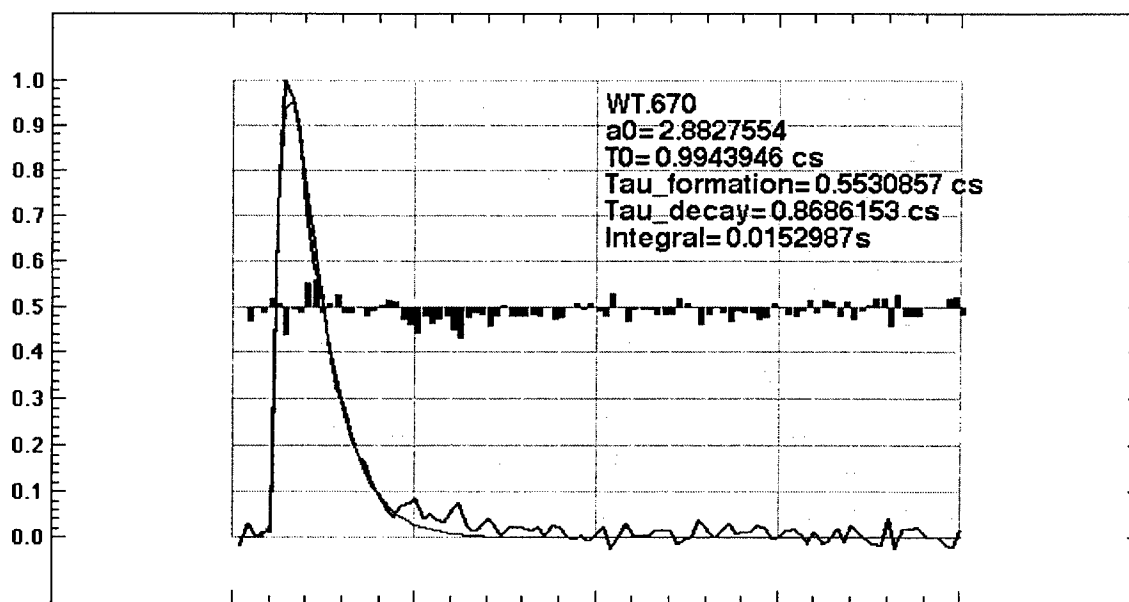
**Figure 3.1.1.2.  E194Q/E204Q : O state decay at 650 nm = 89 ms**

A summary of the results is shown in Figure 3.1.5. and Table 3.1.1; data is compiled for

**Figure 3.1.1.3.  E204Q : O state decay at 650 nm = 102 ms**

all mutants mentioned above at multiple wavelengths and pH values.



Time [cs (s/100)]

chi^2= 0.0120265
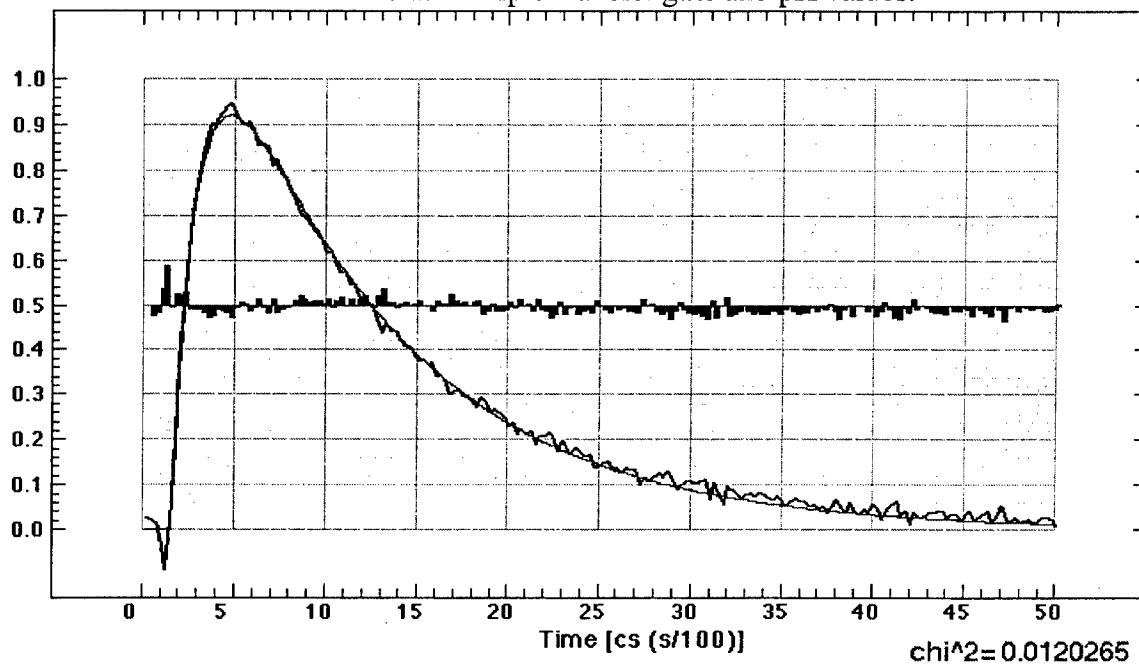
**Table 3.1.1:** Summary of Kinetic Data for BR Mutants

**412**
**nm**

| Protein | pH | OD (Imax) | $\Delta Abs_{max}$ | 412 dec (ms) | exp2 (ms) | lifetime (ms) | integral | Q (412) | X2 |
|---|---|---|---|---|---|---|---|---|---|
| WT | 5 | 1.710 | 0.143 | 5.870 | | 5.890 | 0.006 | 0.092 | 0.001 |
| | 7 | 1.758 | 0.162 | 4.410 | | 6.402 | 0.004 | 0.085 | 0.002 |
| | 9 | 1.637 | 0.166 | 5.326 | 38.956 | 16.670 | 0.021 | 0.087 | 0.087 |
| E194Q | 5 | 1.559 | 0.099 | 11.304 | | 11.323 | 0.012 | 0.066 | 0.001 |
| | 7 | 1.501 | 0.103 | 25.369 | | 25.397 | 0.022 | 0.059 | 0.019 |
| | 9 | 1.517 | 0.104 | 5.788 | 240.560 | 94.995 | 0.103 | 0.074 | 0.028 |
| E204Q | 5 | 1.650 | 0.127 | 6.255 | | 6.266 | 0.006 | 0.078 | 0.001 |
| | 7 | 1.605 | 0.165 | 13.971 | | 13.993 | 0.012 | 0.088 | 0.020 |
| | 9 | 1.576 | 0.104 | 151.072 | 644.129 | 420.014 | 0.386 | 0.060 | 0.013 |
| F208N | 5 | 1.633 | 0.149 | 6.655 | | 6.660 | 0.006 | 0.083 | 0.006 |
| | 7 | 1.586 | 0.151 | 19.845 | | 19.881 | 0.019 | 0.090 | 0.007 |
| | 9 | 1.604 | 0.126 | 490.089 | | 491.633 | 0.451 | 0.072 | 0.030 |
| E194C | 5 | 1.461 | 0.119 | 6.798 | | 7.394 | 0.009 | 0.075 | 0.007 |
| | 7 | 1.765 | 0.137 | 15.922 | | 15.952 | 0.017 | 0.062 | 0.020 |
| | 9 | 1.617 | 0.138 | 8.826 | 130.948 | 69.261 | 0.082 | 0.081 | 0.004 |
| E204C | 5 | 1.442 | 0.144 | 6.443 | | 7.234 | 0.009 | 0.092 | 0.006 |
| | 7 | 1.568 | 0.231 | 12.920 | | 13.004 | 0.015 | 0.119 | 0.016 |
| | 9 | 1.577 | 0.185 | 162.907 | | 162.987 | 0.125 | 0.091 | 0.205 |
| DOUBC | 5 | 1.688 | 0.077 | 10.542 | | 10.755 | 0.013 | 0.042 | 0.013 |
| | 7 | 1.519 | 0.103 | 20.527 | | 20.555 | 0.021 | 0.051 | 0.019 |
| | 9 | 1.683 | 0.114 | 178.155 | | 178.359 | 0.119 | 0.044 | 0.116 |
| DOUBQ | 5 | 1.630 | 0.129 | 7.911 | | 7.930 | 0.008 | 0.082 | 0.006 |
| | 7 | 1.562 | 0.100 | 10.183 | | 10.185 | 0.009 | 0.056 | 0.022 |
| | 9 | 1.489 | 0.116 | 7.916 | 168.810 | 54.853 | 0.070 | 0.074 | 0.006 |

**568**
**nm**

| Protein | | OD (Imax) | $\Delta Abs_{max}$ | 568 dec (ms) | exp2 (ms) | lifetime (ms) | integral | Q (568) | X2 |
|---|---|---|---|---|---|---|---|---|---|
| WT | 5 | 1.710 | 0.272 | 6.777 | | 6.938 | 0.007 | 0.171 | 0.001 |
| | 7 | 1.758 | 0.262 | 5.634 | | 5.636 | 0.005 | 0.144 | 0.001 |
| | 9 | 1.637 | 0.209 | 8.676 | 75.683 | 38.701 | 0.043 | 0.138 | 0.003 |
| E194Q | 5 | 1.559 | 0.207 | 22.999 | | 23.029 | 0.023 | 0.128 | 0.007 |
| | 7 | 1.501 | 0.248 | 38.785 | | 38.809 | 0.036 | 0.144 | 0.018 |
| | 9 | 1.517 | 0.202 | 292.702 | | 292.781 | 0.243 | 0.108 | 0.071 |
| E204Q | 5 | 1.650 | 0.240 | 6.878 | 110.939 | 38.972 | 0.044 | 0.149 | 0.001 |
| | 7 | 1.605 | 0.287 | 10.351 | 104.801 | 48.375 | 0.056 | 0.186 | 0.003 |
| | 9 | 1.576 | 0.217 | 533.828 | | 534.033 | 0.425 | 0.110 | 0.133 |
| F208N | 5 | 1.633 | 0.181 | 109.782 | | 115.548 | 0.127 | 0.124 | 0.045 |
| | 7 | 1.586 | 0.162 | 118.488 | | 136.823 | 0.161 | 0.121 | 0.035 |

15

| | | | | | | | | | |
|---|---|---|---|---|---|---|---|---|---|
| | 9 | 1.604 | 0.014 | 728.308 | | 781.714 | 0.819 | 0.011 | 1.276 |
| E194C | 5 | 1.461 | 0.111 | 42.122 | | 50.249 | 0.059 | 0.090 | 0.006 |
| | 7 | 1.765 | 0.090 | 48.732 | | 74.338 | 0.082 | 0.057 | 0.016 |
| | 9 | 1.617 | 0.087 | 86.145 | | 105.327 | 0.118 | 0.007 | 0.145 |
| E204C | 5 | 1.442 | 0.146 | 25.125 | | 41.568 | 0.044 | 0.123 | 0.012 |
| | 7 | 1.568 | 0.168 | 38.095 | | 54.405 | 0.062 | 0.123 | 0.004 |
| | 9 | 1.577 | 0.021 | 183.153 | | 210.582 | 0.237 | 0.019 | 0.708 |
| DOUBC | 5 | 1.688 | 0.105 | 311.402 | 1315.855 | 624.627 | 0.615 | 0.062 | 0.049 |
| | 7 | 1.519 | 0.101 | 207.137 | 811.638 | 349.799 | 0.386 | 0.075 | 0.045 |
| | 9 | 1.683 | 0.014 | 10.541 | 302.143 | 305.132 | 0.390 | 0.011 | 0.825 |
| DOUBQ | 5 | 1.630 | 0.198 | 14.073 | | 14.108 | 0.014 | 0.118 | 0.038 |
| | 7 | 1.562 | 0.186 | 8.377 | 88.365 | 26.440 | 0.026 | 0.117 | 0.003 |
| | 9 | 1.489 | 0.161 | 53.244 | 400.353 | 171.171 | 0.141 | 0.085 | 0.093 |

## 650 nm

| Protein | | OD (Imax) | $\Delta Abs_{max}$ | 670 dec (ms) | exp2 (ms) | lifetime (ms) | integral | Q (670) | X2 |
|---|---|---|---|---|---|---|---|---|---|
| | | | | | | | | | |
| WT | 5 | 1.710 | 0.034 | 11.377 | | 11.640 | 0.014 | 0.024 | 0.090 |
| | 7 | 1.758 | 0.030 | 9.711 | | 9.854 | 0.012 | 0.019 | 0.054 |
| E194Q | 5 | 1.559 | 0.082 | 28.212 | | 56.502 | 0.056 | 0.053 | 0.007 |
| | 7 | 1.501 | 0.057 | 47.356 | | 61.063 | 0.074 | 0.047 | 0.094 |
| E204Q | 5 | 1.650 | 0.130 | 107.292 | | 113.060 | 0.126 | 0.088 | 0.044 |
| | 7 | 1.605 | 0.120 | 116.191 | | 132.766 | 0.155 | 0.089 | 0.061 |
| | 9 | 1.576 | 0.011 | 773.373 | | 833.933 | 0.848 | 0.009 | 1.493 |
| F208N | 5 | 1.633 | 0.128 | 106.888 | | 113.775 | 0.125 | 0.088 | 0.034 |
| | 7 | 1.586 | 0.117 | 112.218 | | 130.416 | 0.153 | 0.087 | 0.020 |
| | 9 | 1.604 | 0.017 | 494.374 | | 569.839 | 0.619 | 0.011 | 0.525 |
| E194C | 5 | 1.461 | 0.086 | 54.966 | | 62.719 | 0.073 | 0.059 | 0.007 |
| | 7 | 1.765 | 0.031 | 66.785 | | 93.244 | 0.107 | 0.023 | 0.029 |
| E204C | 5 | 1.442 | 0.097 | 28.916 | | 37.678 | 0.044 | 0.078 | 0.006 |
| | 7 | 1.568 | 0.122 | 36.682 | | 53.443 | 0.062 | 0.090 | 0.001 |
| | 9 | 1.577 | 0.023 | 191.149 | | 213.087 | 0.234 | 0.017 | 0.293 |
| DOUBC | 5 | 1.688 | 0.071 | 323.988 | 1305.488 | 633.118 | 0.616 | 0.041 | 0.070 |
| | 7 | 1.519 | 0.077 | 191.097 | 1923.409 | 480.325 | 0.554 | 0.058 | 0.112 |
| DOUBQ | 5 | 1.630 | 0.026 | 82.820 | | 86.588 | 0.098 | 0.019 | 0.019 |
| | 7 | 1.562 | 0.014 | 66.116 | | 69.057 | 0.083 | 0.011 | 0.047 |

With the exception of F208N, all of the mutants are targeted at affecting the nature of the O-state by manipulating the proton release group. F208N has an extremely prolonged O-state, but the mechanism by which this is accomplished is unclear. The Q function defined in **Figure 3.1.1.5** is a quality factor that balances the magnitude of the O-state integral with the time it takes to evolve (with an upper limit of 10 ms). The Q value is

16

defined as the integral under a trace divided by the lifetime of the mutant. Therefore the best mutant will have a short lifetime but a large integral. A high Q value ("Q"=quality factor) indicates a large absorbance change in a short amount of time. By this criterion, the best candidate would appear to be E204C. Although F208N has a large Q-value as well, the lifetime of its O-state precludes serious consideration as a memory material; it does, however, produce P & Q in much larger amounts than the wild-type protein. Unfortunately, E204C was not available in quantities large enough to be evaluated as part of this report, and in preliminary studies involving actual write/read operations, behavior atypical of other BR mutants was observed which decreased its appeal as a potential memory material. Most of this work was done after the contract end date as part of our other funded initiative from AFRL for this project, and results will included in that project's final report. Results from experiments evaluating the performance of both the wild type protein and several of the mutants is described in the prototyping section below.
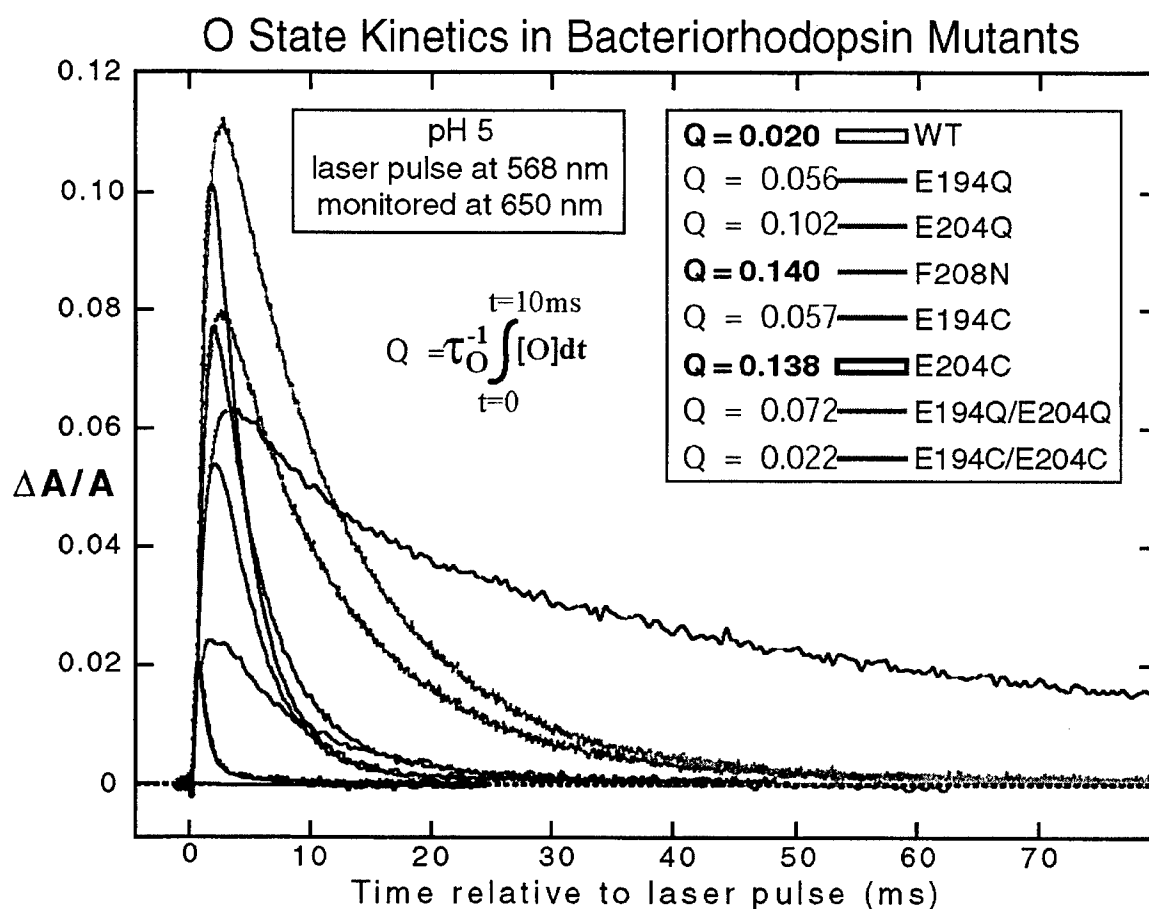


**Figure 3.1.1.5.** Kinetic traces for wild type and all mutants relevant to memory applications as determined within the confines of this contract.

### 3.1.1.6. Characterization of the Q-state in Wild Type Bacteriorhodopsin

17

One of the foremost conclusions of this research effort is that wild-type bacteriorhodopsin is not commercially viable as the active element of the branched-photocycle volumetric optical memory. Although the protein is fully capable of operation as a memory element in three dimensions, low efficiencies result in prolonged writing cycles. For this reason it is necessary to fully understand the nature of the branched photocycle and the P & Q-states.

Too date, the branched photocycle has only been discussed in two publications external to those from the W.M. Keck Center of Molecular Electronics at Syracuse University; Andreas Popp, et al. first described the branched photocycle in 1993 [1], and more recently, researchers in Hungary obtained results by continuous illumination of BR gels (gels similar to those produced for the branched photocycle memory) that could be interpreted in terms of the P and Q states [2, 3]. In an effort to reproduce the latter results, spectra containing a yellow photoproduct were obtain by irradiating a polyacrylamide gel of bacteriorhodopsin with light at a wavelength greater than 620 nm at a pH of 8.0 and a temperature of 35 to 40 °C. The maximum absorbance of this yellow species was found, via spectral analysis, to be 394 nm. This yellow species could be fully regenerated with an ultraviolet lamp at 365 nm (ambient conditions) to render a species that was spectrally equivalent to native bacteriorhodopsin. This is directly comparable to the results obtained by Dancsházy [2, 3].

**Figure 3.1.1.6** shows the overlaid spectra, with the yellow line as the most "Q-like" spectrum that shows a large decrease in the peak at 568 nm and a rise in another peak at about 384 nm. The 2 intermediate spectra were taken following 5 and 10 minutes of exposure to 365 nm radiation, and the red line indicates the fully regenerated species. **Figure 3.1.1.7** shows the difference between the initial spectrum (no exposure) and the other four.

## BR Conversion Spectrum
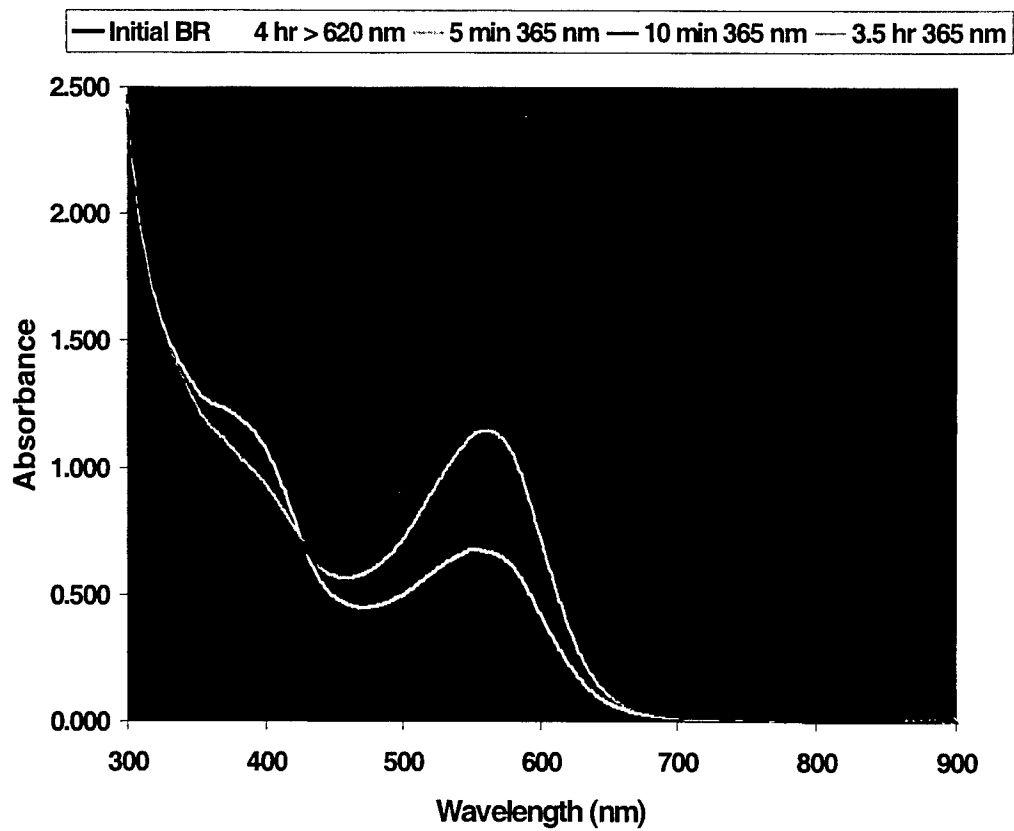


Figure 3.1.1.6: See text for details.

## BR Difference Spectra
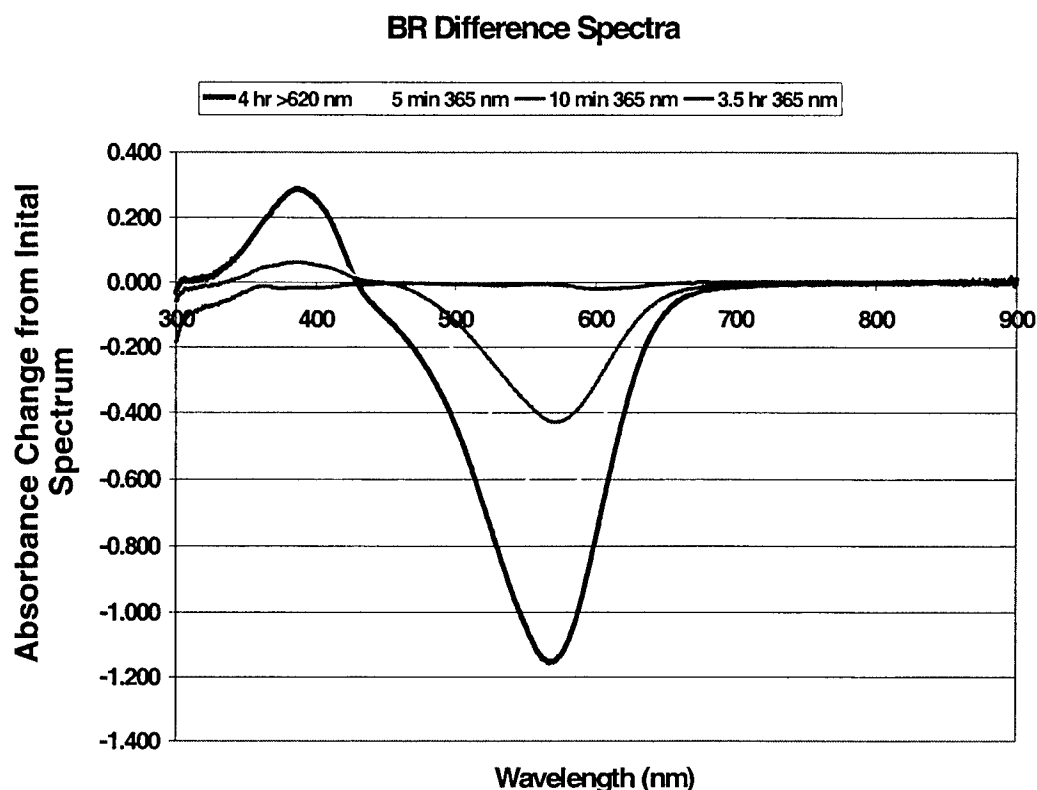


Figure 3.1.1.7: See text for details.

These preliminary results suggest that the yellow photoproduct is the Q-state found by Andreas Popp, et. al [1] because this state had a similar peak absorbance (380 nm), and it could also be restored .

### 3.1.1.6.1. Thermal P and Q Data

In attempt to better understand the nature of the P and Q states, thermal studies were conducted to understand the temperature dependence of the P and Q states. In house experiments show that access to the branched photocycle is greatly facilitated by elevated temperatures of 35-40 C. This is especially true for wild-type bacteriorhodopsin.

Denatured bacteriorhodopsin has a similar UV-visible spectrum to the photochemically generated Q state, but will not regenerate upon illuminattion. (Figure 3.1.1.8) Chromophore extraction studies were performed on both products to explore the possibility that both contain a 9-cis retinal chromophore, thus explaining their spectral similarity.
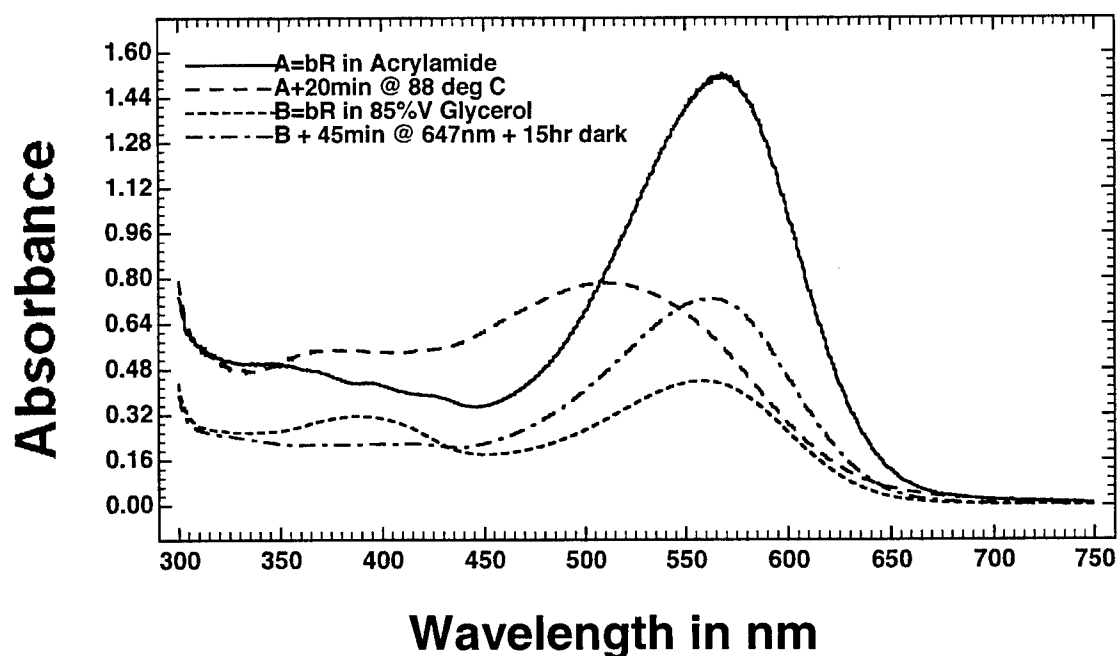
**Figure 3.1.1.8.** UV-visible spectra showing similarity in the 325 to 400 nm region for thermally denatured (upper two spectra), and the photochemical Q state

Figure 3.1.1.9 illustrates the results from two chromatograms from chromophore extraction experiments conducted on the spectrally similar photochemically formed Q state and first permanent thermally denatured state of purple membrane. One should note that while the two products are spectrally similar, only the one formed photochemically can be renatured to natively functional bacteriorhodopsin. The striking result of this figure is that two products come off the column with a similar retention time to the oxime of 9-*cis* retinal, which indicates that this chromophore seems to occupy both of these forms of the protein. The second product in this peak is unknown at this time, and is likely to be a single-bond rotated isomer of the 9-*cis* retinal oxime, or the 15-*anti* 9-*cis* retinal oxime. These results can be interpreted in terms of protein-chromophore interaction. In the photochemical case, the protein is responding to a photochemically induced 9-*cis* chromophore, while in the other case the chromophore is responding to a less restrictive (denatured) binding site. This result is also an indication that a 9-*cis* chromophore is the next highest energy conformation of retinal in the binding site after 13-*cis* and all-*trans*.

21

# Chromophore Extractions:
## Thermal Q in Acrylamide, Photochemical Q in 80% Glycerol
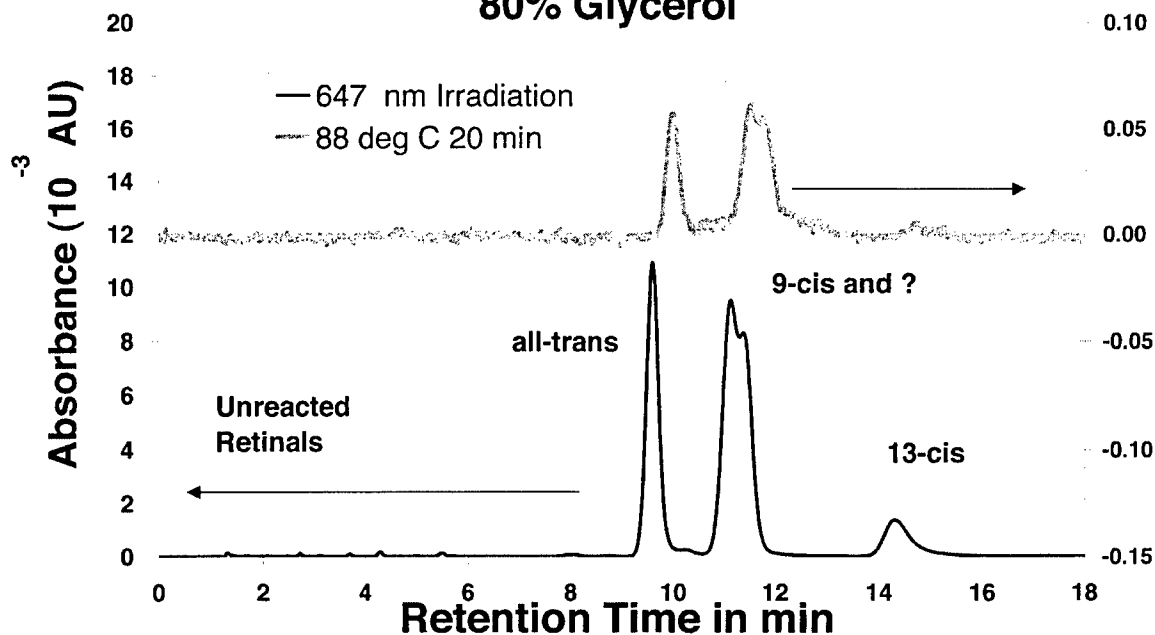


Figure 3.1.1.9. HPLC chromatograms of two chromophore analysis experiments on the renatuarable, photochemically formed Q state(bottom, left vertical axis), and the first permanent thermally denatured state of bR (top, right vertical axis).

## 3.1.1.7. Scatchard Plot Analysis

There has been a debate surrounding the presence of calcium binding sites in Bacteriorhodopsin. Some studies suggest that bacteriorhodopsin has a calcium binding site near the chromophore, while other studies suggest it is near the E194, E204 proton release group region. Some studies suggest that the calcium binding site is near the surface of the protein, in the D102, D104 region. No results have unequivocally shown where the binding sites are, and calcium has been too small to look at with current crystallization methods. Therefore, we have adopted Scatchard plot analysis in combination with mutants affecting the proton release group to further study the location, number, and binding constants of calcium binding sites in bacteriorhodopsin. We seek to identify the impact that cations have on the lifetime and yield of the O state, which in turn affects the use of bR in device applications.

Scatchard plots are a way of determining the ligand binding properties of a given ion. The concentration of calcium cation bound per bacteriorhodopsin molecule (n) is plotted on the X-axis, while the Y-axis consists of n divided by free calcium concentration. This type of information is shown below.

22

Scatchard Plot
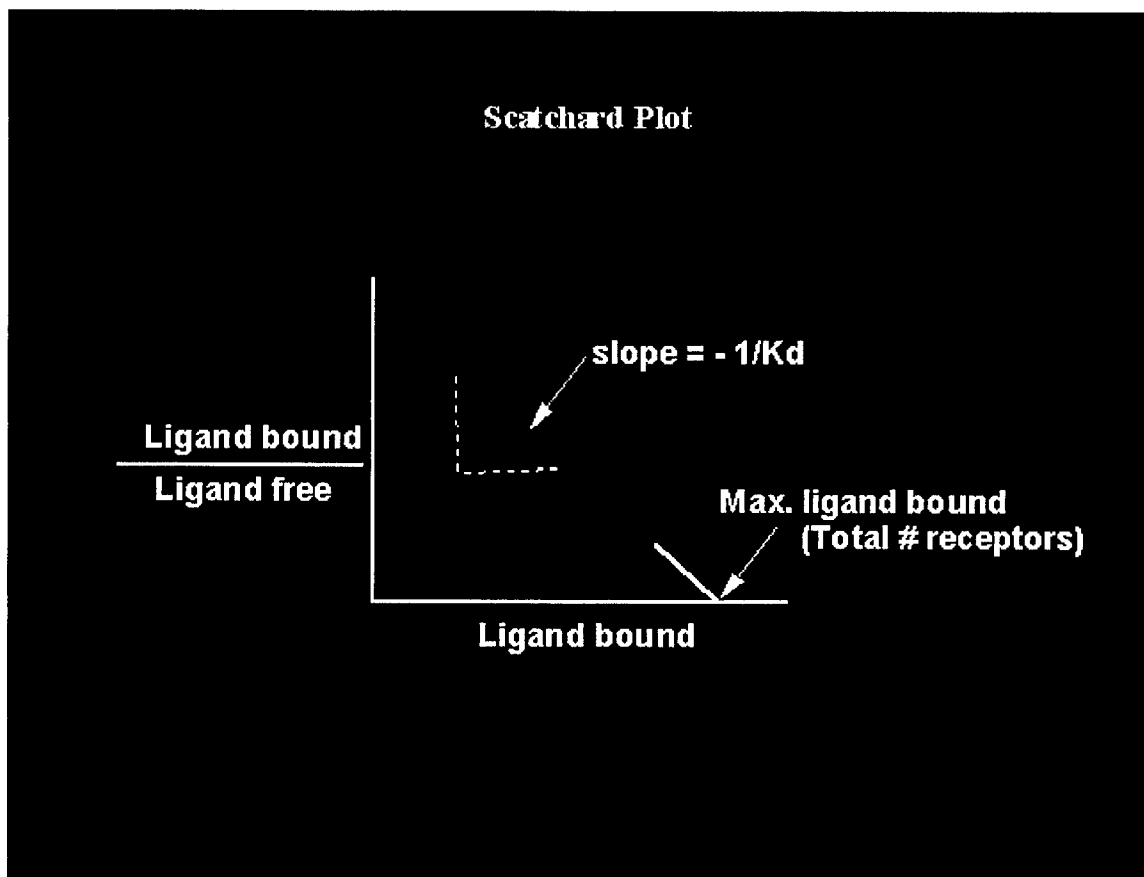
Notice that the useful values that come out of such a calculation are:

X-intercept = number of sites in a given class

Negative slope = binding constant for that particular class

When there is more than one site responsible for binding the ion, a curvilinear plot results, as shown below:

**Curvilinear Scatchard Plot**

Ligand bound / Ligand free (y-axis)

Ligand bound (x-axis)
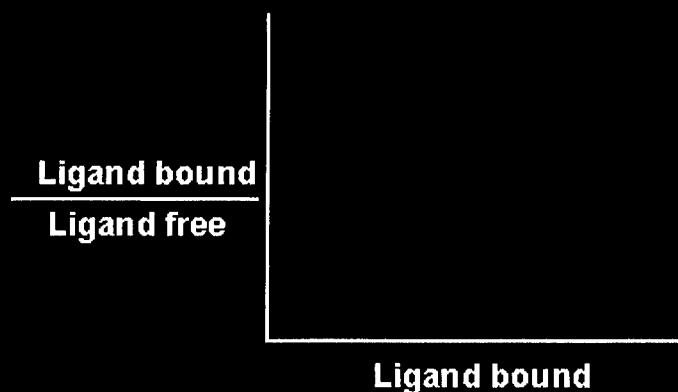
- Multiple classes of receptors with different Kd
- Negative co-operativity of ligand binding

In bacteriorhodopsin, multiple classes of receptors with different binding constants have been identified previously. However, what has not been determined is how the protein will bind calcium in the absence of the proton release group (which coincides with a possible calcium binding site). We believe that we have made a mutant which not only increases the lifetime of the O state by delaying proton release, but also one which removes one of the highest affinity calcium binding sites. We believe this double mutant, E194C/E204C, also introduces a di-sulfide linkage into the protein, possibly constraining mobility of amino acid residues and/or protein helices, or hindering proton mobility. Analysis of this data might be useful in determining whether or not calcium binding plays a role in formation of P and Q by affecting the O-state kinetics. In this context, analysis of Scatchard plots of the E194C/E204C double mutant might also provide useful information on improving memory device applications.
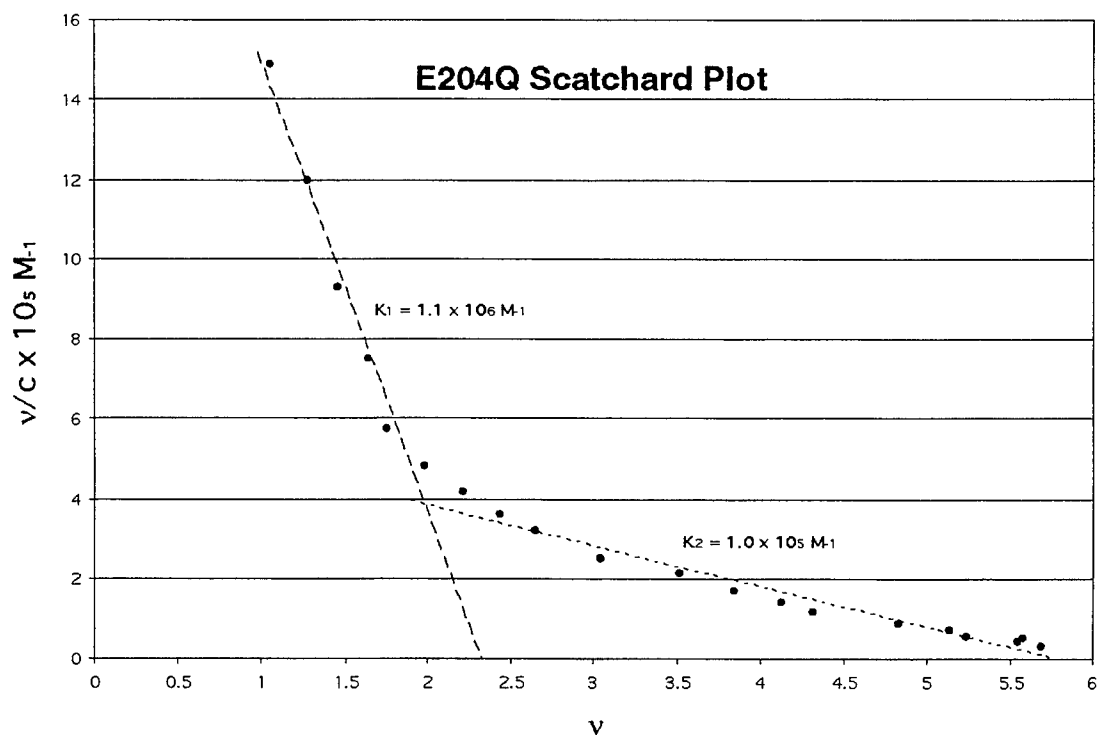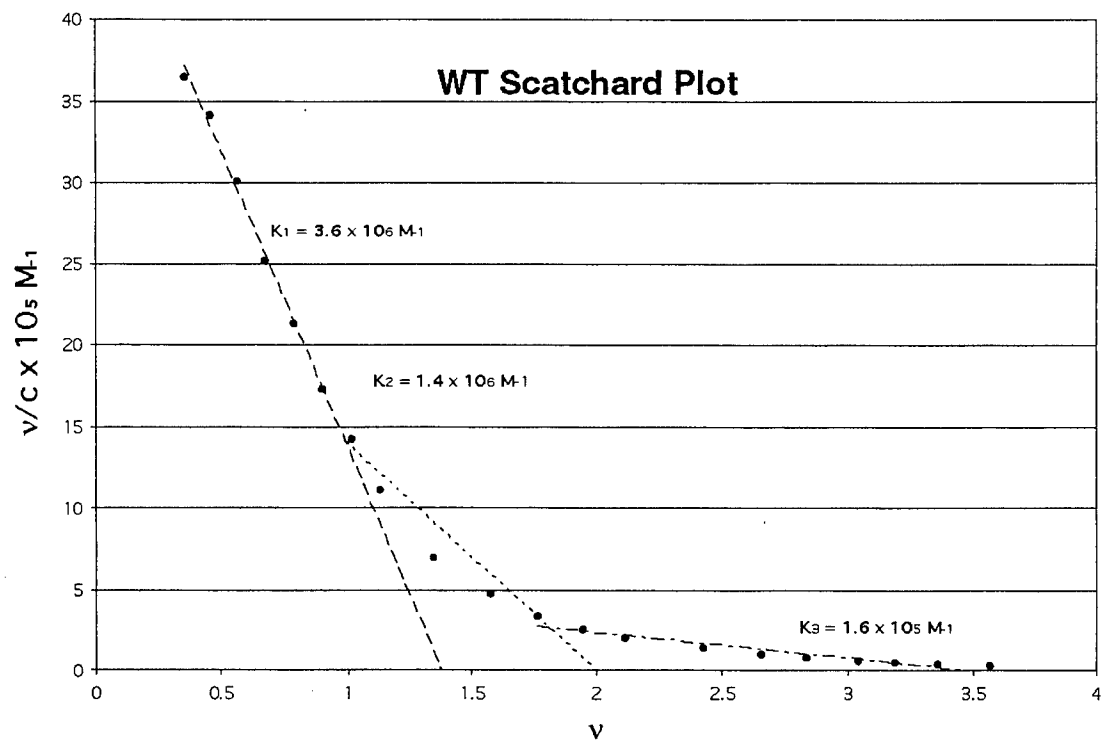
**Figure 3.1.1.10:** Scatchard plots of calcium regeneration into deionized WT and E204Q
protein. 0.01M calcium was titrated into a 15 mL sample of 20 uM deionized blue
membrane protein. Electric potential differences were recorded using an ion-
specific probe and a pH/ion-sensitive electrode meter. Equimolar amounts of 0.01M

calcium were titrated in μL additions to a sample of 15 mL deionized water or a sample of 20 μM deionized protein. ν represents the amount of molar ratio of calcium bound per bR molecule. ν/c represents the molar amount of calcium bound per bR molecule divided by the concentration of free cation in solution. Slopes were calculated to include points of various molar ratios : WT has three slopes calculated as: 1:1 molar ratio of $Ca^{2+}$:bR, 2:1 molar ratio, and all points above a 2:1 molar ratio. Binding affinities are calculated as the negative slope of the line and are shown next to each line. E204Q has slopes calculated from two titration regions: all points below and including a 2:1 molar ratio, and all those above a 2:1 molar ratio.

The WT Scatchard plot is broken into three linear regions corresponding to molar ratio amounts. The first line includes all points up to a 1:1 molar ratio of calcium ion per bR molecule. Literature suggests there is one high affinity binding site in this class [4, 5]. The second linear region corresponds to those points between a 1:1 and a 2:1 $Ca^{2+}$:bR molar ratio. We also expect there to be one site in this affinity class. The third region corresponds to the remaining points, which correspond to molar ratios greater than 2:1. We expect there to be 2-4 ion binding sites in this affinity class.

The E204Q Scatchard plot is divided into two linear regions. The first region corresponds to those points up to a molar ratio of calcium per bR molecule of 2:1. The second line represents all points above a 2:1 $Ca^{2+}$:bR molar ratio. Binding affinities are calculated as the negative slope of each line, and are labeled on the graph, where • = molar ratio of calcium bound per bR, c = concentration of free cation in solution. Therefore, the y-axis is the amount of bound calcium per bR divided by the concentration of free cation.

Scatchard plots have been constructed to examine calcium binding to deionized E204Q protein (dIE204Q). When compared to dIbR, dIE204Q protein has a disrupted high affinity calcium binding site profile. This can be seen in the Scatchard plot of E204Q; the binding of the highest affinity site is either altered to match another existing affinity, or eliminated. It is accepted that the site of highest cation binding affinity corresponds to a non-chromophore residing site, while the second highest affinity cation binding site is near the chromophore binding pocket and responsible for the blue to purple color shift [5]. If calcium is binding to the E194/E204 region, then E204Q should result in disruption or alteration of this highest affinity binding site. Scatchard data of E204Q suggest this to be the case, and support the presence of calcium bound to the E194/E204 region. The binding affinity of the second highest class, responsible for the blue to purple shift, is nearly constant between the Scatchard plot for WT and E194Q ($K_2$ of WT vs. $K_1$ of E204Q). This suggests that the second site, which resides near the chromophore, is unperturbed in the E204Q mutant.

### 3.1.2. Materials Research at Carleton University

As mentioned above, the task of optimizing the polymer host matrix was handed to Professor Wayne Wang of Carleton University. Professor Wang and his student Jeff Franklin were responsible for optimizing the matrix with respect to long-term stability and optical clarity. Their progress during the final year of the contract is detailed below. It outlines initial developments and recent advancements made in the preparation of a suitable polymer matrix for a bacteriorhodopsin based optical storage device.

### 3.1.2.1. Investigation of polyacrylamide hydrogel variables

The effects of variables such as temperature and pH on the stability and light scattering of polyacrylamide (PAm) gels were investigated. It was found that both the pH and temperature display an effect on the light scattering of a given gel as well as the shrinkage or stability of that same gel.

- It was observed that by increasing the temperature of a PAm gel, the light scattering was reduced.

- At lower temperatures (< RT) the light scattering was increased over those gels at RT.

This can be explained by the fact that the light scattering of a given gel is characteristic of the rate of polymer relaxation that has occurred. The greater the degree of polymer relaxation, the lower the observed light scattering. By increasing the temperature of the hydrogel more energy is supplied to polymer relaxation and the rate of relaxation is increased, thereby lower the amount of observed light scattering compared to that of a gel at RT. On the other hand, if the gel is cooled, the amount of energy available for polymer relaxation is a minimum and the rate of relaxation is therefore decreased. This slowed relaxation rate gives the gel a more disordered state and causes a higher degree of light scattering over a gel at RT (see figure 3.1.2.1). However, due to the greater relaxation rate at elevated temperatures, the shrinkage or distortion of the gel is also accelerated, whereas it is slowed at decreased temperatures. This rate of polymer relaxation can also be viewed as polymer "aging."

The effect of pH on the polyacrylamide hydrogels was seen to increase light scattering with decreased pH (figure 3.1.2.1). This is most likely due to the fact that at lower pH values there is a pronouned amount of swelling and polymer degradation. Both of these factors contribute to increased light scattering. In addition, it was observed over long time periods that the rate of shrinkage or distortion of a gel at high pH was slower than that observed for gels at neutral or acidic pH. This finding was later useful in screening alternative polymers for possible hydrogel matrices.

27
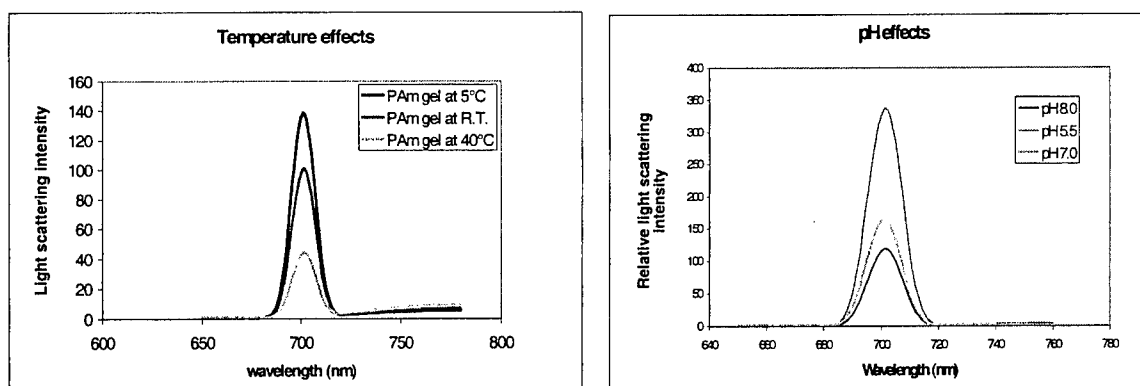
**Figure 3.1.2.1**: Effects of temperature and pH on light scattering of PAm gel.

### 3.1.2.2. Aging studies on hydrogels and the relation to light scattering and gel shrinkage/distortion (deformation)

An aging study on the optimized PAm hydrogel formulation was carried out over the course of 18 months. The study was used to show the amount of polymer relaxation (shrinkage or distortion) that took place for a given hydrogel over a set time period and the amount of light scattering of the matrix corresponding to the amount of polymer relaxation that has occurred. The results for a PAm hydrogel containing 50% sucrose additive and 0.4 mL of BR solution can be seen in Figure 3.1.2.2. Light scattering was monitored at 700 nm. The gel was sealed with wax and epoxy to protect it from the atmosphere. Over the course of 18 months there was an observed vertical shrinkage of 5.0 mm with no distortions or bubbles in the matrix itself (figure 3.1.2.3).

**Figure 3.1.2.2:** Light Scattering of PAm Hydrogel as a Function of Time (aging)
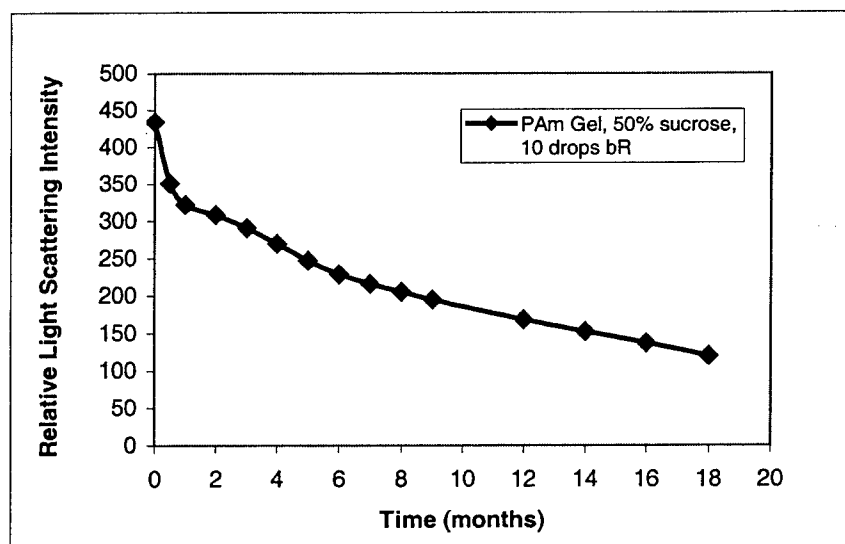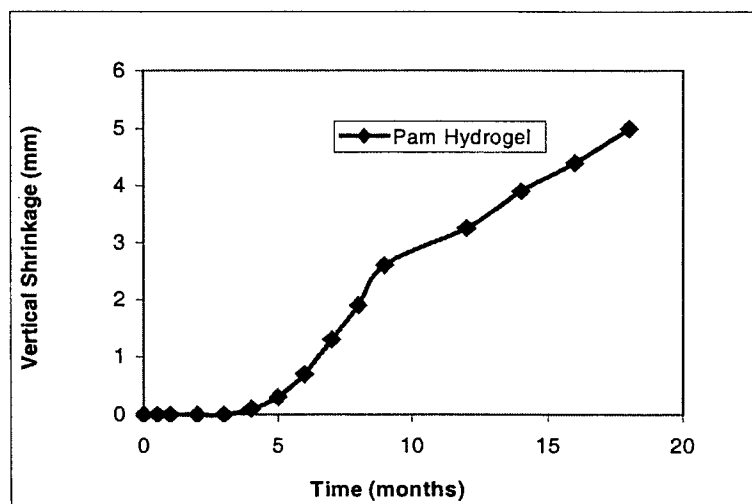
**Figure 3.1.2.3:** Visible aging (shrinkage) of PAm hydrogel over time.

This observed aging trend was seen to vary with various parameters such as temperature and pH. An aging experiment was set up to monitor the light scattering and shrinkage/distortion of various PAm hydrogels under different temperatures and pH. The experiment was run over the course of 8 weeks. Light scattering was monitored at 700 nm. Each gel contained 50% sucrose and 0.2 mL of BR solution. The gels were sealed *via* wax and epoxy. The first part of the experiment looked at the effects of temperature and compared the aging of PAm gels at 40°C, Room Temperature (RT), and 5°C. The results can be seen in figure 3.1.2.4.
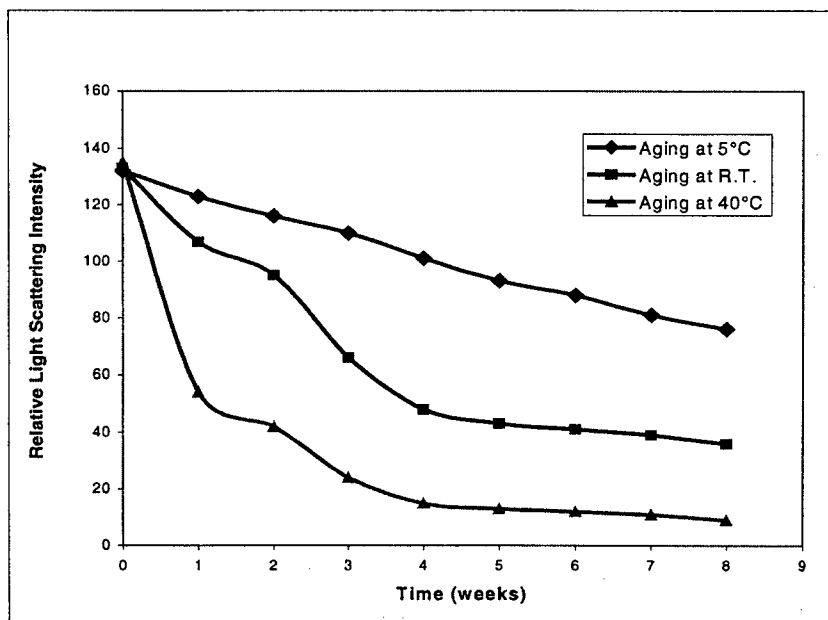


**Figure 3.1.2.4:** Relative light scattering of PAm gels aged at various temperatures over time.

As can be seen from figure 3.1.2.4, light scattering of the PAm gels is improved (or decreased) with increasing temperature. This trend was explained above. The higher the temperature, the more energy available to allow the polymer to relax. The greater the amount of polymer relaxation, the lower the observed light scattering. However, the gels stored at different temperatures exhibited various levels of deformation. The gel deformation can be defined as any visible structural defect such as an air bubble in the matrix, vertical shrinkage, bubbling or pulling away from the cuvette wall, etc. Since all the gels in this experiment displayed various deformation patterns, a percentage value was assigned to each gel for a given time period. The percentage value assigned is an estimated amount of the total space occupied by the original gel structure that has since become deformed or has shrunk with time. The results for each aging temperature can be seen in figure 3.1.2.5.
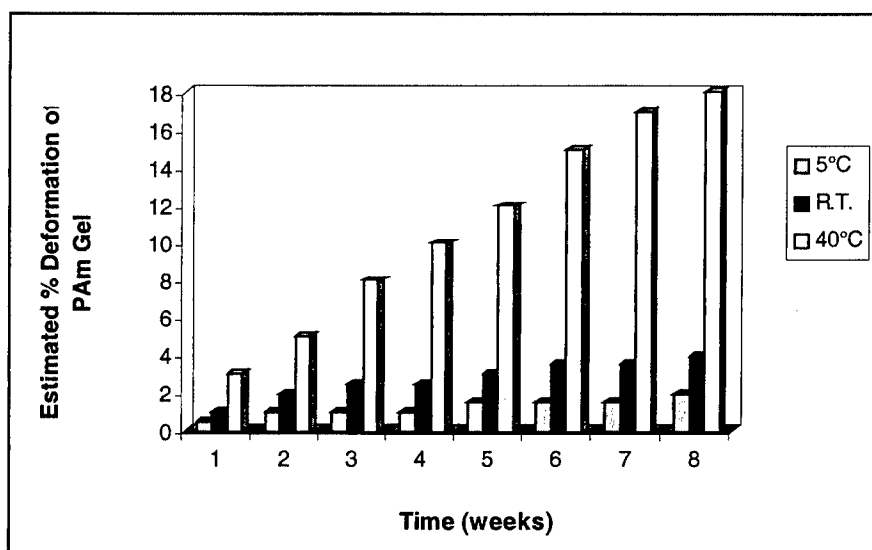


**Figure 3.1.2.5**: Estimated % deformation of PAm hydrogels over time at various temperatures

As can be seen in the bar graph, the higher the temperature, the greater the amount of gel deformation. Gel deformation can be directly related to polymer relaxation in that as a polymer structure becomes relaxed, subtle changes in shape occur. Thus, there seems to be a trade off in that at elevated storage temperatures there is a marked improvement in the observed light scattering of a given gel over one at a lower temperature, but the amount of gel deformation is also greater at elevated temperatures. It is important to note that an experiment was performed in which gels were stored for 2 weeks at elevated temperatures and then soaked in water to remove the deformations present. Gels were then sealed deformation free, but maintained the decreased light

30

scattering values due to their storage at elevated temperatures. This incubation time was seen to slow the rate of deformation for a given gel.

In addition to hydrogel aging being affected by temperature, it is also affected by changes in pH. Another aging experiment was set up to compare the shrinkage and light scattering of PAm hydrogels over an 8 week period at different pH values. The gels were tailored to the desired pH prior to polymerization. All gels contained 50% sucrose, 0.2 mL BR solution and were sealed with wax and epoxy. Light scattering was monitored at 700 nm. The results can be seen in figure 3.1.2.6.
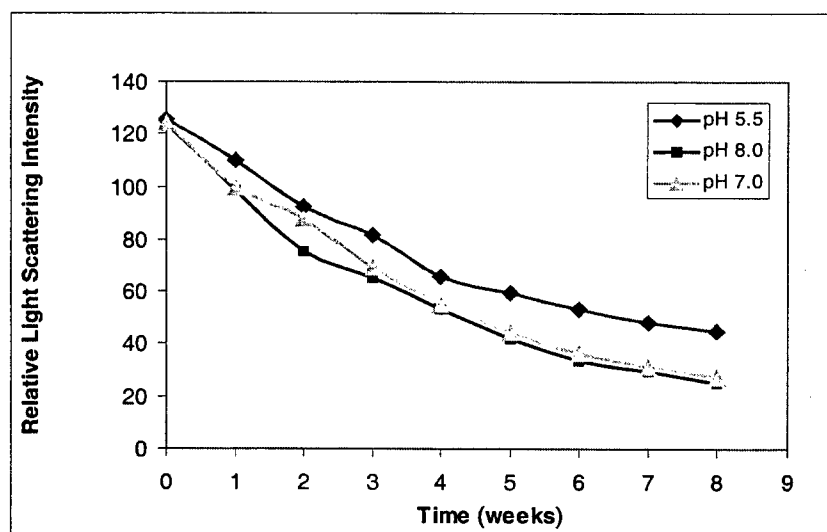


**Figure 3.1.2.6:** Relative light scattering over time (aging) for PAm hydrogels at different pH

Over the course of 8 weeks, it is evident that the gels stored at pH 8.0 have improved light scattering characteristics with time. This may be a direct result of the amount of swelling the hydrogel undergoes at different pH values or it could be related to the degree of polymerization. Since the gels were modified to a set pH prior to polymerization, the lower pH may have resulted in a more incomplete polymerization and thus increased light scattering. However, this is unlikely since all pH values have almost identical initial readings at time "0." It may also be due to the fact that polyacrylamide is more easily degraded at acidic ranges in pH. This could over time lead to higher light scattering than a gel at higher pH due to the presence of degradation fragments. It is also important to note that since gels were set at a pH prior to polimerization, the pH will have changed during the polymerization process to some extent.

The gels displayed various forms of aging patterns; therefore, an estimated percentage value was assigned to each time period for an amount of overall gel deformation that had occurred. The gels were monitored for an 8 week period. The results

31

can be seen in figure 3.1.2.7. It is evident from the bar graph that pH 5.5 has accelerated deformation (aging) than that of a gel at pH 7.0 or at pH 8.0. Again, this is probably due to the increased swelling of PAm under acidic conditions. The added tension that the swelling may induce on the network may in turn accelerate the polymer relaxation process to some extent. The more water that the polymer absorbs, the more likely the crosslinking points would stand out as points of high local density, and thus the system would likely demonstrate more pronounced "point inhomogenieties" which would likely lead to the increased light scattering characteristics of these gels. Also, it is known that at acidic pH, PAm is more easily degraded which would also contribute to the overall % deformation observed in each gel.
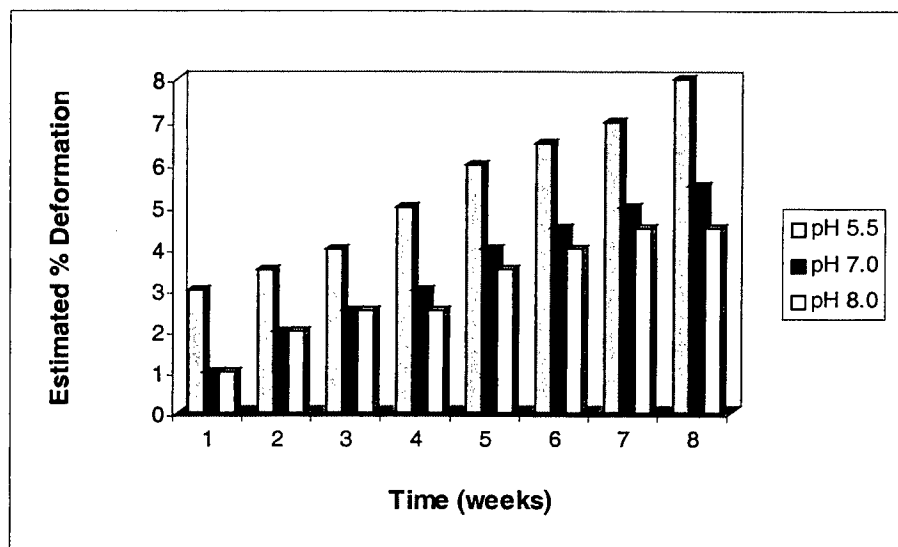


**Figure 3.1.2.7:** Estimated % deformation of PAm hydrogels over time at different pH

### 3.1.2.3. Investigation of additive effects on hydrogel light scattering

Sucrose was the additive of choice to evaluate the preliminary effects of biocompatible additives on the light scattering of PAm. However, several alternative additives were investigated with promising results (figure 3.1.2.8).
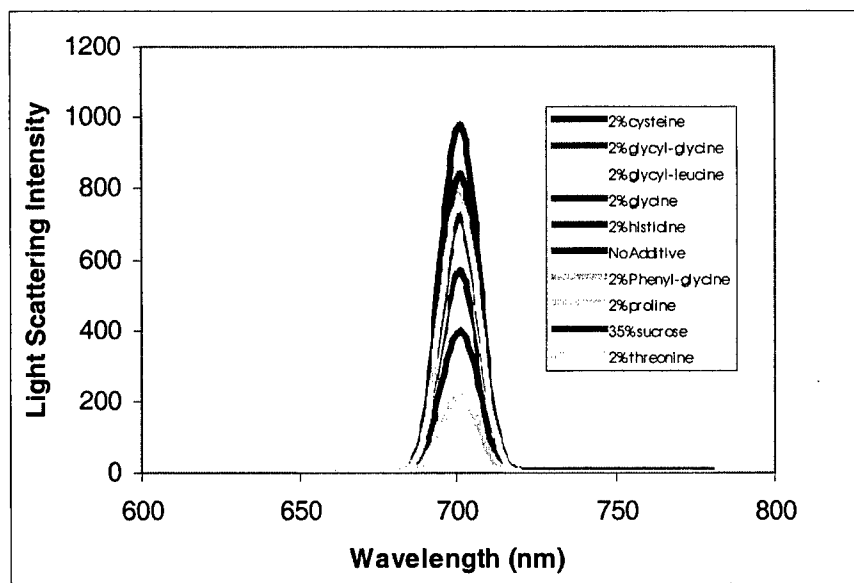
**Figure 3.1.2.8:** Comparison of light scattering within PAm hydrogels with the incorporation of various biocompatible additives.

It can be seen from the results that several additives produce lower light scattering within PAm than sucrose at much lower concentrations. Thus it may be more beneficial to utilize alternative additives (or combinations thereof) to decrease light scattering of a given hydrogel. In terms of cost, most of the additives investigated have a comparably low cost, however there are a few exceptions (figure 3.1.2.9) as well, the amount needed to produce a desired light scattering level will determine the overall cost required for a given additive.

**Figure 3.1.2.9:** Comparison of additive cost per 5 gram sample.
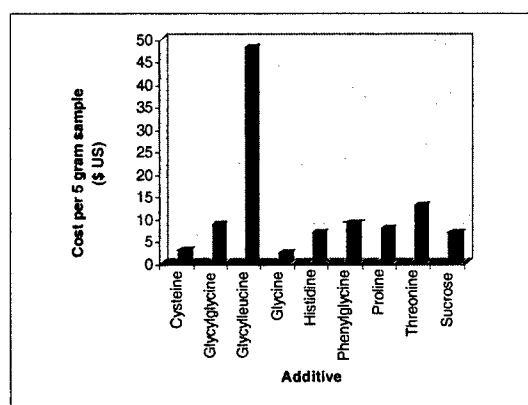


*Photo-crosslinkable hydrogels :*

The copolymer of dimethyl acrylamide and 2-hydroxyethyl acrylate was modified with cinnamoyl chloride as previously described. The attempt to add a cinnamoyl group was important because it would act as the photoactive crosslinking group. Finally, after many polymerizations and crosslinking attempts a successful photo-crosslinking reaction was observed. The modified copolymer was UV irradiated for ~5 min and it formed a cloudy gel structure (figure 3.1.2.10). The fact that the reaction actually took place was very encouraging. However, attempts to improve the cloudy nature of the gel or optical transparency have thus far failed.

**Figure 3.1.2.10**: Photo-crosslinked copolymer of N,N
    Dimethyl acrylamide and 2-hydroxyethyl acrylate.
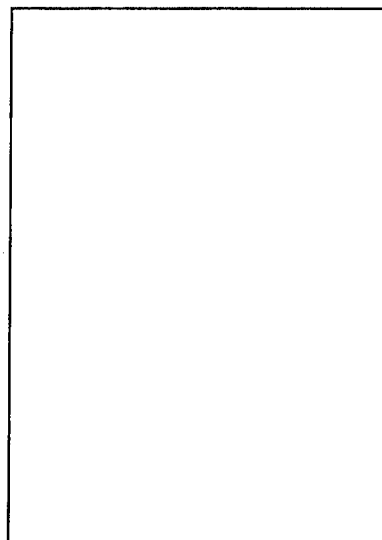
### 3.1.2.4. Alternative hydrogel systems

Once the polyacrylamide hydrogel system was optimized for light scattering characteristics, there still remained the problem of gel shrinkage. From the optimized formulation, a hydrogel cube once incubated, soaked with water, then sealed air tight could remain stable for approximately 5 – 6 months before signs of polymer aging or relaxation were observed. Thus, alternative hydrogel systems were investigated for their improved stability and light scattering characteristics. Several monomers were screened in various combinations. For example, copolymers of

1. acrylamide + 2-[(methacryloyloxy)ethyl dimethyl (3-sulfopropyl) ammonium hydroxide] inner salt + Methylene bis acrylamide;

2. acrylamide + hydroxyethyl acrylate; and

3. 2-[(methacryloyloxy)ethyl dimethyl (3-sulfopropyl) ammonium hydroxide] inner salt + Methylene bis acrylamide

were investigated over varying concentrations of monomers and additive. In addition, combinations of polymers such as PAm + gelatin, and PAm/HEA copolymer + gelatin were also investigated for light scattering properties with and without the additive "sucrose" over various concentrations. Figure 3.1.2.11 displays the light scattering measurements of these various polymer systems. All gels used in this comparison contained the same amount of bacteriorhodopsin. As can be seen in the figure, some hydrogel systems displayed better light scattering properties than that of the optimal PAm system, while others displayed higher scattering than seen in the current PAm gels. From this study, two interesting findings were made.

34

The first was that when polymerizing acrylamide with 2-hydroxyethyl acrylate, if the concentrations of the monomers reached a so called "threshold" value, then gelation was observed to occur in the absence of crosslinking agent. This was presumably due to the extensive amount of hydrogen bonding occurring between the two monomers. Thus the polymer chains formed "physical crosslinks" with other polymer chains through these hydrogen bonds. As can be seen in the figure, due to the absence of chemical crosslinks, these gels scatter less light than that of the optimized PAm system. It was also observed that as the concentration of monomers increased above this threshold value, the strength and rigidity of the gels increased as well. Several concentrations of the two monomers were examined and their stability up to 80°C was investigated. This



**Figure 3.1.2.11**: Light Scattering Comparison of Various Hydrogel Systems.

demonstrated that none of the physical hydrogels became fluid or lost rigidity at elevated temperatures.

In addition to this important finding, it was also observed over time that the hydrogel composed of polyacrylamide and 2-[(methacryloyloxy)ethyl dimethyl (3-sulfopropyl) ammonium hydroxide] inner salt was much more stable than that of the optimized PAm formulation. It had a slowed deformation rate over that of just PAm hydrogels. This is likely due to the previous observation made from the effect pH has on aging. Since the monomer used in this copolymer is a ammonium hydroxide inner salt, it likely imparts a fairly basic environment to the polymer which in turn imparts an increased stability to the hydrogel.

### 3.1.2.4.1. PAm/HEA copolymer hydrogels

As already mentioned, it was discovered that these gels are formed from intensive hydrogen bonding of the polymer chains with each other. Therefore, there are no chemical crosslinks present in the network several different combinations of monomer concentration were investigated for both acrylamide and 2-hydroxyethyl acrylate that induced gelation. These gels were then tested for their light scattering characteristics (figure 3.1.2.12) and compared to polyacrylamide hydrogels crosslinked with MBA. All gels in this experiment contained 40% sucrose and were allowed to sit for 2 days prior to reading.
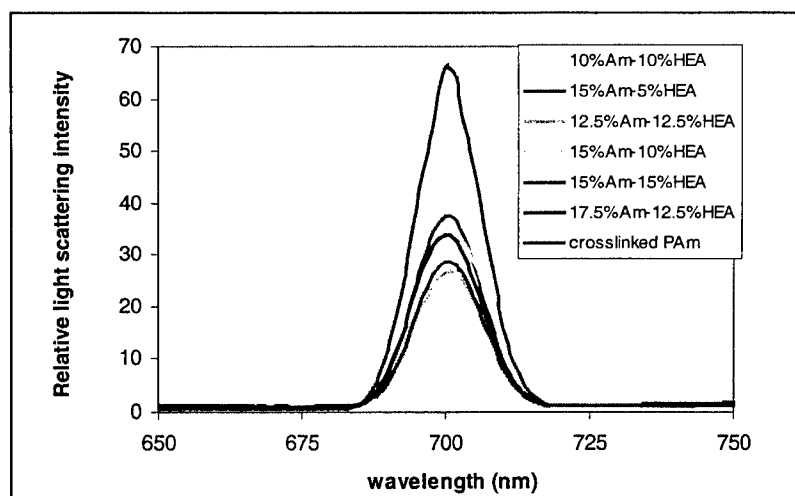
**Figure 3.1.2.12**: Relative Light scattering comparison of Am/HEA physically crosslinked hydrogels to the regular chemically crosslinked PAm gel.

The polyacrylamide hydrogel in figure 3.1.2.12 contained 10% (w/v) of acrylamide (usual) with 0.2% (w/v) MBA (usual) as well as 40% sucrose.

As one can see from the figure, all the copolymer gels of Am/HEA displayed improved light scattering characteristics over that of the chemically crosslinked PAm. As previously mentioned, the strength of these copolymer gels was dependent on the concentrations of monomers used. For optimum strength and light scattering, it is evident from figure 3.1.2.12 that monomer concentrations of either 12.5%(w/v) for both acrylamide and HEA, or 15%(w/v) for both acrylamide and HEA are necessary.

An interesting occurrence was noticed during the polymerization of these Am/HEA copolymer gels. That is when BR is incorporated into the polymerization solution there is an observed color change from purple to pink. This does not occur when only acrylamide is used as a monomer, therefore it is likely as a result of the toxicity associated with the 2-hydroxyethyl acrylate monomer. During the polymerization, the BR remains a light pink color. Post polymerization the color changes slowly with time back to a deep purple. This occurrence was monitored by UV/vis to show the spectral changes in BR during the polymerization process. The results can be seen in figure 3.1.2.13.
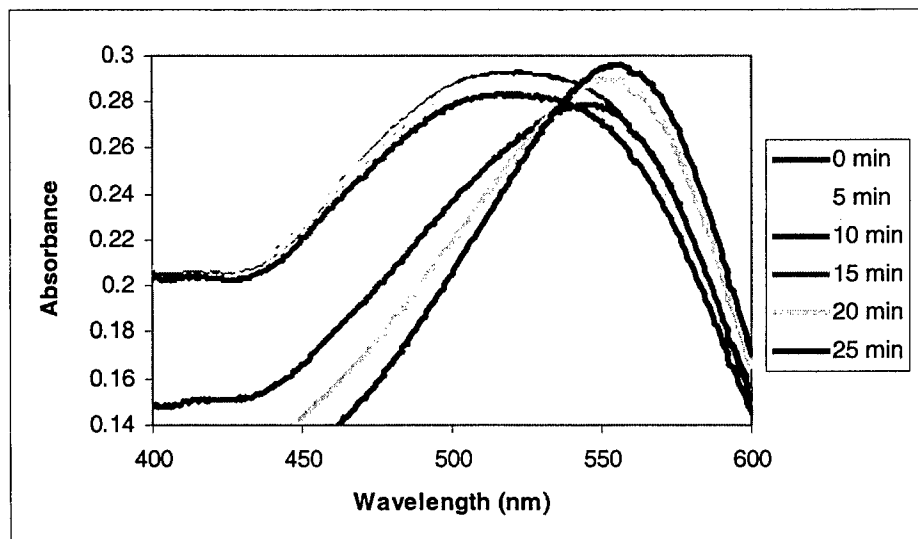
**Figure 3.1.2.13**: Spectral shift of BR during Am/HEA copolymerization

The times for each spectrum refers to the time elapsed from initiation of the polymerization reaction. As can be seen in the figure, after 25 minutes the protein returns to its normal absorption spectrum. At time 0 until time 10 minutes, the BR has an absorption maximum at 525 nm. At time 15 minutes the absorption maximum shifts to 550 nm which corresponds to the N state intermediate of the protein.

### 3.1.2.4.2. Polymer Hydroglasses

With the advancements made in light scattering reduction for a given polymer, the main problem left to be solved for this project was the issue of polymer relaxation/gel deformation. As seen outlined in the above text, there are ways to prolong the deformation or slow down its rate, however, it will eventually occur over time. Thus, there was no clear-cut solution to this problem. Upon analysis of the situation, it was determined that deformation was occurring because the gel was soft and pliable, which in turn inevitably allowed it to succumb to the relaxation of the polymer. If the polymer could be synthesized to be so rigid and hard that no deformation would be permitted then the problem could be solved. Therefore, investigations into forming such polymers began. The result was the production of "hydroglasses".

The formation of the desired "hydroglass" structures was accomplished using acrylamide and methacrylamide as monomers, and piperazine diacrylate as the crosslinking agent. The reaction was carried out in water as the term "hydro" implies. Very hard, rigid structures were produced that could be removed from the mold in which they were made (i.e. cuvette). Several different shapes were made in different containers such as; NMR tubes, glass vials, cuvettes, etc. The resultant glass-like structures displayed a high degree of hardness. Some of these polymer structures were cut using a



**Light Scattering Comparison of Current Gel Systems With that of a Hydro-glass**

Legend:
— Hydro-glass
— PAm gel no additive
— PAm gel 50% sucrose

Wavelength (nm)

**Figure 3.1.2.14**: Comparison of relative light scattering intensities of the current Pam hydrogels to that of the newly formed hydroglass
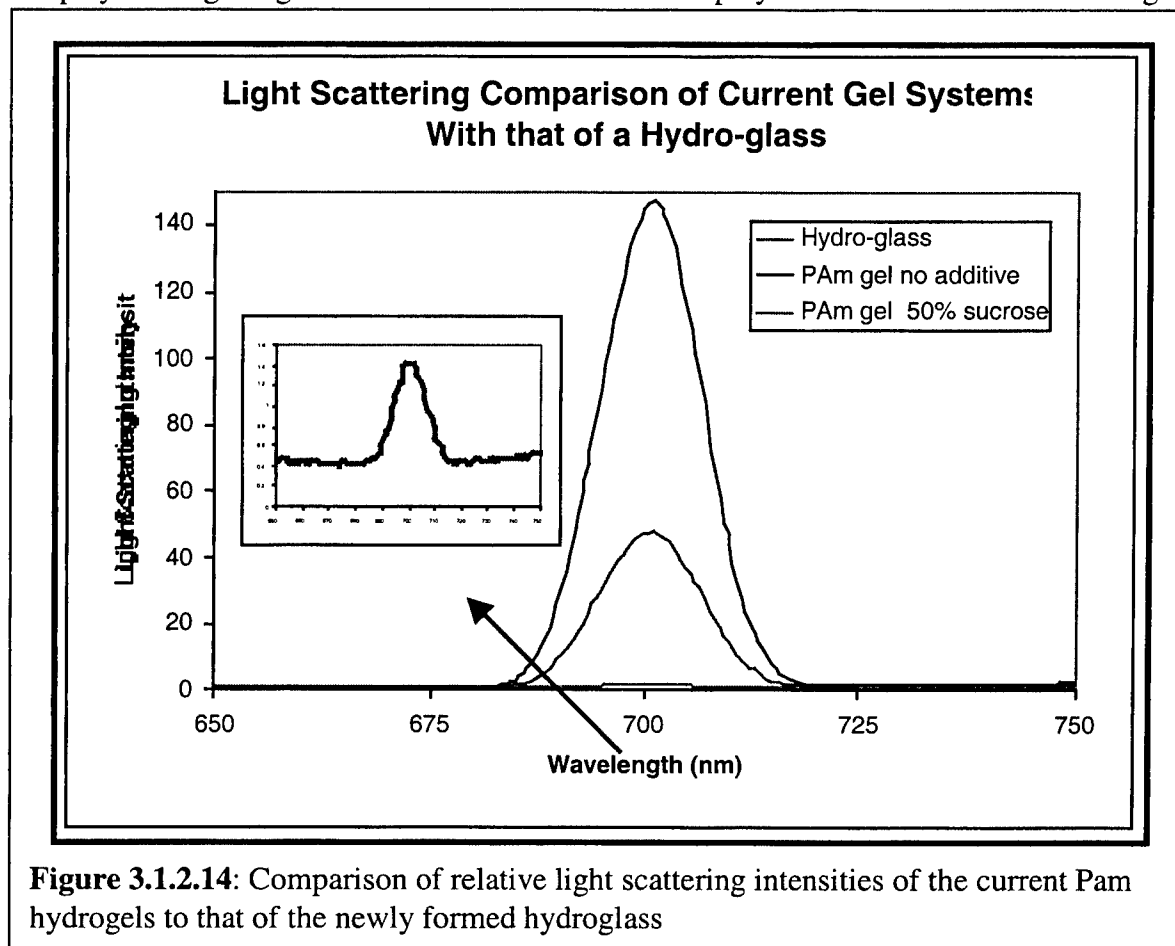
glass-cutting instrument, which demonstrated their ability to be subjected to mechanical stress without fracture. The light scattering of a hydro-glass cube was tested on the fluorimeter as done for all hydrogel cubes to this point. The scattering was compared to that of a polyacrylamide hydrogel without additive and to one with 50% sucrose (current system) (Figure 3.1.2.14). As can be seen, the hydro-glass cube has a marked reduction of light scattering over the current system. It should be noted that the hydrogels were run on the fluorimeter in plastic cuvettes, while the hydro-glass cube did not require a plastic cuvette to contain it.

Upon further investigation of the reaction conditions it was found that excessive amounts of heat are generated during polymerization of these hydroglasses. The polymerization was monitored using a thermocouple and found to reach temperatures around 105°C. The temperature only remained above 100°C for approximately 25 seconds, however, the temperature was just too high for bacteriorhodopsin to be

successfully incorporated. Thus, attempts to fine-tune this aspect of the reaction to a more acceptable temperature for BR incorporation were made. By varying the amount of catalyst, the reaction was slowed somewhat and by placing the cuvette in a water bath during the reaction, successful incorporation of BR occurred. This incorporation was not 100% successful; approximately 40% of the BR was denatured from the exothermic reaction, while approximately 60% remained. This was assumed through the color of BR added and that left in the polymer (i.e. the less BR present, the lighter the purple color). Therefore, alternative hydroglass systems were also investigated. The methods used for the acrylamide, methacrylamide system were applied to other monomers.

Several hydroglass structures were successfully formed using various monomers such as hydroxy ethyl acrylate, hydroxy ethyl methacrylate, N-(hydroxymethyl) acrylamide, N-(hydroxymethyl)methacrylamide, 2-[(methacryloyloxy)ethyl dimethyl (3-sulfopropyl) ammonium hydroxide] inner salt, N, N-dimethyl acrylamide, methacrylamide, and acrylamide. Monomers were used in various combinations to yield hard, glassy structures. However, depending on concentrations used and the types of monomer, some structures were found to be more rigid and hard than others. It was also found that when using large amounts of hydroxy ethyl methacrylate or hydroxy ethyl acrylate the protein was denatured due to the toxicity of these compounds. Hydroglasses formed from acrylamide and the inner salt monomer have been used for the successful incorporation of BR. This hydroglass is not as rigid and hard as the methacrylamide/ acrylamide structures but it is much more biocompatible towards the protein. Both the toxicity and the heat of reaction for this system are more suited to incorporation of BR. A comparison of the light scattering of these BR incorporated hydroglasses to the PAm hydrogels containing BR was made. As seen in figure 3.1.2.15, the two samples both contain 0.6 mL of BR solution. As well, it should be noted that the hydrogel contains 50% sucrose and was aged for 18 months while the hydroglass contains no additive and was aged for about 1 month. However, despite this the hydroglass still has a marked reduction of light scattering over the PAm hydrogel. The hydroglass was also sealed with an optical epoxy and was therefore not contained in a cuvette. The biocompatibility of these hydroglass structures was also checked by monitoring the absorption maximum of BR in the medium compared to that of BR in a PAm hydrogel. The results can be seen in Figure 3.1.2.16. To date, the only problem associated with these hydroglass structures is the ability to seal them evenly and effectively creating an airtight seal with all faces of the cube remaining flat. The epoxy currently being used seals the cubes but creates convex curves to each face on the cube. Thus, an alternative method of sealing or an alternative sealant must be used. This is more of an "engineering" problem that should not pose as too much of a problem—its only a matter of time. An epoxy sealed hydroglass structure can be seen in figure 3.1.2.17.

**Figure 3.1.2.15**: Light scattering comparison of BR incorporated hydrogel and hydroglass.
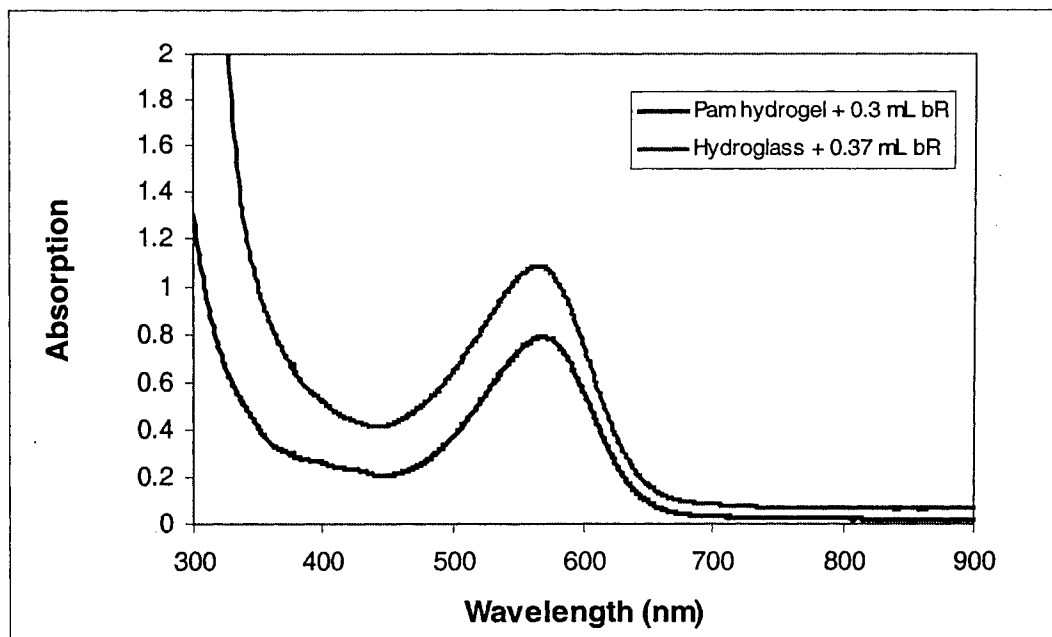


### 3.1.2.5. Future Work

The next year of this project (through 10/2001) will be focused around optimizing this hydroglass polymer system such that all conditions of the required device are met. As of now, the BR hydroglass cube has exceptional low light scattering characteristics, excellent biocompatibility, and a hardness that should alleviate the shrinkage problem to date. The only problems to deal with are manufacturing issues such as sealing and polishing etc. Ongoing with this research, investigations into the PAm hydrogel system will continue to focus on tying up all the "loose ends" for a more complete understanding of this process and the factors involved in shrinkage, light scattering and polymer degradation. As well, means to maximize production of these optical cubes will continue such that the device can be produced in greater amounts in a minimal amount of time.

**Figure 3.1.2.16**: Biocompatibility comparison between both the hydrogel and hydroglass matrices for BR incorporation
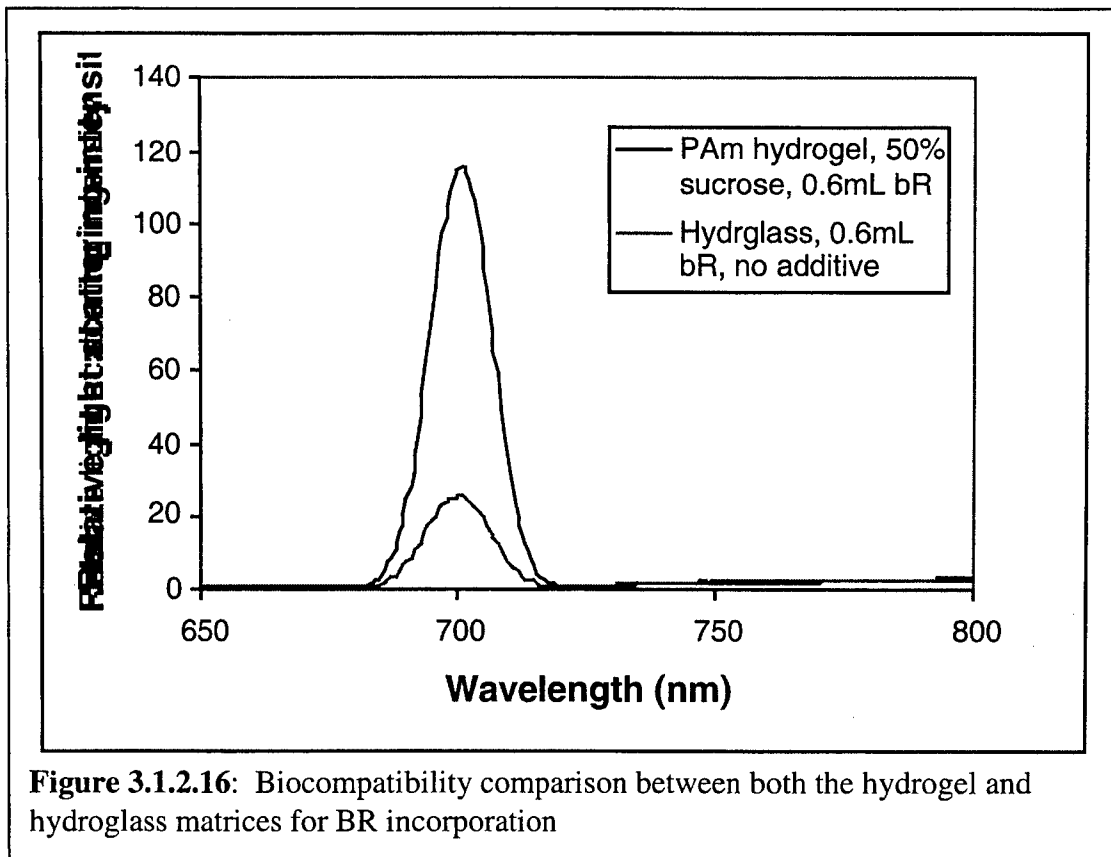
**Figure 3.1.2.17:** BR-Hydroglass sealed with UV cured epoxy
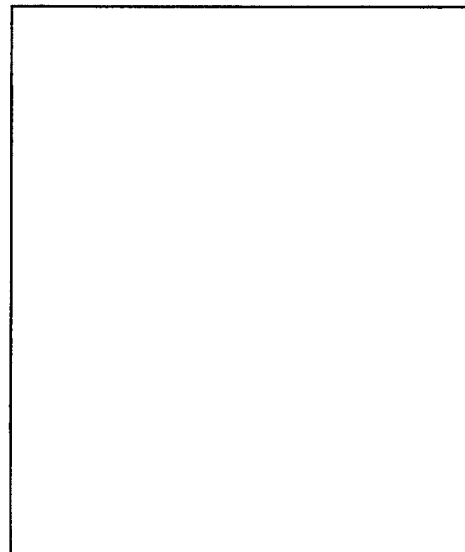
## 3.2. Miniature Prototype Development

### 3.2.1. Prototype Design

#### 3.2.1.1. Overview

In addition to the modular prototype, part of the effort for the contract included producing a miniature or portable prototype. The emphasis for the miniature design was simplification, while still providing proof of concept. The miniature design has been used to demonstrate reading and writing, as well as erasing a single volumetric element, or "voxel" within a BR cuvette. In other words, it has been used to demonstrate complete functionality of a three-dimensional BR based memory system.

We assume that the ultimate goal is to produce a removable medium drive, analogous to a zip drive. The storage medium, of course, will be a one cubic centimeter cuvette of polymer-encapsulated bacteriorhodopsin. An advanced design would be interfaced to the computer through a standard such as the SCSI interface. The components required to produce such a drive are shown in the figure below.
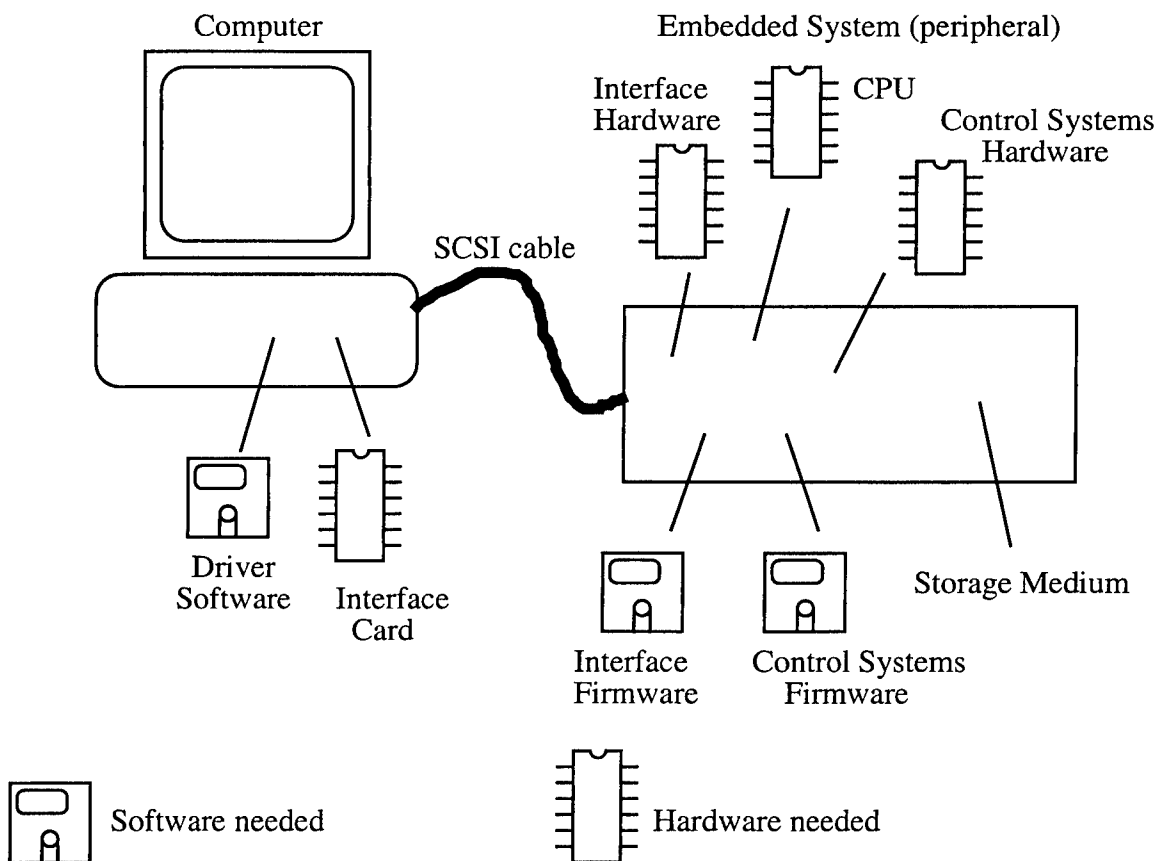


Fig 3.2.1: Block diagram of the components required for an advanced storage device.

42

The software items shown in the figure include a driver that resides on the host computer, interface firmware, and control systems firmware. The term firmware refers to software that resides on a read only chip, ROM, so once it is written it can not be changed. The hardware shown in the figure includes an interface board, interface hardware, a CPU, and control systems hardware. In the SCSI world, the host driver software is standard and should be the same for every removable medium storage device regardless of the manufacturer or storage technology. The interface card can either be plugged into the mother board of the host computer or integrated as part of the mother board. On the host side of the project, the items are relatively cheap and standardized, assuming a host computer is already available.

Most of the development occurs on the embedded systems side of the project. First dealing with the hardware, the interface hardware and CPU are referred to as the platform. The CPU is heart of the computer system, and is embedded on the peripheral. Common platforms are the Motorola 68k family, or the Intel 8051. The SCSI interface hardware consists of standard components designed specifically for interfacing purpose and are readily available for most platforms. Complete interface and embedded systems hardware packages can be purchased relatively cheaply as a single unit. The control systems hardware typically include power-type driving circuits (e.g., a laser driver) as much of the control is handled directly by the embedded system.

The software on the embedded system constitutes a major financial investment. For example, the development of a complete SCSI interface firmware requires two man-years of effort for a new platform from the ground up. As mentioned above, control systems software is also very complex—much of the timing and feedback control are left to the software.

### 3.2.1.1.1. Simplifications for the miniature prototype

A good portion of the control involved in the modular prototype is required for the spatial light modulator (SLM) and the CCD array or PDA devices. This complexity has been eliminated in our miniature prototype by making the paging laser and data laser project beams as opposed to pages or images. Of course this limits writing to one bit at a time, but is, nevertheless sufficient for the purposes of proof of priciple demonstration.

Because only one bit is written at a time, data rates are very slow. Therefore we do not need to use a high throughput interface such as SCSI and can use a simple serial interface. Also at such low data rates, our firmware platform can be simplified. A very simple Motorola 6800 device complete with serial interface hardware and firmware was chosen.

Every host computer has a serial interface complete with a serial driver. Therefore, by using this interface any host such as an Apple or IBM compatable PC can be used. The "driver" software produced is actually a communications program and not a

43

real driver. In other words, the drive does not appear as the "E:" drive, for example, to the host computer.

With respect to the optical design, creating paging and data beams (as opposed to pages or images) maximizes light intensity from the laser sources. Light intesity is a concern for the advanced prototype. Measurements derived from the miniature prototype have yielded acurate numbers from which to work when designing the paging and spatial light modulating systems. The sensitivity required for the CCD array or PDA is of concern, and again the measurements made using the simple prototype have yielded invaluable data required for an advanvced prototype design.

By incorporating these simplifications, the block diagram of the miniature prototype appears in the figure below.

Computer                                Embedded System (peripheral)

Interface Firmware, Hardware,
and CPU are included on                 Control Systems
68HC912EVB evaluation board             Hardware

Serial Cable

Serial interface
card included on
all computers                           Miniature optical
                                        table and
"Driver"                                Storage Medium
Software

Control Systems
Firmware
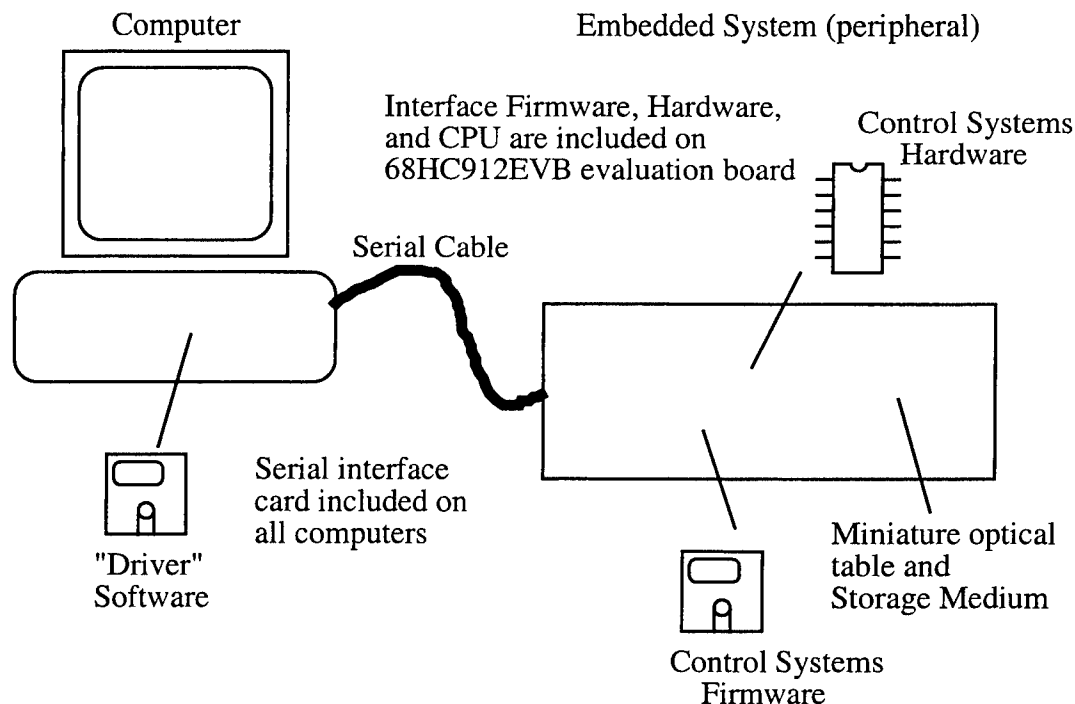
**Fig 3.2.2:** Block diagram of the components required for the simplified prototype.

The following text will describe the details to date of the design of each of the components shown in the figure above

### . 3.2.1.1.2. Driver Software

As previously mentioned, the driver for the first miniature prototype is not actually driver software, but a serial communications software program. The software has been developed in Real Basic so that it works in on both Apple and IBM compatible

44

computers. The implementation of actual driver software is much more complicated, and has not been developed for the miniature prototype. There is truly no value in producing this off the shelf software component until a device competitive with current hard disk technology is demonstrated.

### 3.2.1.1.3. Interface Firmware, Hardware, and CPU

The miniature prototype is implemented with a 68HC912EVB micro-controller card. This card is a 6800 based CPU with 32kbytes of embedded firmware known as Debug12. The evaluation board comes complete with serial interface firmware and hardware as well as much of the required control systems hardware. A user program of less than 768 bytes has been developed and is stored in on-chip EEPROM to make the system a completely bootable stand-alone device.

### 3.2.1.1.4. Control Hardware

As mentioned previously, much of the control hardware is contained on the embedded micro-controller itself. This includes all timing, analog output, and analog input circuitry. Remaining pieces of hardware were required to drive the blue Erase LEDs, control the cuvette temperature, move a neutral density filter in place for reading, as well as to implement the actual detection of the signal. Because the read signal is quite small, a special section on detector design is included in this report.

### 3.2.1.1.5. Miniature optical table

As an interface to the BR cuvette, a simple miniature optical table was made. The table was made on a quarter inch piece of aluminum, and was configured to move with the use of a stepper motor stage to implement the writing and reading of multiple bits. A layout of the optical components is shown in the figure below.

Silicon Photodiode

3cm square hole for bR cuvette holder

Blue LED

Movable dimming filter for Read operation

635 nm laser module

670 nm laser module

Screw terminal for electrical connections
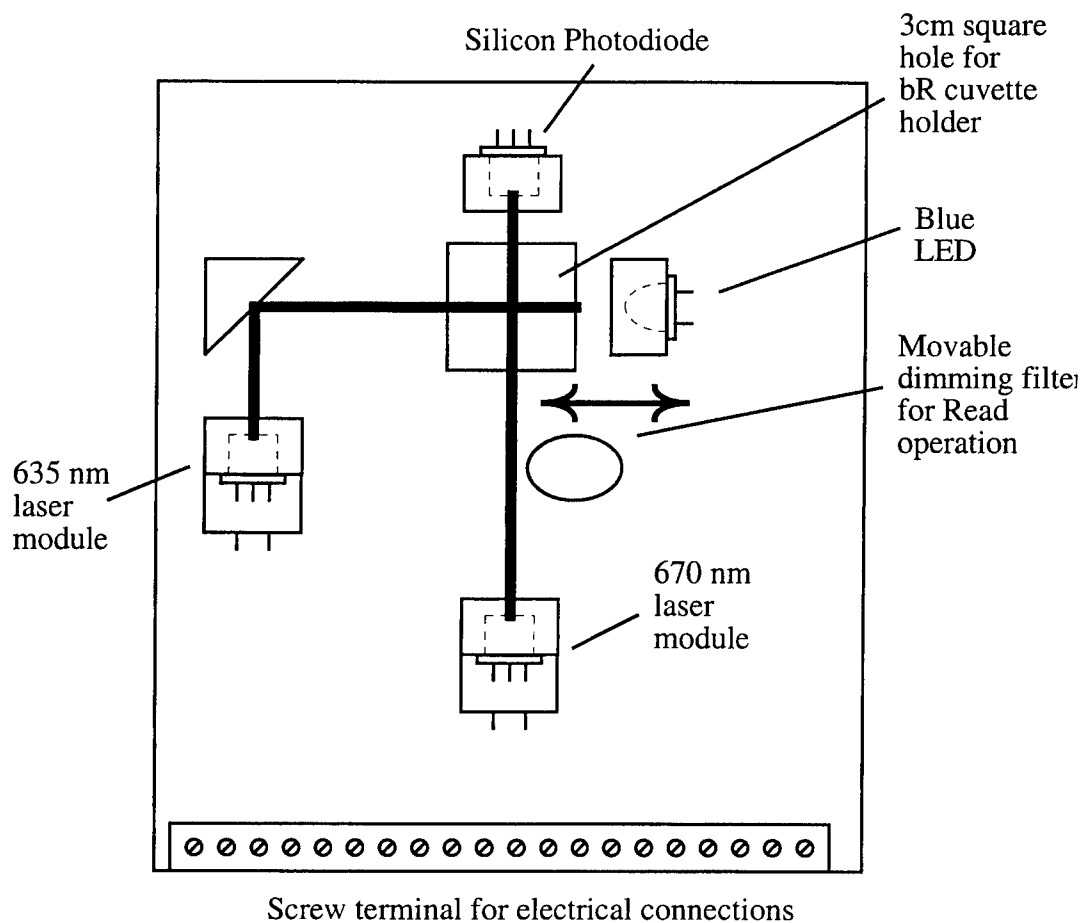
**Fig 3.2.3:** Block diagram for optical table installed in miniature prototype

### 3.2.1.2. Detector

In order to observe O-state, an optical detector is necessary that is sensitive enough to register a very small decrease in brightness of a very bright signal. The circuit shown below was used to operate the detector.
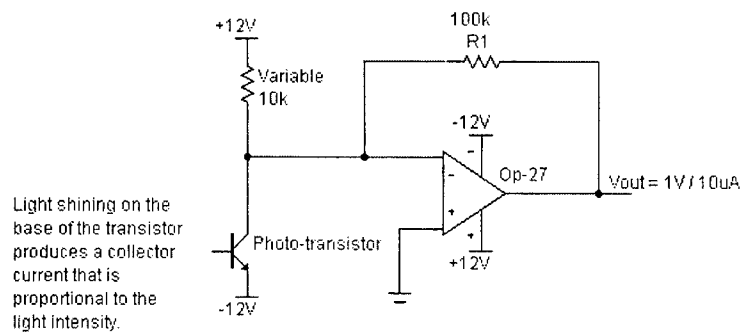
**Fig 3.2.4:** Initial design of optical detector, with manual light cancellation circuitry.

The light impinging on the detector produces a current. This current is supplied through the resistor from the positive power supply. Because the detector current is perfectly balanced by the resistor current, no current enters the amplifier. A slight decrease in light causes the detector current to decrease, while the resistor current remains the same. The excess current from the resistor now flows into the amplifier. Therefore, only changes in the light intensity will get amplified. The circuit is balanced so that when the 690nm writing laser is on, the output voltage is 5V. As the 690nm-laser light becomes slightly dimmer due to production of O-state, the voltage at the output will drop from 5V. The A/D converter in the computer can detect this signal and a time dependent variation of the absorption can be observed.

When the laser is on, the detector sinks about 6 milliamps of current. When the circuit is balanced we see approximately 20 microamps peak-peak of noise at the output at 120Hz, or about a 2V peak-peak signal. At this sensitivity level no noticeable change due to O-state absorbance was observed.

Improvements were made in the detector amplifier, primarily by replacing the phototransistor with a photodiode. The new detector achieved a sensitivity of 1V/100nA. The circuit still contains the feature for canceling background light (the laser light itself) while amplifying only changes in the light intensity. After calibrating with respect to the optical intensity of the laser, the amplifier produced 400 kilovolts/Watt change in optical intensity. With this improved sensitivity, the BR photocycle could be observed.

For the miniature prototype, the amplifier design was further improved to provide automatic zeroing of the output. This was accomplished with a feedback system, capable of canceling the photo-diode output current due to the read-laser shining on the detector. In order for the transient O-state signal to be measured, the response of the feedback amplifier had to be made slower than the signal. Although this technique works fine, the amplifier requires about 30 seconds to stabilize after the read laser was turned on. This amplifier, part of the x-y motorized miniature prototype, achieved a sensitivity of 4 Megavolts/Watt. A block diagram of this detector circuit is shown below.

**Block Diagram of Detector Circuit used in the Miniature Prototype**

Slow Integrator, cancels signals up to 1Hz.
settles in 30 seconds.

Σ

Signal Out

photo-diode
detector

A

Trans-impedence amplifier
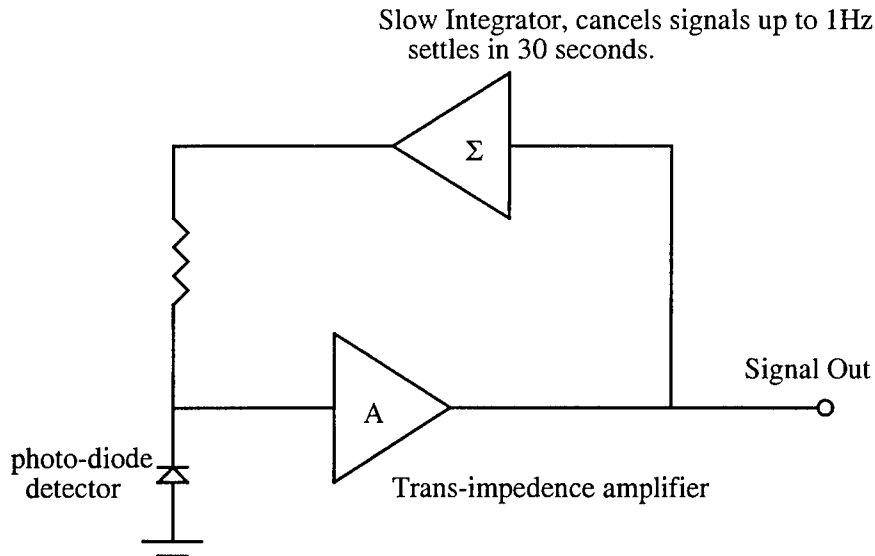
**Fig 3.2.5:** Block diagram of detector amplifier which automatically zeros the amplifier output.

Another problem with this detector system is that any change in laser light intensity is integrated and appears as an output signal. It was found in the miniature prototype that a small power glitch was caused by pulsing the page laser. This glitch modified the intensity of the read laser creating a pulse, which was integrated and appeared as a signal at the output of the device. Therefore, prior to upgrading to the final detector design, operation of the read laser had to switch to battery power.

Both the long-term stability issue and the requirement for battery operation of the laser have been eliminated by using a sample-and-hold technique in the feedback loop of the amplifier. To operate this amplifier, an additional digital Sample/Hold signal from the micro-controller needed to be programmed. A block diagram for the new detector circuit is shown below.

**Block Diagram of Final Detector Circuit used in screening systems**

Fast Integrator, cancels signals up to 1kHz.
settles in 3ms.

Sample and Hold Circuit

Σ

Signal Out

A

photo-diode
detector

Trans-impedence amplifier
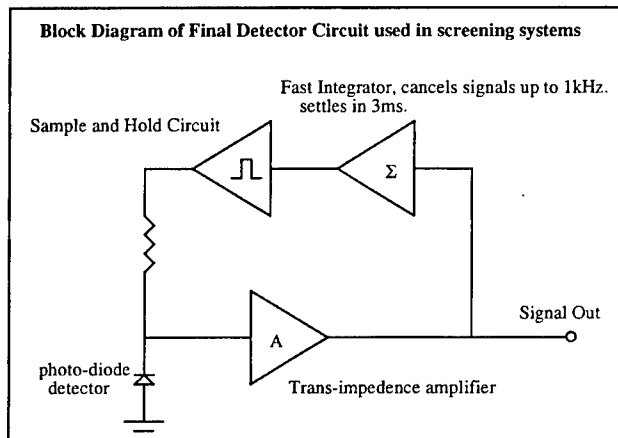
**Fig 3.2.6:** Block diagram of detector amplifier used in the screening apparatus. This detector achieves a sensitivity of 40 Megavolts/Watt.

The response time for the integrator portion of the feedback loop could now be decreased to 1ms. Although the feedback loop became unstable for faster response times, 1ms turned out to be adequate for this

48

application. The sample and hold circuit stabilizes in a matter of microseconds, and does not limit the amplifier response in any way. The response time for the detector amplifier has now been decreased from 30 seconds to 3ms, greatly speeding up the time required for the read process. The figure below shows the amplifier response for O-state in a BR cuvette. The data is the average of 16 read traces, a measurement that was completed in 3.8 seconds, as compared to over 30 seconds for one trace required by the previous detector.

RoomTemperature O-state Waveform for a BR cuvette using the new Sample-and-Hold detector
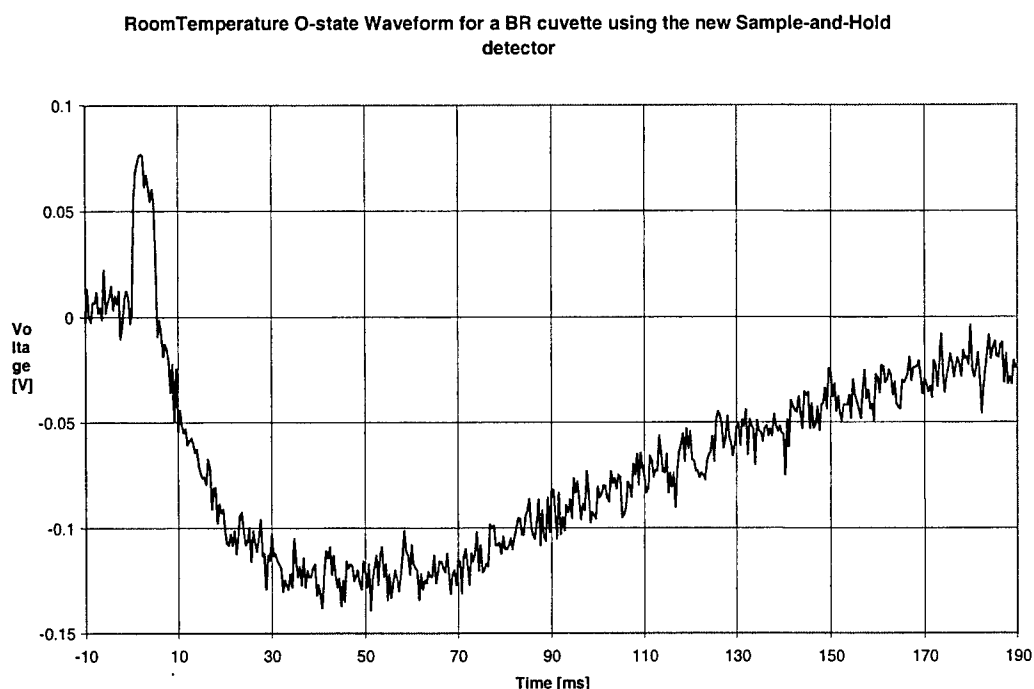


**Fig 3.2.7:** Output of S/H detector amplifier during a read of the BR signal. (In the screening apparatus 40 Megavolts/Watt is achieved by inverting and amplifying this output signal by a factor of 10 before A/D conversion.)

The second problem with the original detector was the requirement for battery operation. The figure below shows a measurement performed exactly as the one above, however the cuvette has been replaced by a blank cuvette (polyacrylamide gel only). It is evident that either scattered light or a power glitch has effected the read laser intensity during the page laser pulse. Although the pulse is present in the output waveform, once the page laser turns off the signal becomes completely flat. In the original detector the square pulse would have been integrated and would appear just like an O-state measurement. Extreme care was required in the previous system to eliminate this pulse so only the real signal would be amplified.

49

**RoomTemperature Blank Cuvette (PA Gel only) using the new Sample-and-Hold detector**

**Fig 3.2.8:** Output of S/H detector amplifier during a read of a blank
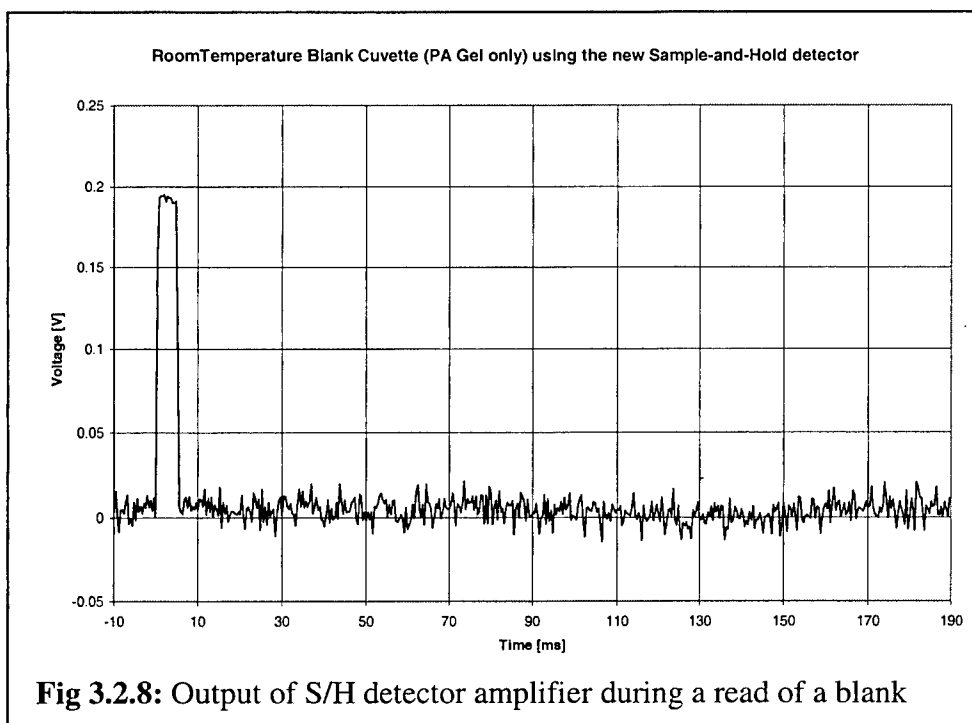
Just to see if the pulse was due to scattered light or to a power glitch, the page laser beam was blocked with an opaque shutter and the experiment was repeated. The result is shown in the figure below. The fact that the pulse is still present shows that it is again due to a power glitch, as well as a combination of scattered light. However the new detector was able to accurately distinguish the difference between the BR cuvette and a blank cuvette even in the presence of the intensity glitch, something the original detector could not do.

To better understand the new detector, an attempt was made to read with just one page pulse and no averages. However, the results indicated that allowing only 3ms for stabilization of the data laser was not sufficient. (In the above figures, which are averages of 16 traces, the first trace is completely ambiguous and only averaging produces the signal.) Although the new detector amplifier is ready in 3ms, the laser itself is not stable enough to perform the read operation. The time allowed for laser stabilization was slowly increased and it was discovered that approximately one half to one second is required before the laser is stable enough to do a read operation. This indicates that the amplifier is now much faster than the laser. The ultimate sensitivity achieved using this new type of detector was 40 Megavolts/Watt change in optical light intensity. Using this extreme sensitivity, the wild-type BR photocycle at 690nm can be completely resolved with 8 bit resolution.

50

**RoomTemperature Blank Cuvette with Page Laser Blocked, using the new Sample-and-Hold detector**

**Fig 3.2.9:** Output of S/H detector amplifier during a read cycle with the incident laser beam blocked. The spike is due a power glitch that occurs while pulsing the page laser.
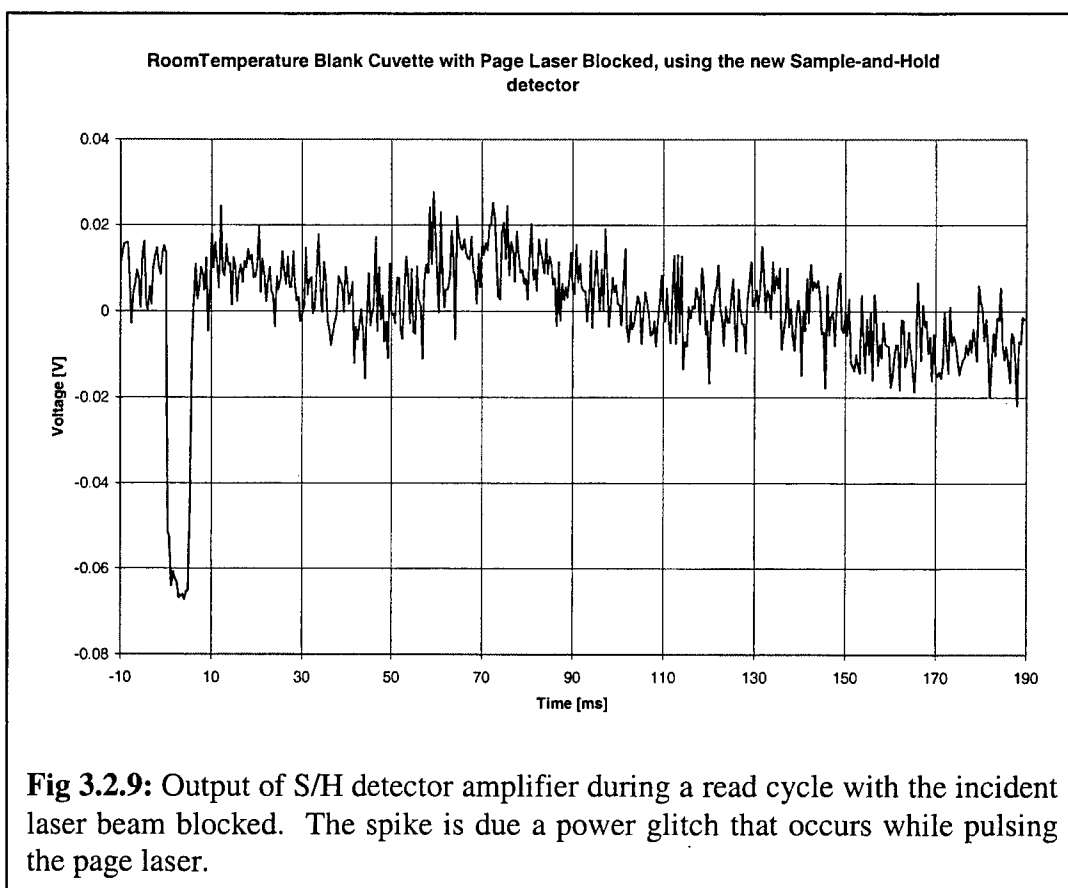
### 3.2.1.3. Motorized System for miniature prototype

The drawing below shows a block diagram of a complete miniature prototype that has been produced as part of this research effort.

The external connections to the prototype include a computer, two power supplies, and an oscilloscope. The standard connections for a typical external drive are the computer and small power supply. It was necessary to include a high current power supply because the heater requires about 2.5A at 12V and the each stepper requires about 0.75A at 5V. Connections to an oscilloscope, mainly for debugging purposes, have also been included.

Inside the memory, there is an electronics section with four circuit boards. The micro-controller is the M32HC912EVB. The three remaining boards have been hand-made in-house. Each has a set of wires connected to the micro-controller and performs a different function within the memory as detailed in the drawing. In a more advanced system, many of these functions would either be programmed into software using a more sophisticated micro-controller or programmed into integrated circuits yielding a very compact system with only a couple of IC's.
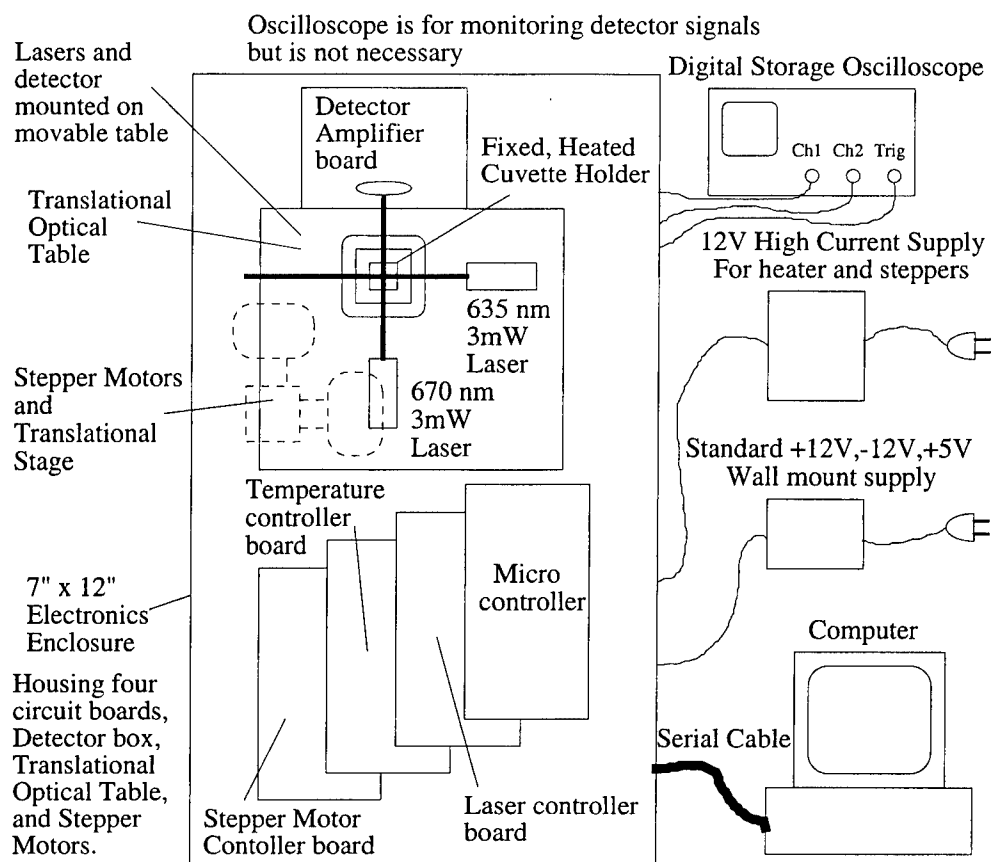
**Fig 3.2.10:** Block diagram of the miniature prototype.

Two stepper motors have been set up with a translational stage in order to move the optical table in both the X and Y directions. This motion control has allowed testing of the memory architecture concerning reading and writing bits along both the paging and data laser axes. A miniature optical table with a full range of motion in two dimensions under stepper control is mounted on top of the translational stage. The lasers and detector module are mounted on this optical table, as are all of the optical components so that alignment has to be performed only once. The lasers are both from LaserMate and are only 3mW; however they have integrated focusing lenses so the beam diameter is set to about 0.3mm x 0.5mm. The laser modules also have an intensity control signal, so that a read operation is performed by optically dimming the laser module as opposed to inserting a neutral density filter in the optical path.

The cuvette holder is a fixed unit complete with a heater and temperature sensor. The optical table moves about the holder allowing intersecting laser light to impinge on different points within the data cuvette. The holder is tall enough to stick through the cover of the electrical enclosure, allowing the cuvette to be added and removed from the device just like a disk in a disk drive.

### 3.2.1.4. Screening System

A very important piece of equipment required for improving the material is a standardized screening system. This will be a key device in implementing random mutagenesis (as part of the subsequent research effort). The screening system is a simplified version of the x-y miniature prototype. To screen for an optimal protein (BR variant), all that must be accomplished is to measure the rate at which writing occurs in the material, in addition to verifying that the photochemistry is branched. A block diagram of the screening system fabricated is shown below.
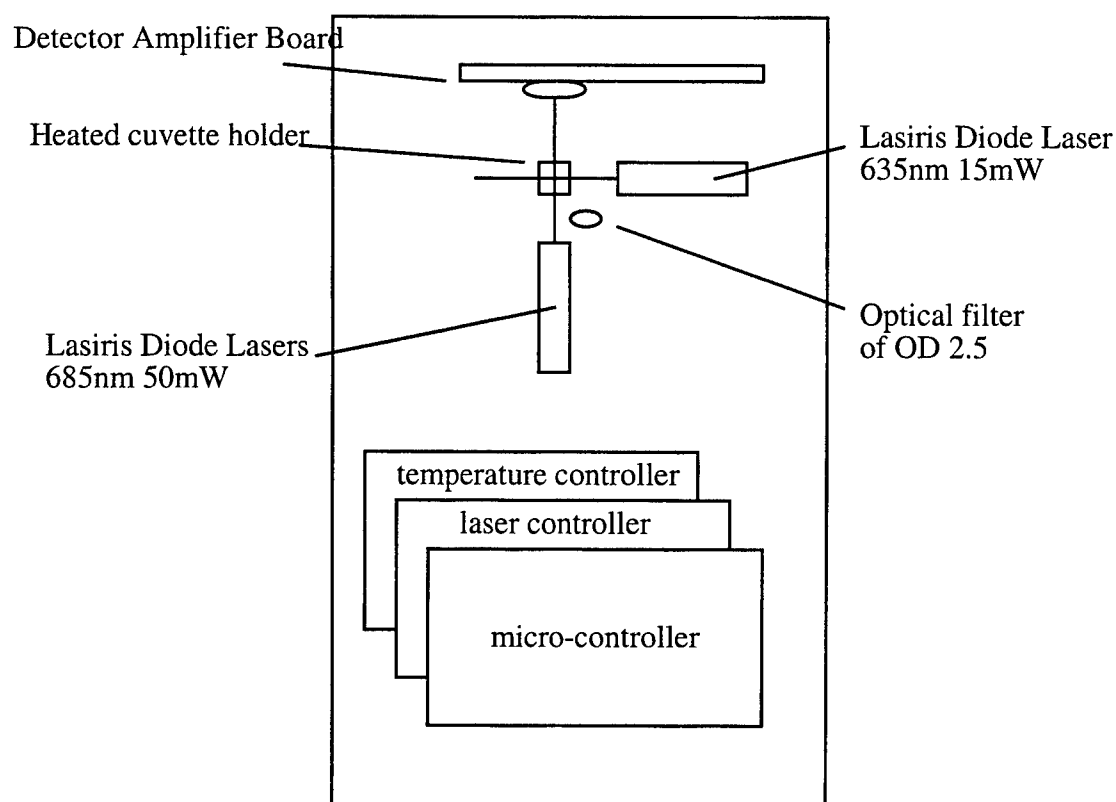


**Fig 3.2.11:** Block diagram of screening system that will be used for material improvement. Two such systems have been fabricated.

As a higher throughput of screened BR variants is needed, additional identical systems can be added to the PC. Up to four of these devices could be easily connected to one PC. For each cuvette screened, an estimate of about one milligram of protein should be required. Two such devices have been manufactured so that screening of cuvettes can take place in parallel.

### 3.2.2. Measurements

### 3.2.2.1. O-state Measurements (Reading)

The three-dimensional read procedure is a simple monochromatic time resolved spectrometer problem (a simple pulse-probe experiment). The first successful measurements using the miniature prototype are described below. A cuvette was prepared using a buffer solution to keep the pH at 6.5. The optical density of the cuvette at 568nm was 2.8. Although the amplifier outputs a voltage, the measured optical intensity can be calculated based on the sensitivity described above and the background cancellation current. The figure below shows the optical intensity as a function of time. To make this measurement the 690nm laser is left on continuously, while the 635nm laser is pulsed.

**Photo-production the O-intermediate observed at 690nm**
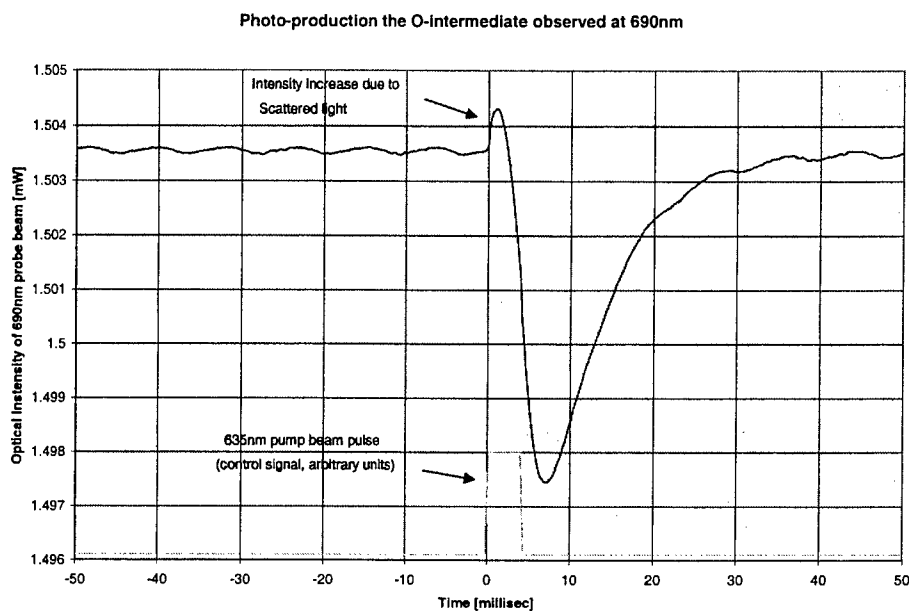


**Fig 3.2.12:** An amplifier output waveform that has been calibrated to demonstrate light intensity observed at the detector.

It is interesting to note that the detected signal represents a change of only 0.40% in the brightness of the laser light passing through the cuvette. The laser module actually has instabilities greater than the measured signal, and therefore an average of 64 measurements of the waveform is required to cancel this instability. In comparison, the stability of the 635nm Lasiris Module was tested and determined to be superior to the 690nm Power Technology Module. Laser stability is not considered to be a great problem because a differential detector and an integrating measurement system can be used to eliminate stability noise. The figure above was produced using a digital storage scope for data presentation; however, the peripheral itself is configured to make this measurement using the A/D converter. Automated data acquisition enables the collection

of data for temperature and pH dependent analysis of the O-state photo-products of BR and its mutants.

Through analysis of the above data it is possible to predict the amount of O-state formed in the cuvette as a percentage of the total BR concentration. Consider the geometry shown below.

Cuvette with bR in a poly acrilimide gel



690nm Probe Beam
1.504mW Intensity
Transmission = 49.03%
OD = 0.3096

5mm

690nm Probe Beam
Incident Intensity 3.068mW
(Determined from Spectrometer data)

with production of O-state
this reduces to 1.498mW
Transmission = 48.83%
OD = 0.3113

635nm Paging Beam
(in and out of page)
Estimated to be 0.3W/cm^2

10mm
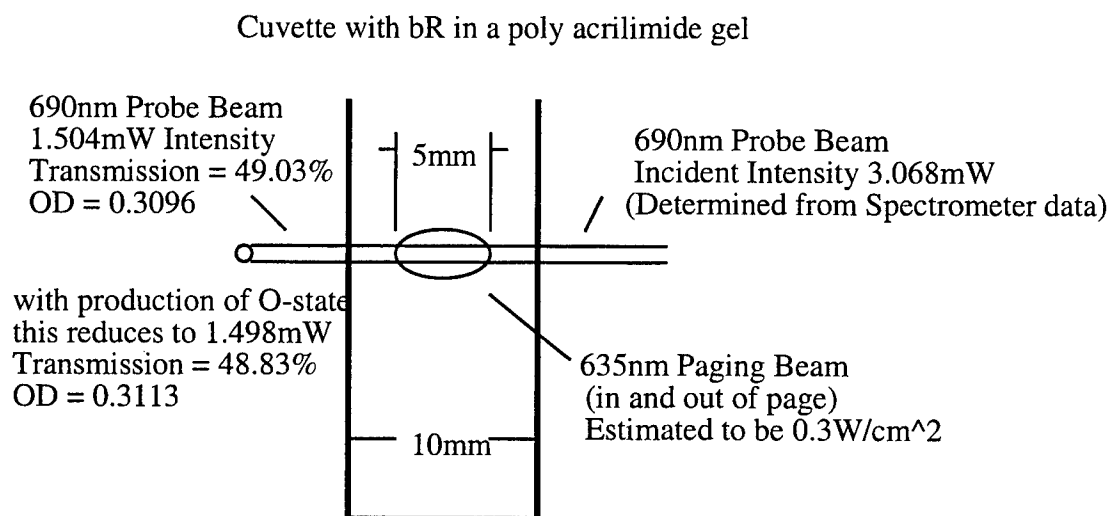
**Fig 3.2.13:** Geometry of laser pulses impinging on cuvette for the data shown in the previous figure.

Data in the figure above is shown out to four decimal places; despite the fact that only difference data was recorded, the absolute magnitudes are given as an indication of scale. Spectrometer data was used to calculate the incident intensity of the probe beam. The actual measured value was very close to the 3mW listed, reduced from the 20mW laser power due the aperture in the system. The optical density of the cuvette was measured to be 0.3096 at 690nm with the spectrometer. The production of O-state increases the optical density to 0.3113. The optical density of a blank was also recorded, in the form of a cuvette prepared without protein (i.e., polyacrylamide only). Subtracting the blank and dividing by 2 to account for a 5mm paging beam, an optical density of 0.0444 due to BR within the doubly-irradiated region was determined, which increases to 0.0461 when O-state is produced. Analysis shows us that 0.21% of the BR material was converted to O-state.

### 3.2.2.1.1. Temperature dependent O-state measurements

Using the same cuvette and system as described above, temperature dependent O-state measurements were produced. At the optical density of the cuvette an amplifier decrease of 1V corresponds to about 0.15% of the BR converted to the O-state. The figure below shows the amplifier output voltage as a function of temperature. The 635nm pulse starts at time=0 and has a width of 2 ms.



**Detector output voltage for 690nm Laser (Measured)**
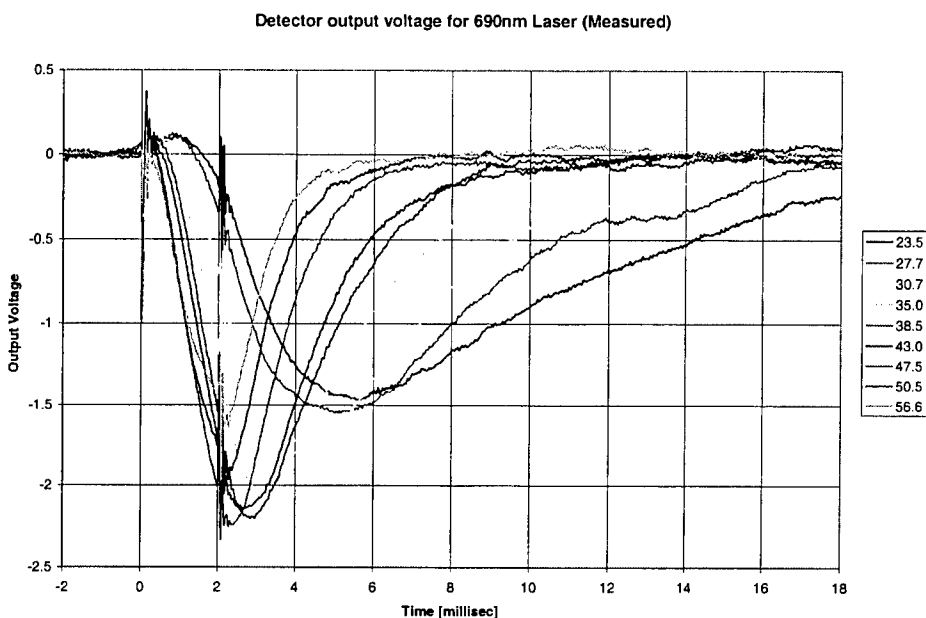
**Fig 3.2.14:** Temperature dependent O-state curves measured with an early version of the miniature prototype.

### 3.2.2.2. P-state Measurements (Writing)

The first measurements of the formation of the P-state were discovered somewhat by accident. It takes conditions of both relatively high temperature and relatively high pH to increase the rate of formation of the P-state to where it can be observed in a reasonable amount of time. The first observation of P & Q were serendipitous; during testing of the temperature circuitry, a laser was left shining on a sample. It was found that a single wavelength of laser light that overlaps both the bR and O-intermediate spectral states can be used to form the P-state. In addition, as the P-state forms, the purple (red absorbing) bR is converted to the yellow (red transmitting) P-state photoproduct. Therefore, by simply shining a red laser on the cuvette and monitoring the intensity of light transmitted, one can observe the formation of P-state in real time. The material that forms the P-state the fastest should be the best candidate for the memory. Note that this process will not form the photoproduct in an isolated three dimensional

location; this process generates P only along the axis of irradiation and is therefore strictly two-dimensional.

The figure below shows the procedure attempted on a cuvette of wild type BR at 40C.
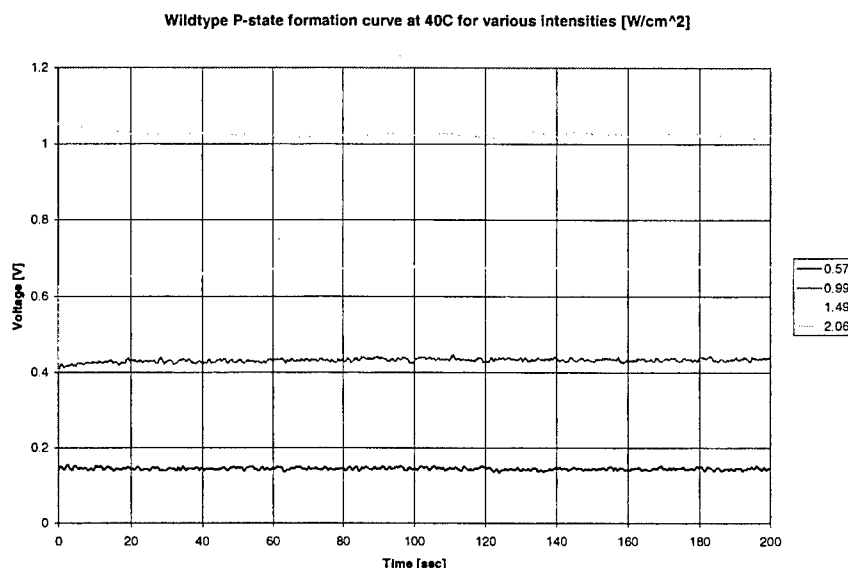


**Fig 3.2.15:** Light intensity transmission through a wild type cuvette under continuous illumination at 40C as a function of time.

The figure shows no signs of P-state formation. The digital oscilloscope sampling system could only acquire data for a maximum of 200 seconds. However, when the protein cuvette was exposed for much longer times (on the order of 10-20 minutes) a yellow hole was "drilled through the cuvette". This means in order to take data for wild type protein at these intensities longer sampling periods would be required.

The figures below show the same procedure at 40C carried out on protein gels made from the mutants F208N and E194Q respectively. The gels were made in a manner identical to that described previously and buffered at a pH of 6.5.

**F208N P-state formation curve at 40C for various intensities [W/cm^2]**
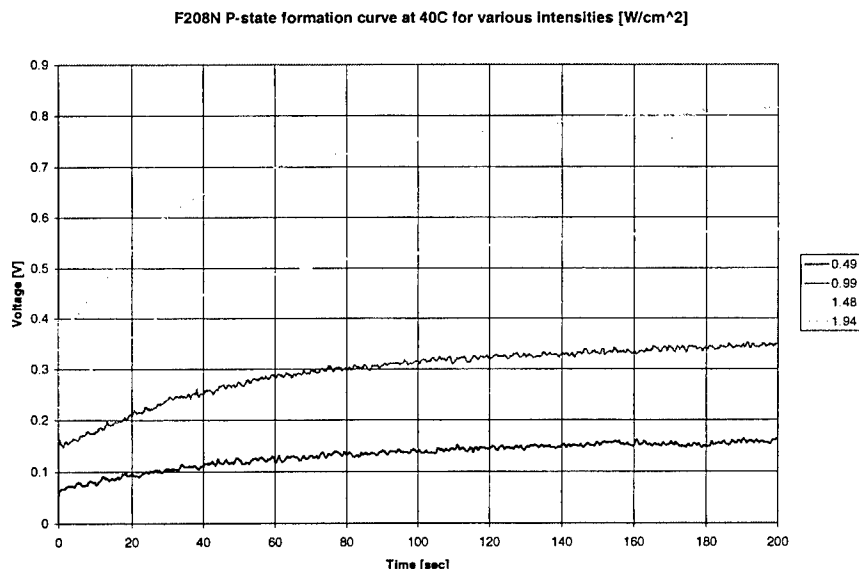


**Fig 3.2.16:** Light intensity transmission through a F208N cuvette under continuous illumination at 40C as a function of time.

**E194Q P-state formation curve at 40C for various intensities [W/cm^2]**
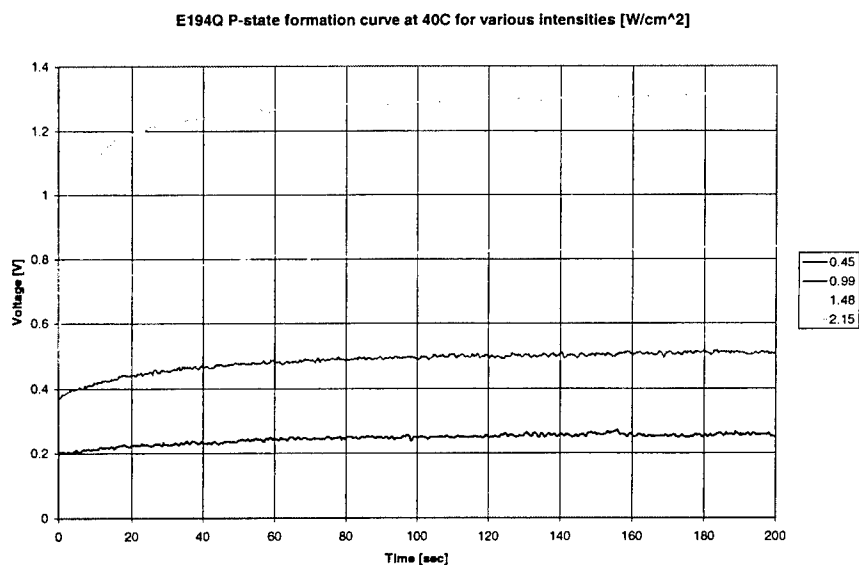


**Fig 3.2.17:** Light intensity transmission through a E194Q cuvette under continuous illumination at 40C as a function of time.

Both of the genetically-engineered proteins (mutants) showed an increase in transmission of the laser beam within the 200 second sampling time. The increase in transmission appears to be dominated by a simple first order photo-reaction. In other words, an exponentially decaying conversion process is responsible for the photochemical conversion. The time constant should be mostly related to the O to P reaction. The actual analysis of the curve is quite complex because all the photo-

58

intermediates are present in the illuminated sample and slowly decay in a quasi-steady state manner, and the optically dilute approximation for first order kinetics cannot be made because of the high optical density of the cuvette.

However, if we assume a simple first order process, a time constant can be determined for each of the curves. The time constants are shown in the figure below. The E194Q mutant has the fastest time constant and therefore should be a better candidate for an optical memory storage medium. Several other mutant proteins still remain to be tested.
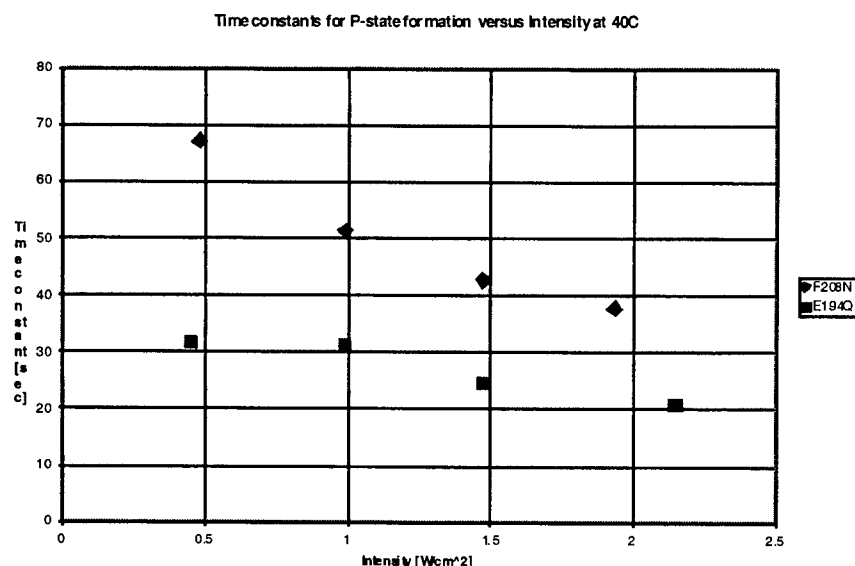


**Fig 3.2.18:** Time constants for F208N and E194Q associated with the rate of rise in optical transmission taken from the two previous figures.

### 3.2.2.2.1. Three-dimensional formation of the P-state photoproduct

It was determined that if the sample was exposed to continued laser irradiation at elevated temperatures, a yellow photoproduct would appear at the exposed location. Encouraged that this was possibly due to production of the P-state, experiments were designed to demonstrate two things: (1) the yellow photo-product could be formed as a volume element suspended completely inside the cuvette, and (2) that the yellow photo-product was due to a branched photo-cycle.

In order to suspend a bit in the middle of the cube, the assumption was made that it was necessary to first flash the paging 635 nm laser and then flash the writing 690 nm laser. The controller was programmed to perform this flash-flash sequence continuously.

The pulse width was set to 0.5 ms for each laser with the flash sequence repeated every 8ms (corresponding to a duty cycle of 6.25%). With gel equilibrated at 40°C, the flash-flash sequence was exposed to the sample overnight. By morning, definite yellow spot contained completely inside the cuvette was visible. In order to obtain more quantitative results, a read operation needed to be performed on the bit (voxel) while it is being written. Unfortunately, the read operation requires continuous exposure to the 690 nm laser, corresponding to a very long writing time(due to the small duty cycle). However, it was determined that the yellow photo-product would change the absolute transmission of the 690nm laser beam. Therefore, the 690 nm laser pulses could be monitored during the write process using the photo-detector to observe the drift in the absolute intensity reaching the detector as P-state was formed. (The detector used for this experiment had manual light cancellation as described above.) The figure below shows the 690 nm laser pulses measured with the detector at various times during the write procedure. The "ringing" in the waveforms is due to the "power on" transient of the laser light controller. However, despite this fact, a definite increase in the average value of these waveforms can be observed, due to increased optical transmission.
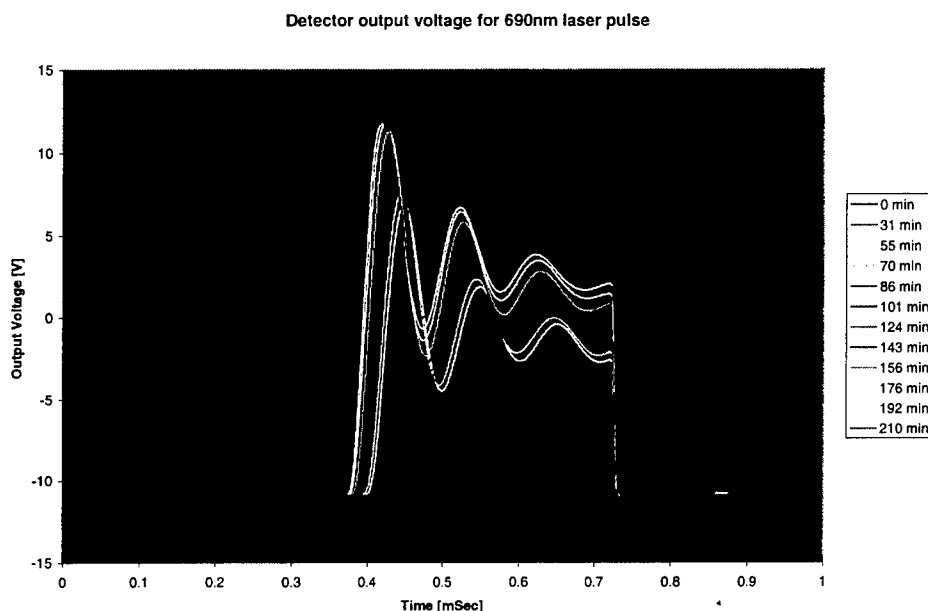


**Fig 3.2.19:** Write laser pulse observed by the detector circuit with manual light cancellation circuitry. The increase in the average value of the detector output voltage is due to increased transmission caused by formation of the yellow P-state photoproduct during the write process.

To monitor the amount of photo-product produced as a function of time, the average value of the waveforms shown in the figure above can be plotted as a function of time. In order to show that this photo-product is produced from a branch out of the main photocycle, the experiment was repeated flashing both lasers simultaneously. Because both lasers are used, the same exact number of photons will enter the bit volume under both the sequential and simultaneous flash experiments. However, because less O-state is produced when the lasers are on simultaneously, the amount of P-state produced should decrease if it is due to the branching reaction. The figure below shows the average voltage from the pulsed waveforms for both experiments. Clearly the slope on the simultaneous flash experiment is less than the slope on the sequential flash experiment, proving the existence of the branched photo-cycle and confirmation of P-state production.

**Amount of yellow photo-product produced versus time as measured by 690nm transmission**
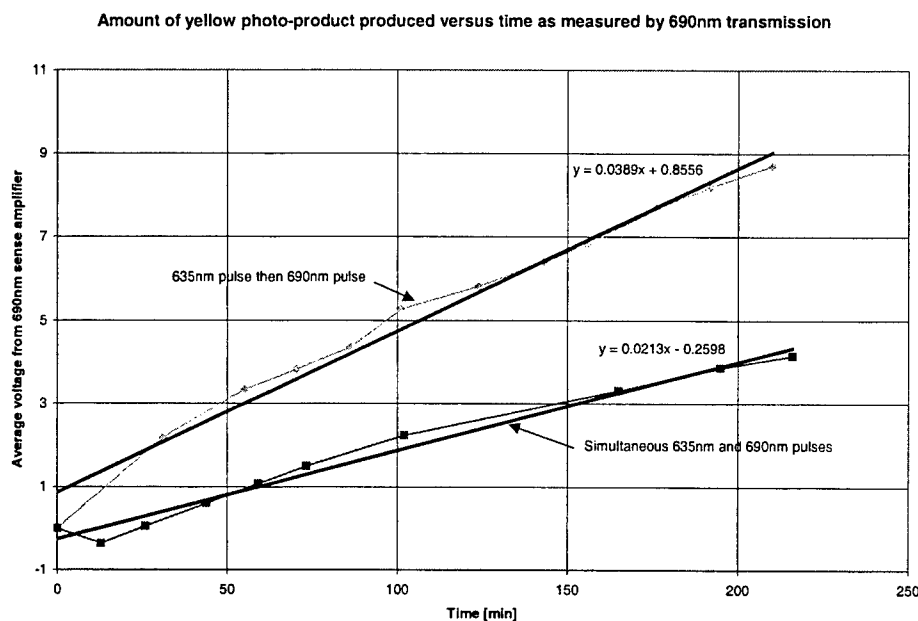


**Fig 3.2.20:** Average voltage plotted as a function of time during the write process for both the flash-delay-flash experiment and the simultaneous flash experiment. Faster formation of the P-state photoproduct for the flash-flash experiment confirms branched photochemistry.

### 3.2.2.3. Exposure Curves (Read, Write, Erase)

The integral of the O-state curves described in Section 2.1 are used as a measure of the amount of protein within an irradiated volume that is photo-cycling. An "exposure curve" is generated by first measuring and recording this integral. A write procedure is then performed for a fixed amount of time (Usually 2-5 minutes), which is then followed by another measure of the O-state integral. As protein is converted to the P and Q states, less BR is available for photocycling, indicating that the integral will decrease as a

61

function of time. The rate of formation of the P-state photoproduct can be measured for both the sequential flash or a simultaneous flash writing operations,

The exposure curve can be interpreted as a performance curve for the screening process. Enhanced O→P conversion efficiency is an important factor for improving the protein, but can not be detected using simple O-state screening. This means that the exposure curve is the most appropriate screening technique for determining the best protein. Experimentally, this curve uses a true volumetric read procedure, just as will be used in the functional memory. The figure below shows the first measured exposure curve and the difference in the rate of formation of P-state photoproducts for both the sequential flash and simultaneous flash experiments.



**Percentage of WT BR converted to the P/Q-state determined through measuring the integral of the O-state at 46C**
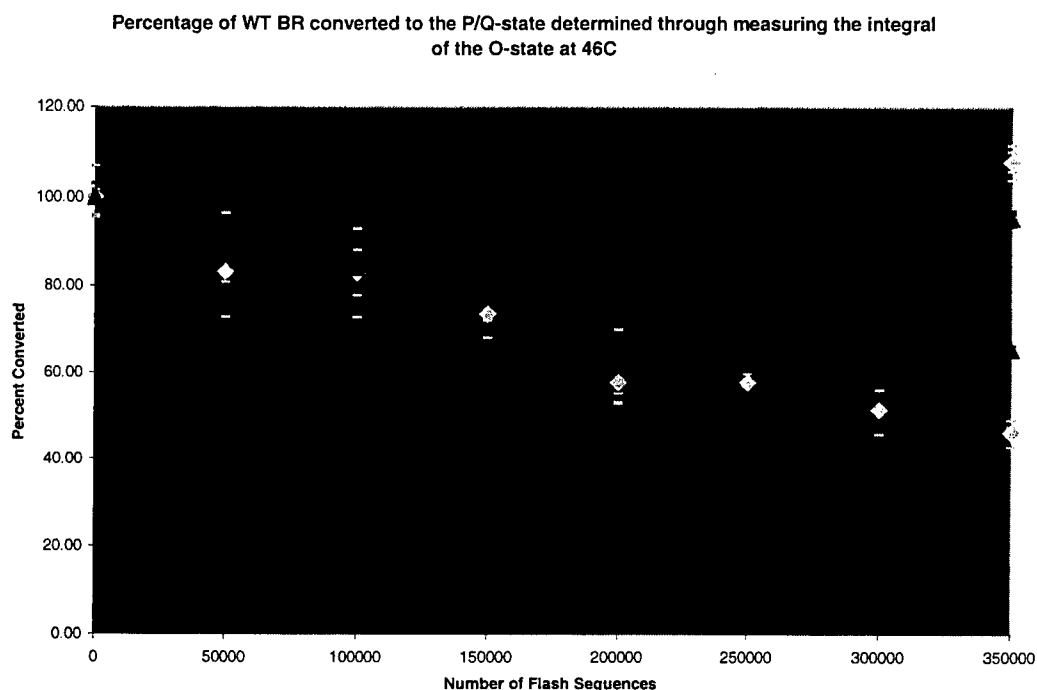
**Fig 3.2.21:** First experimentally measured exposure curve, proving the existence of branched photochemistry using the true volumetric reading procedure.

The first automated measurement of the exposure curve, shown below, has enough resolution to show that a first-order type photochemistry results from both the sequential flash and simultaneous flash exposures. Here, the x-axis has been represented in real time as opposed to the number of flashes. This method of presenting the data will create a more accurate comparison for proteins with varying time constants. Because the data is represented with time on the x-axis, an exponential fit and resulting time constant can be made for the data. The screening effort can simply compare the time constant of formation to determine the best cube.

**Integral of O-state versus time for writing Wildtype BR at 40C**
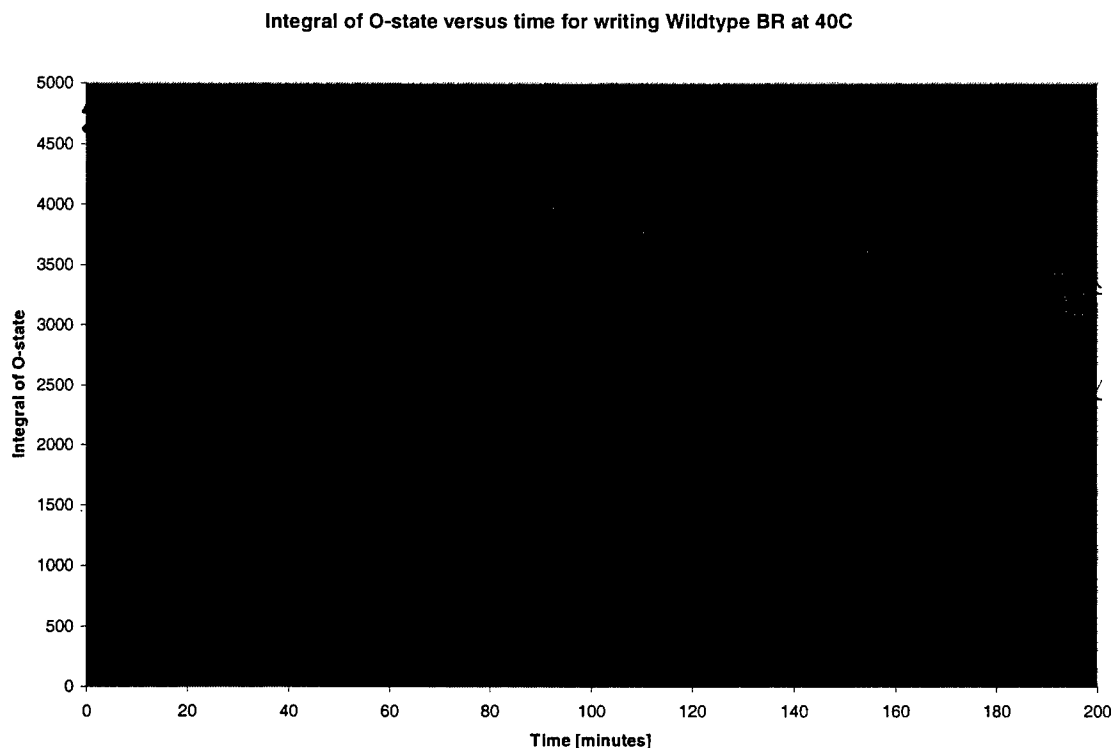


**Fig 3.2.22:** First automated exposure curve for wild-type protein.

Measurements were also made for one of the long O-state mutant proteins, E204Q. The preliminary result, shown below, produces no difference in the time constant between the sequential flash and simultaneous flash experiment. This result means the mutant E204Q will not be a candidate for the volumetric memory project, although the yellow photo-product forms by about a factor of ten faster than wild-type protein. Of course the duty cycle when operating E204Q for branched operation is very low (about 1:200, on:off). If one is not concerned with branched photo-chemistry and the duty cycle is made continuous, the yellow photo-product forms in a very short time (seconds), which may make E204Q an important candidate for a permanent, yet erasable, holographic medium.

**Integral of O-state versus time for writing Mutant E204Q BR at 40C**
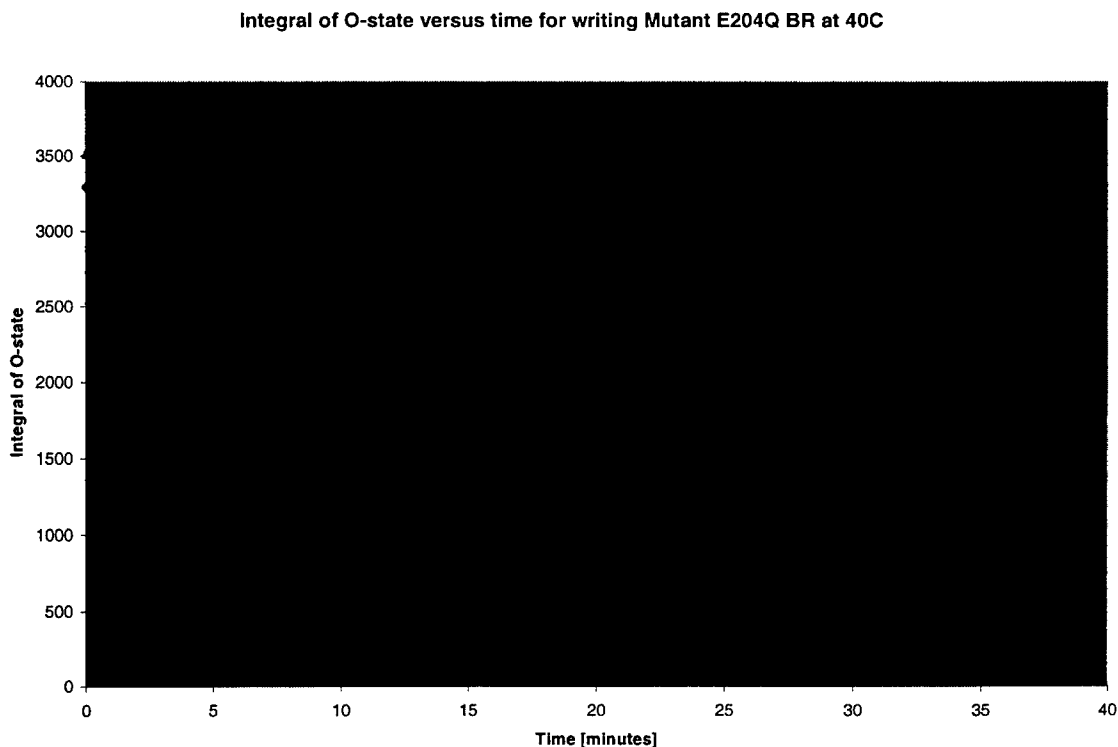
**Fig 3.2.23:** Automated exposure curve for the mutant E204Q. The results show that the photochemistry from E204Q is not branched.

The final exposure curve shown below was made possible by installing two 470nm blue LEDs aimed at the intersection point of the paging laser and the data laser. The operation of the LEDs is controlled automatically by the prototype system. For the first experiment evaluating the ability of the LEDs to erase data, a bit was written for 150 minutes and then erased for 450 minutes. Every five minutes during the procedure a read cycle was performed to determine the integral of the O-state. The cuvette was kept at 40C during the entire duration of the experiment (80 hours), with the write/erase cycle repeated 8 times. The screening effort will consist of producing these exposure erase curves for each mutant. Note with the capability of automatic erasure, the simultaneous flash and sequential flash experiments can be carried out many times in an overnight run.

**Write/Erase Cycles of WT BR at 40C (Write 150min, Erase 450min)**
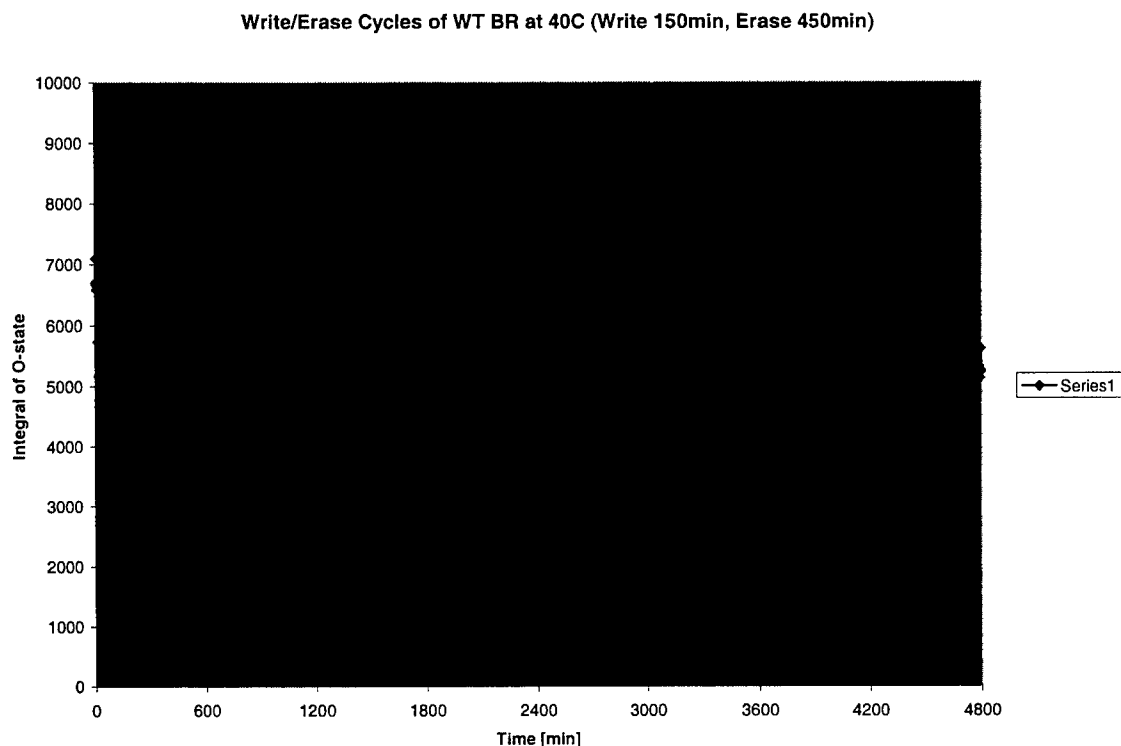
**Fig 3.2.24:** Automated exposure curve and erase measured eight time on the same point.

It is evident from the figure that the LEDs can perform the erase cycle completely in 90 minutes. However, there seems to be some BR that eventually enters a state that cannot be restored to functioning protein. A concern developed that this could be due to the different absorption bands of the P intermediate and the Q intermediate. The Q-state has a deeper blue absorption band and it is possible that the 470nm LEDs do not return this photoproduct completely back to the BR resting state. At present, 430nm diodes are used in the prototype, which appears to minimize the this problem.

### 3.2.2.4. Position Dependent Measurements (Verification of 3D Memory)

In order to prove that three-dimensional reading can be performed, data must be written and read in more than one location. A quick test of this process was accomplished by moving the translational stage by hand before the stepper motors were attached. The experiment tested the ability to distinguish binary "1" and "0" data along the paging laser. The experiment started by ensuring that the cuvette was completely erased, followed by a read operation at three locations along the paging laser axis. The cuvette was then moved to the middle position to perform the write operation. Upon completion, the cuvette was returned to the same three locations for read operations. The figure below shows the six photocycle O-state traces that resulted from this experiment. The cuvette of F208N mutant protein was held at 40C during the experiment.
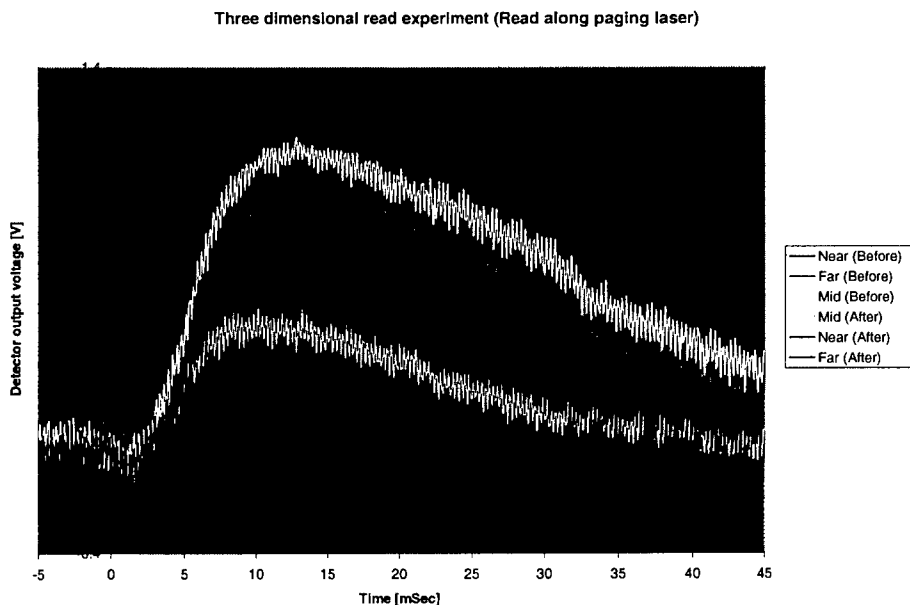
**Fig 3.2.25:** Position dependent measurements of the O-state photoproduct before and after writing.

There are several interesting details visible in this data. The terms Near, Mid, and Far, in the legend refer to the location of the bit relative to the direction of the paging laser. Before and After refer to when the data was taken in relation to the write operation. Notice that the magnitude of the response before the write decreases as the location is moved farther away from the paging laser. This is expected to be due to absorption of the paging beam as it passes through the cuvette.

Also note that after the write operation, the magnitude of the response at all locations is diminished. The write operation consisted of a 5 millisec paging pulse repeated every 50 millisec., with the 5 millisec data laser flash delayed by 5 millisec following the paging laser. The duration of the total write operation was 1 hour (72000 cycles). Under these conditions the paging laser is on while a significant amount of O-state is present, causing the paging laser alone to perform the write operation. If the paging pulse duration was decreased and the duty cycle increased to reduce this effect, the time required to write a bit would increase significantly. Methods to improve the difference between a "0" and a "1" bit include increasing the paging laser intensity and using a mutant with a shorter O-state lifetime. The read operation was performed with the data laser set at an intensity of a factor of 10 lower than during the write operation. For the experiment described in the figure, a magnitude discriminator of 0.5 Volts was used to distinguish between a binary "0" and "1" bit.

### 3.2.2.4.1. Contour Plot of a bit (Integral of O-state versus position)

After the exposure curve above was made, the gel was returned to the miniature prototype and a position dependent x-y map of the integral of the O-state was measured.

66

The figure below shows the normalized data for the F208N mutant cuvette displayed as a contour plot. The data has been inverted to facilitate viewing (i.e., a post is easier to see than a hole in a contour plot). The data has also been spatially filtered, first by a low pass filter, followed by a high pass filter (for data smoothing to eliminate surface noise).

The bit written in the center of the cuvette along with a small "channels" of unwanted photochemistry along both the paging laser axis (minor) and the data laser axis (major ridge). The data laser has caused much more writing in the "O" portion of the data axis due to the fact that it was continuously operated during the entire read operation, in order to complete the exposure curve.



**x-y Map of F208N cuvette after previous exposure curve**
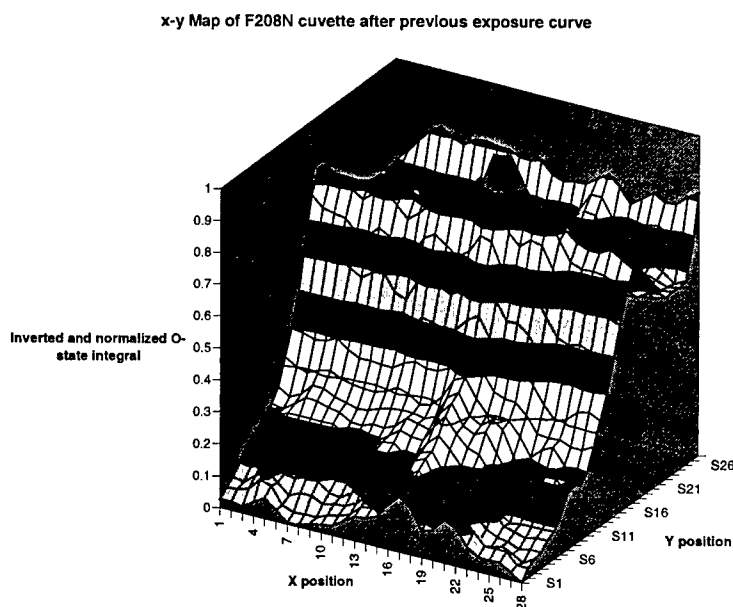
**Fig 3.2.26:** Contour plot showing the formation of a bit selectively at the intersection of two laser beams. The z-axis data was measured using a true three-dimensional read.

### 3.2.3. Modeling

As a parallel research effort Real Basic program was written for the purposes of modeling the BR photocycle. It included all of the optical time constants, efficiencies, and temperature-dependent thermal time constants required to model the transient production of intermediate states of the BR photo-cycle. A fourth order Runge-Kutta subroutine in this program is used to approximate the solution to the coupled system of rate equations, which describe the BR photocycle. All of the relevant terms included in the rate equations are qualitatively illustrated in the figure below.

67
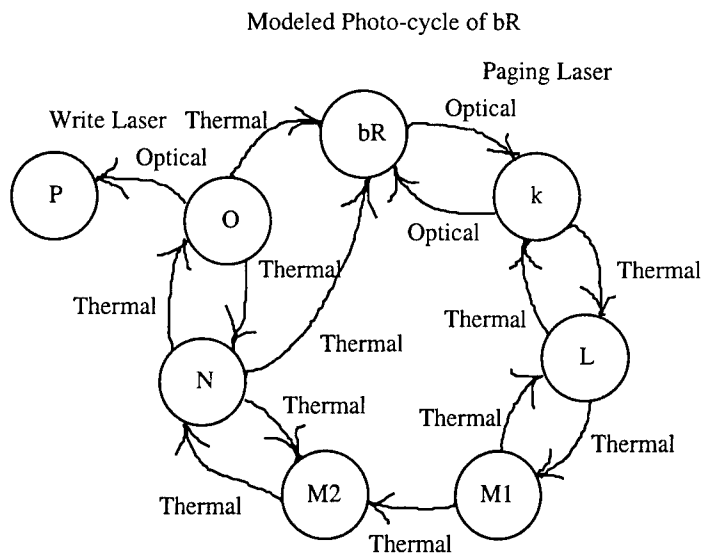
**Fig 3.2.27:** State diagram for the photocycle of BR. Each branch represents a first order rate equation. Modeling the population in each state requires a coupled solution of all the rate equations.

The goal of this phase of the project was to model the BR photocycle in order to more fully understand the results of the observed production of the O-state described in the previous section. With the input variables set as close as possible to the conditions used in the experiment, the simulation predicts that about 1.5% of the BR should be converted to O-state. Recall that experimentally only 0.21% conversion was observed. This order of magnitude error is most probably due to diminished intensity in a real experiment due to reflection, absorbance in the gel, and scattering, none of which are accounted for by the program.

By incorporating the geometry of the experiment and the gain of the amplifier, the model was capable of producing the amplifier voltage as a function of time. To make the model match the measured result, the modeled intensity of the 635nm laser was varied until the peak magnitude of the room temperature response matched that of the model. This match occurred with a laser intensity of $30mW/cm^2$. The estimated intensity of the actual laser is about $300mW/cm^2$. (This is the factor of ten discrepancy described above.) The figure below shows the modeled amplifier output as a function of temperature.

Detector output voltage for 690nm Laser (Model)
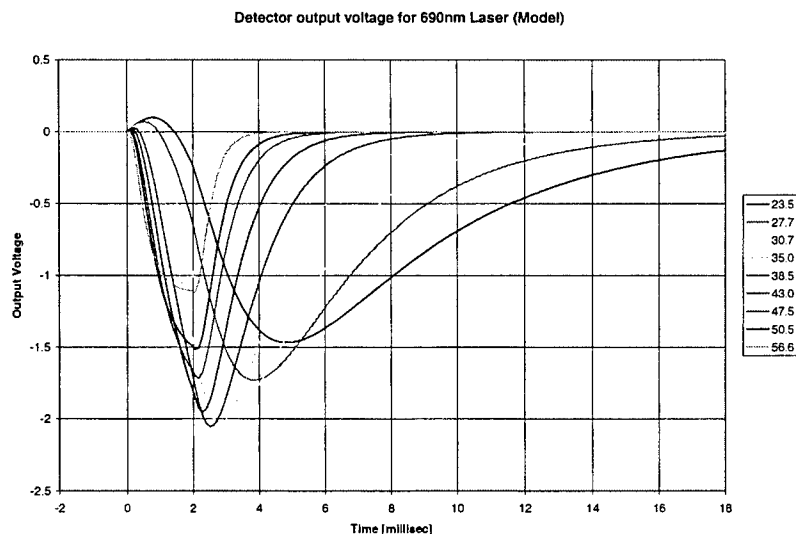


**Fig 3.2.28:** Solution of the O-state kinetics model shown in the previous figure as a function of temperature. Compare this result with the measured result of Fig. 14.

Compare this data to the temperature dependent data presented in the measurements section. The very good comparison between the measured and modeled data is a measure of how well the main wild-type BR photocycle is understood. To further compare the model with the measured data, there are several important quantities that can be extracted from these figures, including the O-state decay time. The figure below compares the measured and modeled decay times—the model predicts a slightly faster decay time, but it should be noted that a minor temperature calibration error could account for this difference.
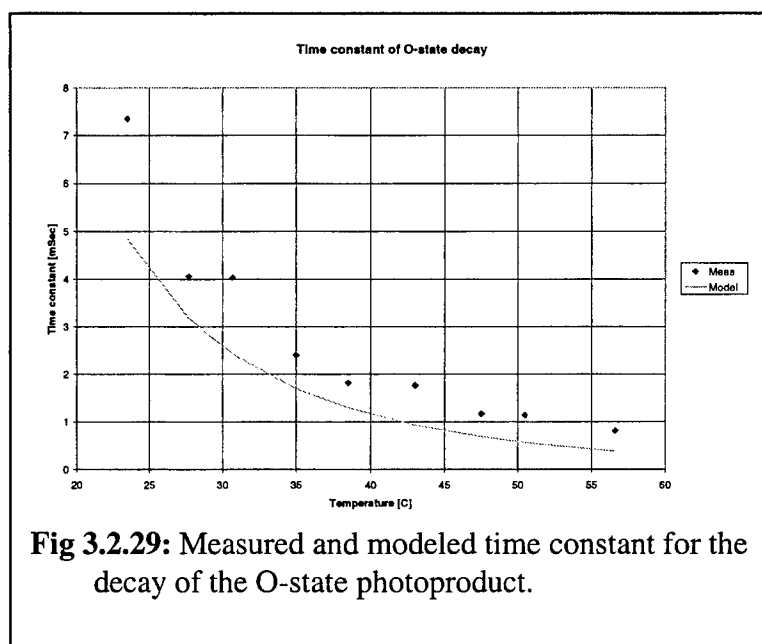


**Fig 3.2.29:** Measured and modeled time constant for the decay of the O-state photoproduct.

Another important quantity is the amount of O-state produced as a function of temperature; the O-state is favored over the N-state at higher temperatures. This can be determined by dividing the integral of the O-state versus time curves by the time constant. The measurement compares the amount of excited molecules relaxing back to bR through the N-bR branch versus the amount relaxing back through the O-bR branch.

69

Good agreement means that the model is describing the important final states of the cycle (M-N-O-bR) properly. The figure below shows the measured and modeled values.



Normalized Integrated concentration of O-state photo-products
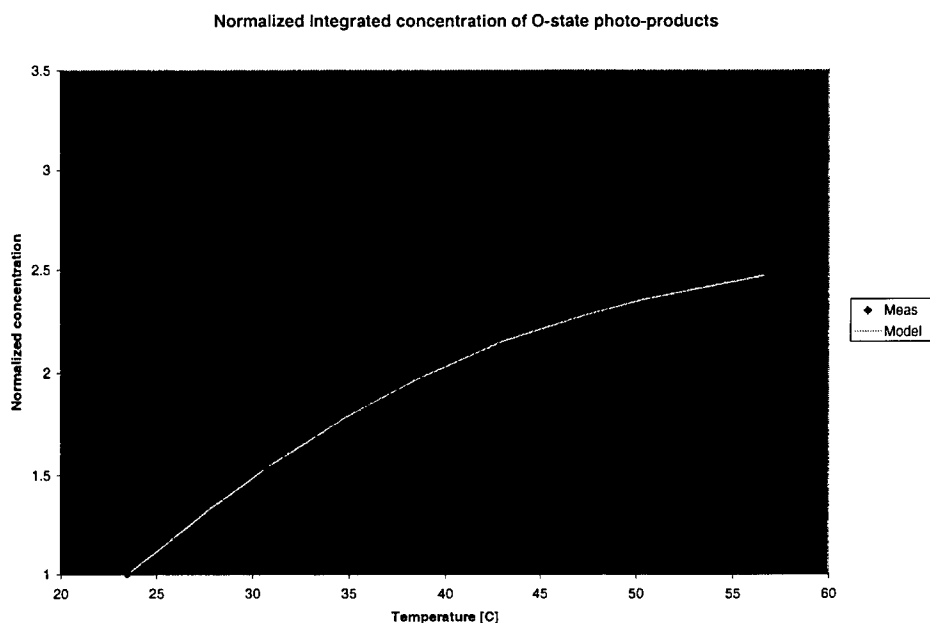
**Fig 3.2.30:** Measured and modeled concentration of the O-state photoproduct.

### 3.2.3.1. P-State Modeling

Because the model works so well for the production of O-state in wildtype BR, the result can be applied to P-state production. The figure in Section 2.2, which describes the rate of production of the P-state photoproduct through measuring the average transmitted intensity, was simulated using the model.

First, the sequential-flash experiment was simulated using the program. An incident intensity of $30\text{mW/cm}^2$ was assumed for both lasers and the O-P conversion efficiency was adjusted until the modeled output voltage of the amplifier reached 8.3V after 2 hours of flash-flash exposure. The required conversion efficiency to make this match at 40°C was 6.4%. Using the same conditions in the simulator we repeated the simultaeous flash experiment. After 2 hours the simulated output voltage was 2.2V, in fairly close agreement to the measured output voltage of 4.0V. The important point of this simulation is that under simultaneous flash conditions a slope greater than zero should indeed be observed.

### 3.2.3.2. Problems With Modeling Mutant Kinetics

With a working kinetic model for wild type BR available, the usefulness of such a model in predicting important quantities such as O to P conversion efficiency is evident, especially for the new mutants. One problem in deriving a solution to the model is that the system of equations describing the kinetics of the BR photocycle is referred to as a stiff system. In the numerical method texts, such a system is described as having small local truncation error while still experiencing problems with global stability. In practice

this means that several close-time steps will result in a small truncation error; the natural conclusion would be that the step size could be increased. However, if the step size is increased the model "blows up" because the global stability criterion is not met. The wild-type model calculation takes approximately one minute to complete. If the same model is to be applied to a mutant, it must be simulated for at least a factor of 10 times more, without the benefit of increased the step size to speed the simulation. The possibility of repeating the simulation many times in order to fit the model to experimental data requires a large computational burden. To model the P-state conversion rate curves a factor of 10000 more simulation time would be required—again a large computing burden. Further, the temperature dependent kinetics model is not as well understood for mutants with respect to the wild-type protein.

An attempt to fit the model with measured mutant data has been attempted. The data was collected from a time-resolved spectrometer measuring BR in solution, excited by a pulse from an XPO laser set at 568nm (data taken and reported by Kevin Wise). For the purposes of fitting the model, three time resolved traces were obtained, one at 412nm (the peak of the M-state), one at 568nm (the peak of the bR-state), and one at 650nm (near the peak of the O-state). For the purpose of the memory, only the slow time constant portion of the bR photocycle is of interest, and therefore only the time constants associated with the branches shown in bold in the figure below were adjusted.

Modeled Photo-cycle of bR
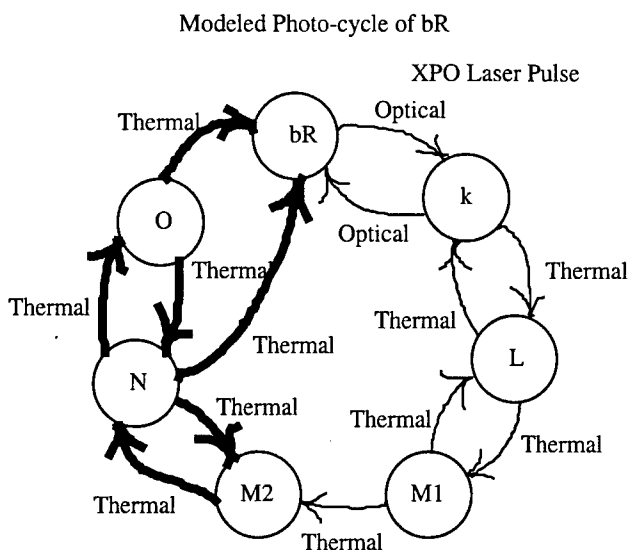


**Fig 3.2.31:** The time constants for the branches distingushed in bold were adusted in an attempt to fit measured data to modelled data.

A "steepest descent" algorithm was used to adjust the time constants in order to minimize the difference between measured and modeled data. The original model results and measured traces for wildtype BR at pH=7 are shown in the figure below. It is evident that the model predicts a faster response at all wavelengths compared to the measured data.
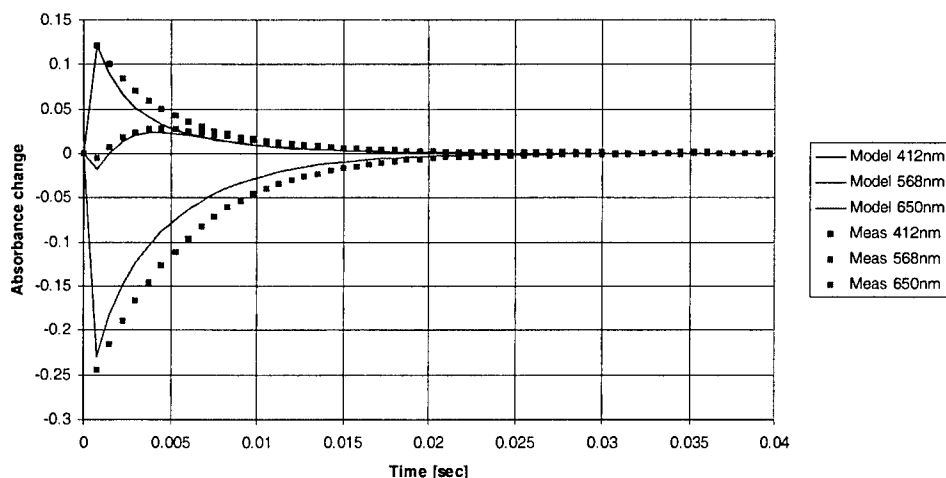
**Fig 3.2.32:** Initial BR model and measured data for the photocycle of BR.

To implement the algorithm the point-by-point difference, or error, between the three measured traces and the three modeled traces was calculated. An attempt to minimize the sum of the squares of these error terms was done by defining a Jacobian matrix as the partial derivative of the error terms with respect to each time constant, holding all other time constants fixed. The Jacobian matrix is found by changing a time constant by 10%, performing the simulation again, and calculating the error terms. Finite difference equations are used to estimate the partial derivatives. Once the Jacobian is found, a unit vector pointing in the direction of the steepest descent is calculated. Two additional error terms are calculated along this vector. A polynomial approximation is then made to determine where the local minimum is located along the steepest descent vector. This information is then used to update the time constants, thereby completing the iteration. The figures below show three iterations of this procedure as applied to fitting the wild-type BR model to measured data for wild-type BR.
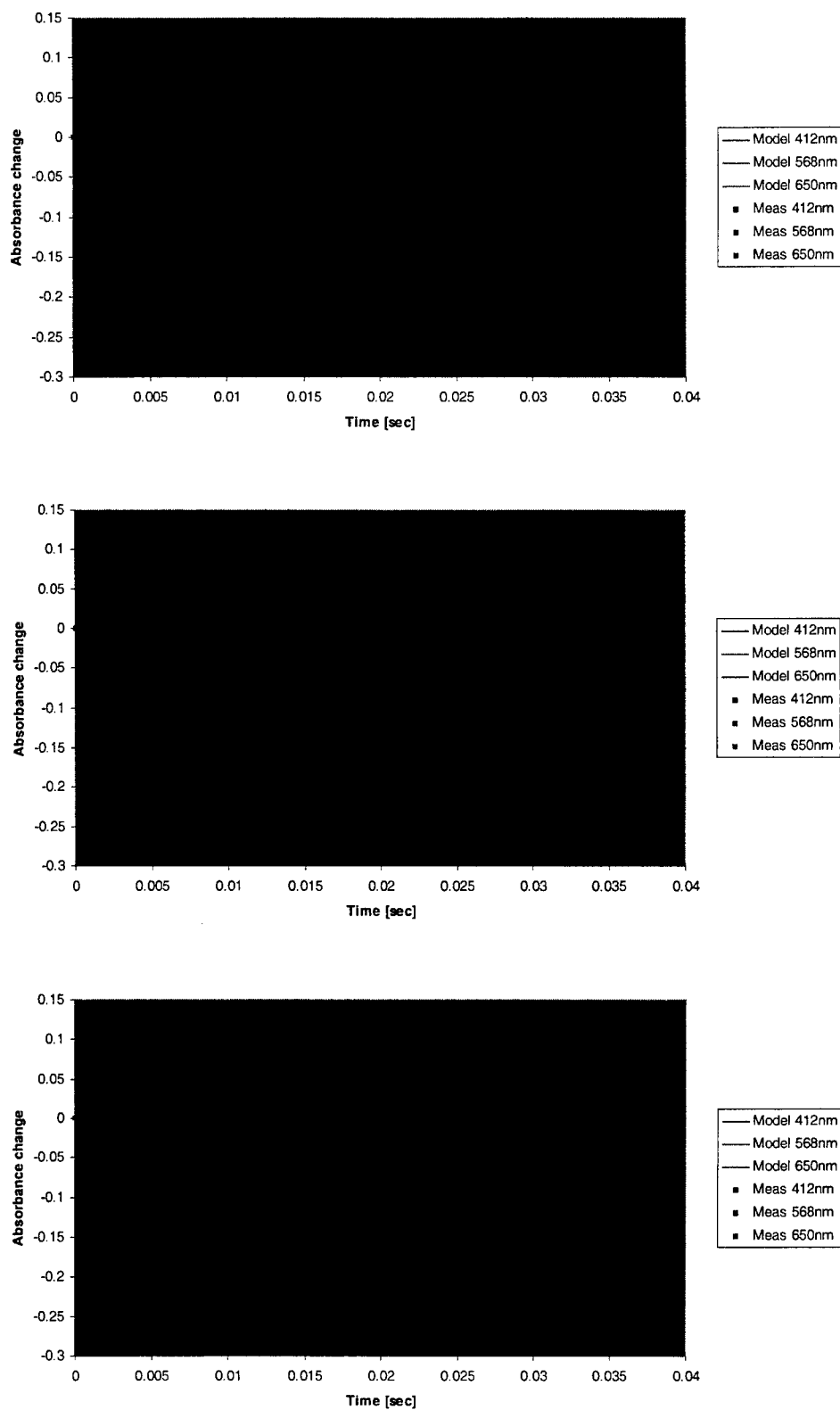
**Fig 3.2.33:** (a, b, and c). Iterations of the steepest descent algorithm. Notice convergence of the model with the measured data.

73

The table below shows how the times constants were changed as each iteration was performed.

**Table 3.2.1:** Time constants as updated by the steepest descent algorithm.

| Time Constant [millisec] | Original | First Iteration | Second Iteration | Third Iteration |
|---|---|---|---|---|
| M2 - N | 1.5 | 1.8 | 1.8 | 1.8 |
| N – M2 | 3.5 | 2.7 | 2.7 | 2.8 |
| N - O | 2.6 | 2.5 | 2.5 | 2.5 |
| O - N | 1.8 | 1.8 | 1.8 | 1.8 |
| N - bR | 2.9 | 4.8 | 4.1 | 3.8 |
| O - bR | 4.7 | 7.1 | 6.3 | 5.9 |

The ultimate goal in using this procedure is to find a new model for mutant strains of BR. To overcome the step size problem resulting from global stability issues, the modeling algorithm was modified to first solve the complete set of equations until the K, L, and M1 intermediates decrease to below 0.001% of the total bR. A simplified set of equations that does not contain the rapidly decaying intermediates is then solved for the rest of the simulation. A step size of 0.5 millisec is easily accommodated without instability in this model. Using this technique the transient response of BR can be modeled over a time period of 600ms. The figure below shows measured F208N mutant data and the original wild-type model.

Attempts to adjust the time constants using the steepest descent algorithm have not worked correctly. The convergence is extremely slow and after five iterations the time constants were for the most part unchanged. The problem is most likely due to a poor guess at initial conditions because F208N is so much slower than wild-type BR. One possible solution would be to choose a mutant with a faster response than F208N but a slower response than wild-type BR. The algorithm could then be used to fit the intermediate mutant—the resulting time constants could then be used as an initial guess for the F208N mutant. A possible concern is whether the time constants that are found using this technique represent a unique solution to this problem.
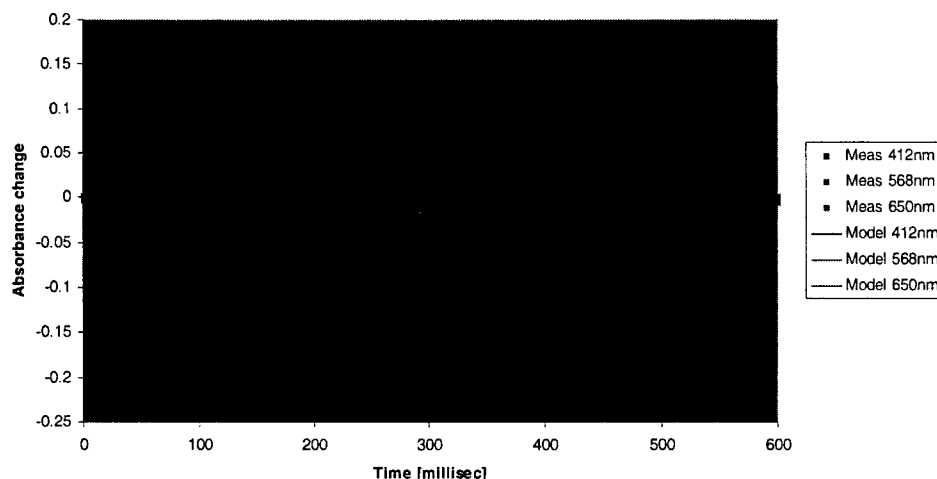
Fig 3.2.34: Initial BR model and measured data for the photocycle of F208N.

### 3.2.4. Complete Prototypes

#### 3.2.4.1. Motorized 2D System

The miniature prototype has been completed and packaged as a self-contained unit—this represents the culmination of seven months of design and research and has been used to prove the functioning of the architecture for the protein based volumetric memory. Below are figures of the prototype and some highlights of the accomplishments made with this device.
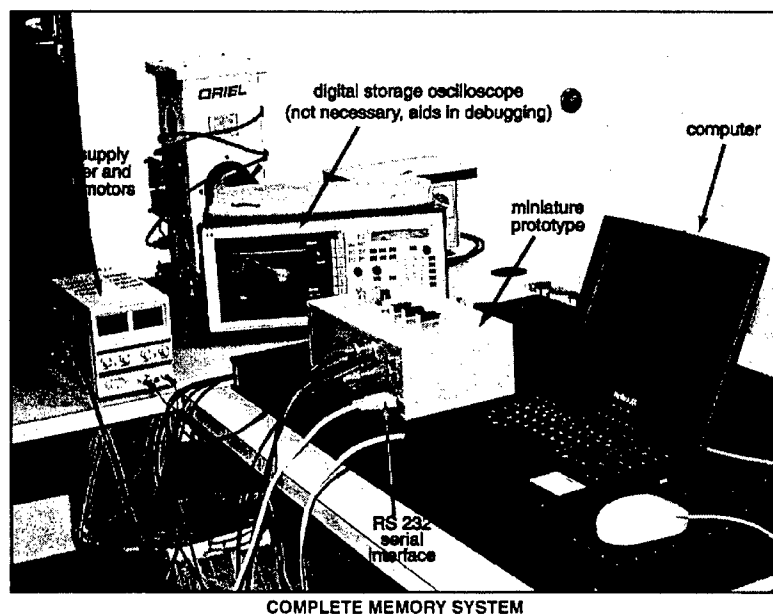


Fig 3.2.35: Miniature prototype

INTERIOR VIEW OF MINIATURE PROTOTYPE
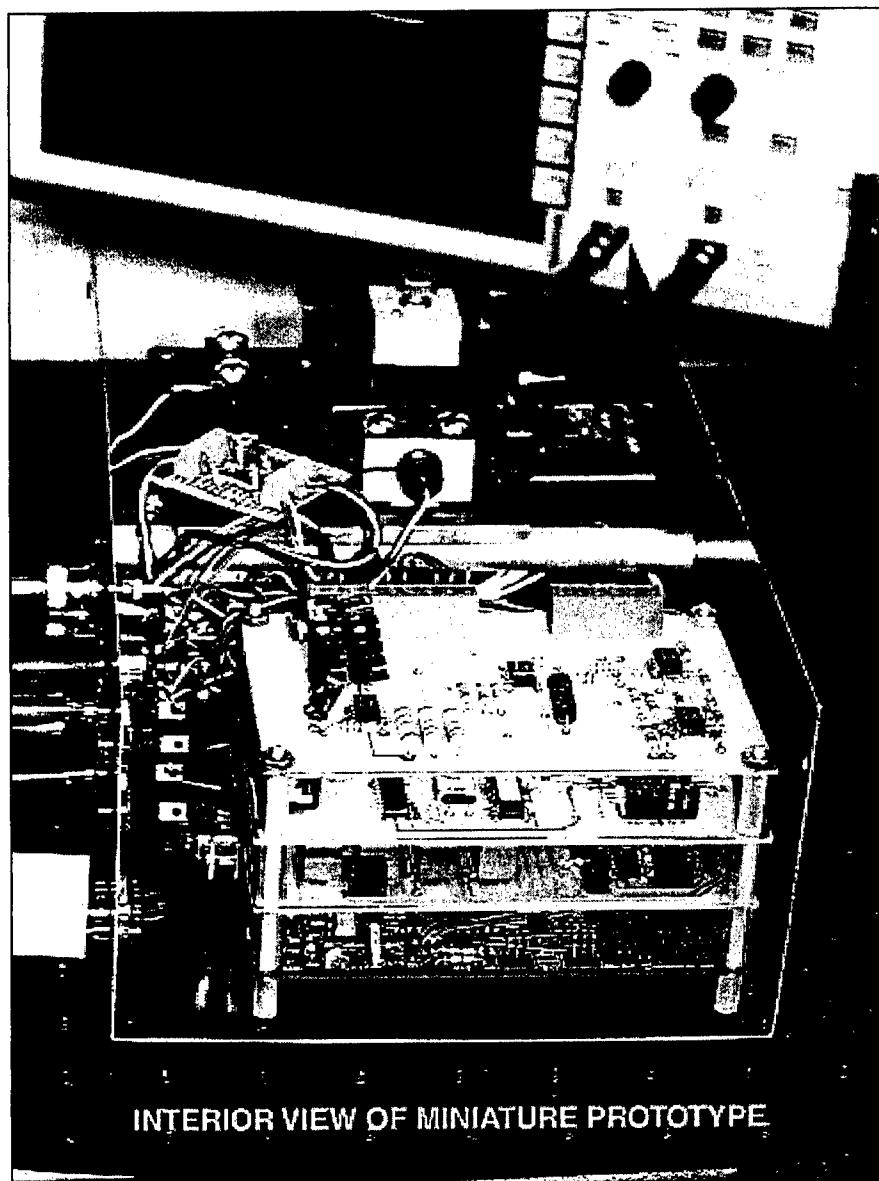
**Fig 3.2.36:** Interior view of the miniature prototype.

### 3.2.4.1.1. Highlight of the Accomplishments

The miniature prototype was used to meet the following objectives:

- Observation of temperature-dependent signals due to the transient red absorbing photoproduct of bacteriorhodopsin, the O-state. The reading procedure for the volumetric memory architecture requires observing this transient signal.

- Production of the long-lived blue absorbing photoproduct, the P-state through a writing operation. This could be seen as a yellow spot floating completely within the volume of the cuvette. As such, this represents the first successful attempt at a volumetric write using a gelled suspension of bacteriorhodopsin.

- Demonstration that the formation of the P-state was indeed a branch from the main photocycle of BR. This observation is crucial to the architecture of the volumetric prototype.

- The first true volumetric read was performed by observing diminished "O-state" formation in a region where P-state has been formed. This experiment confirmed the volumetric memory architecture.

### 3.2.4.2. Screening System

Two screening systems have been produced. The screening system is a complete memory architecture (including erase capability) without position control that can be used to generate exposure curves so that the sequential- and simultaneous-flash experiments can be carried out repeatedly at a single point. This simple exposure curve can be generated overnight and gives a complete picture of branched versus unwanted photochemistry, rate of formation of P-state, rate of erasure, and cyclicity, all with a system that operates precisely as the proposed volumetric memory architecture. Using these systems we will be able to screen a large variation of protein candidates for the memory. A photograph of the two systems is shown below.



Fig 3.2.37: Two screening devices.

### 3.2.5. Proposed System for Future Prototype Development

The results gathered from the prototypes described in this report have indicated that the next prototype should have differential detection. To perform this task a dual beam must be passed through the cuvette, sampled by a dual detector. To date, the prototypes have relied on absolute detection of the O-state signal, while the proposed volumetric memory design has always incorporated differential detection. Much higher noise performance should be obtained with a differential system, which will require much less writing time to form a detectable bit. Other than the differential detector, the prototype will be same as those produced to date.

The new prototype will be produced by a professional embedded system design firm called Critical Link, based in Syracuse, NY. The close proximity of this company to Syracuse University facilitates communication between their design team W.M. Keck Center scientists, an extremely important consideration. Included in this report is the scope of work that was prepared by Critical Link after several discussions on the details of this project. Not shown in this task list are additional sub-contracts required for the design of the mechanical and design of the optical systems. Each of these sub-contracts are much smaller than the embedded systems design project and are still being put together. At the writing of this report the Critical Link effort is fully under way as part of the sister grant to this contract.

Task Summary

| | Man-day Estimate |
|---|---|
| **System Design** | |
| **Requirements** | |
| Requirements review | 2 |
| System architecture | 3 |
| **High-level hardware design** | |
| Component selection (inc. Processor, USB chip set) | 3 |
| Laser selection | 3 |
| Laser control circuitry design | 2 |
| Laser dimmer design | 3 |
| Analog front-end design | 10 |
| **High-level software design** | |
| RTOS selection | 1 |
| Software design | 3 |
| **Hardware Development** | |
| **Low-level design / Schematic Capture** | |

| | |
|---|---|
| Processor / processor support | 3 |
| USB chip set | 3 |
| Laser control circuitry | 2 |
| Stepper motor control | 2 |
| PLD design/simulation | 3 |
| Laser dimmer control | 2 |
| Temperature control | 2 |
| Temperature sensor | 2 |
| Analog Front End | 3 |

**Component Procurement**

| | |
|---|---|
| Component procurement | 2 |

**PCB fabrication / test**

| | |
|---|---|
| PCB layout / routing | 5 |
| PCB fabrication. | |
| PCB prototype assembly. (2 units) | 1 |
| PCB test and debug. | 15 |
| PCB pass 2 layout / routing | 2 |
| PCB pass 2 fab | |
| PCB prototype assembly. (2 units) | 1 |
| Pass 2 test | 7 |

**Firmware Development**
**Port Real-Time Operating System**

| | |
|---|---|
| Create board support package | 3 |
| Debug RTOS on target hardware | 5 |

**Low-level I/O Functions**

| | |
|---|---|
| USB interface | 5 |
| Laser control | 2 |
| Laser dimmer control | 2 |
| Stepper motor control | 2 |
| Temperature sensor | 2 |

**Firmware Integration / Test**

| | |
|---|---|
| Integration / Test | 10 |

**Host Side Software Development**
**PC Driver Development**

| | |
|---|---|
| Develop USB driver | 5 |
| Develop simple user interface utility | 5 |

**MAC Driver Development**

| | |
|---|---|
| Develop USB driver | 20 |
| Develop simple user interface utility | 10 |

**System Test / Integration**

| | |
|---|---|
| System Test / Integration | 20 |

**Totals**

| | |
|---|---|
| Total Labor | 176 |

### 3.3. Modular Prototype

During the first year of this effort, a considerable amount of time and effort was put into the construction of a modular prototype where optical and electronic components could be easily integrated into the memory system, but just as easily removed for further modification and optimization. This portion of the research effort was directed by Dr. Enrique Izaguirre here at Syracuse University. Unfortunately, factors beyond Dr Izaguirre's control made it necessary for him to leave Syracuse and take up a teaching position with CUNY. It was also at this time that it became evident that efficiency issues with the protein were going to redirect the research toward the simpler one-bit screening prototypes described above. With the wildtype protein, the laser intensity needed to illuminate a page through a spatial light modulater (SLM) is not possible from commercially-available diode lasers—the design of the modular prototype (see Figure 3.3.1) utilized an SLM, and had an optical layout based on the design illustrated in Figure 2.5. It was determined that at this point it was not worth pursuing this design, which will only be possible with the development of improved bacteriorhodopsin analogs. However, Dr. Izaguirre remained on the contract as a consultant and continued his work with several aspects of the modular design. His progress is summarized below.

### 3.3.1. Spatial Light Modulator Development:
After determining that transmission-based spatial light modulators would result in too much optical loss, a micro-mirror spatial light modulator (MMSLM) was determined to be the best approach for encoding page-based data into the memory gel matrix. Computer control was established for the MMSLM, such that computer defined images could be projected from the unit. After determining that too much optical distortion resulted from any attempt to reduce the projected image, it was decided that the optical system had to be reversed to allow more facile image reduction. Optical distortion and loss was estimated at approximately 20%

and 10% respectively, for the un-optimized system. By the end of the contract, the MMSLM had been installed on an optical bench and was being evaluated with respect to short distance image projection.

### 3.3.2. Paging Optics Development

Designs have been made to combine the power from several diode lasers to produce both the paging and data beams using fiber optics. The paging laser design employs an optical line generator. Arrays of 2 x 2, 3 x 3, and 4 x 4 diode lasers have been modeled to give a final power of 1.8 W. Coupling of the lasers is accomplished
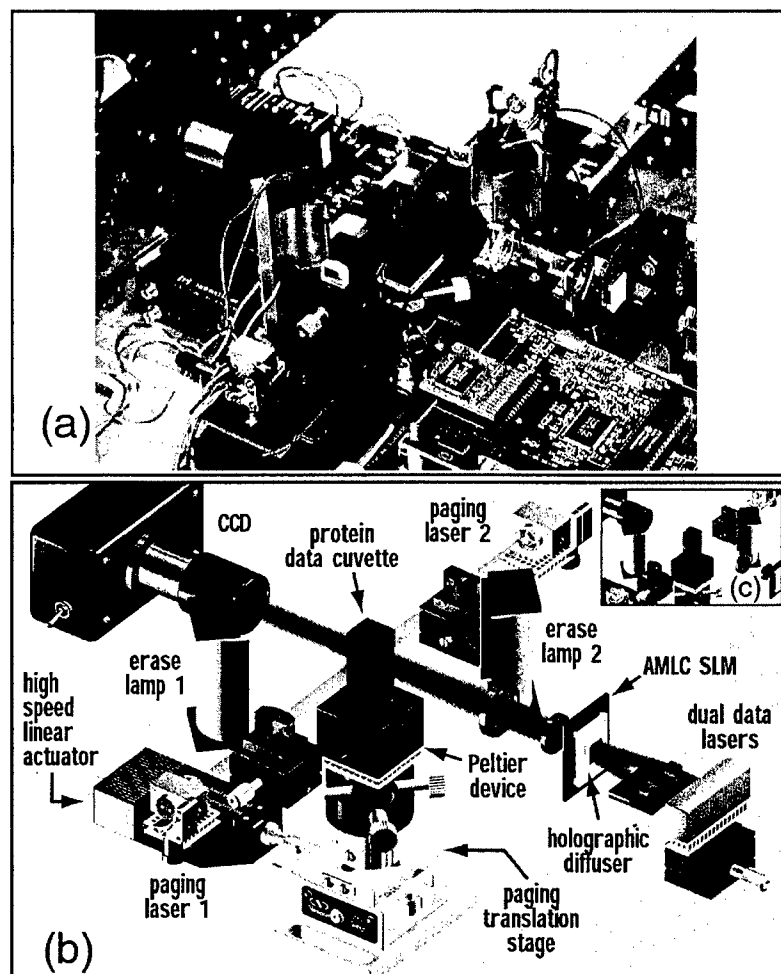


Figure 3.3.1: Photograph and labeled schematic of original modular prototype.

by fiber optic assemblies and controlled by a TTL pulse. Refractive micro-lenses at the fiber output are used in the design to concentrate the beam and control the beam intensity distribution. The refractive micro-lenses have been tested with an optical fiber to form a beam from three diode lasers. The output from the three lasers was successfully coupled into the optical fiber, and focused by the refractive micro-lenses. In the final design, optical fibers and linear array of gradient index lenses will be used to couple the lasers to the memory cell micro lenses for the paging beam. This optical arrangement has already been simulated for one paging beam, and the next step is to simulate such an arrangement on both sides of the cube for higher intensity; this will provide valuable data on the beam homogeneity and interference effects originated by the partial coherence of the lasers. The use of cylindrical axicons to extend the Rayleigh's range of the paging beam was also examined. Further modeling of the proposed optical designs of both the fiber-optic mediated paging and data beams continues.

### 3.3.3. CCD Camera

A circuit capable of controlling the exposure time of the CCD camera was built and evaluated using Lab View to acquire and process data images. Unfortunately, the experimental results obtained indicated that a different method would be necessary for detecting that data signal by the CCD. In light of difficulties concerning the efficiency of the bacteriorhodopsin branched photocycle, it was determined that further evaluation of signal detection at the CCD was not warranted at this time.

### 3.3.4. Light Scattering

An apparatus to measure scattering as a function of the active optical elements (the membrane patches) and the non-active part of the medium (the hydro-gel) has been constructed. The set-up utilizes differential optical techniques for the purpose of evaluating the scattering of polarized vs. non-polarized light; it is important to mention that this technique will provide information on the scattering of unpolarized light and the conservation of polarization. The study of the conservation of polarization in the memory cell is of fundamental importance for the implementation of multiplexing by means of orthogonally polarized beams. As of 8/00, problems with system noise had precluded the acquisition of meaningful data.

## 3.4. The W.M. Keck Center for Molecular Electronics Beamline Facility Report

This section details the progress made at the beam line facility at the Center for Advanced Microstructure and Devices (CAMD) by researchers Peter Dowben (Department of Physics and Astronom, University of Nebraska) and Phil Sprunger (Center for Advanced Microstructure and Devices (CAMD), Louisiana State University.

### 3.4.1. The Grating Fabrication

A major success of this research program has been discovery that one class of unique, thin-film polymers, namely poly vinyidene fluoride (PVDF) and poly vinylidene fluoride trifuoroethylene, P(VDF-TrFE), copolymers can be directly photoetched using synchrotron-based X-rays. Exploiting its ferroelectric, piezoelectric, pyroelectric properties, the results of this research project demonstrate that development of microstructure devices, which exhibit these unique properties, can be easily fulfilled. As an example, the figure at the right shows an example of a PVDF



Figure 3.4.1. Direct etching of PVDF: ~ 4•m denth

microstructure directly patterned, without any needed post processing and/or development, upon exposure to synchrotron radiation (broad band X-rays).

In order to optimize this effect, ultraviolet photoemission spectroscopy (UPS) and mass spectroscopy was used to elucidate the photodegradation mechanism of (PVDF) and P(VDF-TrFE) copolymer thin films. Upon increasing exposure to X-ray white light (hv~1000 eV), UPS measurements reveal that substantial chemical modifications occur in both in ~ 100 Å PVDF and 5 monolayer P(VDF-TrFE) films, including the emergence of new valence band features near the Fermi level, indicating a semi-metallic photodegradeted product (see spectra at left). The photodetached fragments of the PVDF and copolymer P(VDF-TrFE) consist mainly of $H_2$, HF, CHF, $CH_2$. This X-ray exposure study demonstrates that PVDF and P(VDF-TrFE) films, possessing unique technologically important properties, can be directly patterned by x-ray lithographic processes. This capability



Figure 3.4.2. UPS spectra of the surfaces of (a) a pristine PVDF thin film and (b) that of a sample degraded by X-ray white light irradiation.

leads us to develop the direct pattern transfer technology and new type of novel masks (one US Patent has already been applied for using this technique). Additionally, using this direct pattern transfer and ferroelectric properties of PVDF and its copolymer, we can build an optical grating and/or second harmonic generation devices.
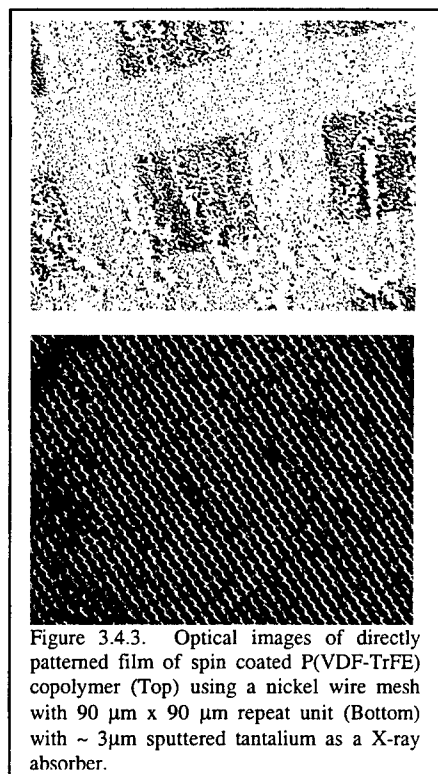


Figure 3.4.3. Optical images of directly patterned film of spin coated P(VDF-TrFE) copolymer (Top) using a nickel wire mesh with 90 μm x 90 μm repeat unit (Bottom) with ~ 3μm sputtered tantalium as a X-ray absorber.

We also have large array grating in PVDF and PVDF-TrFE. As an example, spun coated P(VDF-TrFE) copolymer thin-films were exposed to a synchrotron radiation and it results in a directly patterned array with well order. Consequently, this can be utilized, based on the nonlinear materials properties, as a two-dimensional diffraction grating. Work continues on this project.

We have also probed the interface of an electrode material with the ferroelectric polymer material we have patterned with X-rays. Unfortunately, we now have conclusively shown that the Al-PVDF-TrFE polymer interface is not abrupt. Experiments with polypyrole and other polymer materials are underway.

We have also fabricated large grating arrays in cobalt and Co/Pt and have undertaken scattering of these grating using neutrons, and optically and have shown that we can vary the Kerr rotation in different diffraction beams. Visible optical scattering and magneto-optic Kerr effect signals have been taken off the 15th order diffraction spot.

## 3.4.2. The Beamline Upgrades.

The 3 m TGM beamline and end station are now functional and we are now taking data. The new gratings have been installed. The new gratings, should greatly enhance the resolution and beam flux transmission of the beamline. Utilizing this new beamline, we have investigated the UV photodegredation of polyvinylidene-trifuoroethylene sued in making some of the patterned gratings and other patterned films discussed below.



Figure 3.4.4. Jaewu Choi (left) and Phil Sprunger (right) standing in front of now operational 3m TGM beamline

In addition, photoemission experiments on adsorption and desorption of metallocene and palladium complex have been completed along with experiments on other doped and undoped conducting polymers such as polypyrrole. The doping is key to understanding the electron-phonon coupling which plays an important role in determining of the metallicity, heat capacity, and Pauli susceptibility in these one dimensional conducting polymer systems. These macroscopic properties crucially depend upon the appearance of a finite density of states near the Fermi level ($E_F$) in either occupied or unoccupied side. Ultimately, this information will be important to the device performance of these materials.

### 3.4.3. Commissioning status of the 3m-NIM beamline is as follows:
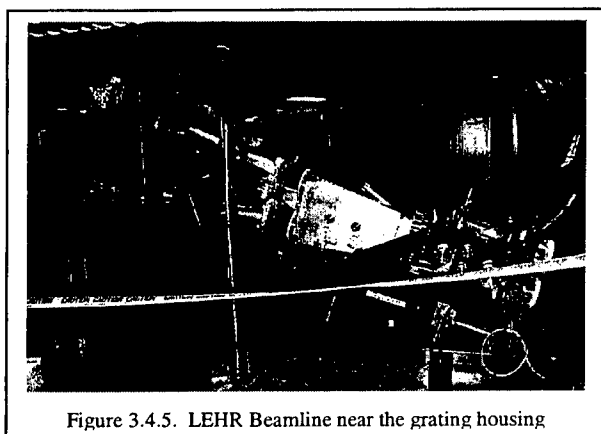


Figure 3.4.5. LEHR Beamline near the grating housing

Throughout the funding period, considerable progress has been made on the low-energy, high-resolution (LEHR) normal incidence monochromater (NIM) beamline at the CAMD facility. Entrance slit, exit slit and gratings (high and low energy) have been installed and aligned.

By using well aligned laser beam, the slits and the gratings were aligned at zero order (white beam condition). Monochromator wavelength scanning (this requires rotation and translation of the grating) was also tested. Reproducibility of the laser beam (zero order light) at the exit slit was found to be excellent.

In addition, grating translation motion was confirmed to be exactly on the beamline axis. With actual beam from synchrotron, beam position is slightly off in vertical direction at the both entrance and exit slits, but which can be adjusted easily in situ by using a manipulator for grating (fine) adjustment.

In addition to the NIM beamline, substantial progress has been made on the LEHR experimental end-station. This includes the construction of a custom mu-metal chamber, to minimize magnetic field penetration, and preparation chamber. At present, the SCIENTA analyzer, in combination with a custom designed cryostat manipulator, is being tested with the use of a UV-resonance lamp. With the addition of the preparation chamber, final construction of this end-station will be completed in late summer, 2000.



Figure 3.4.6. LEHR endstation with SCIENTA analyzer (at left)

### 3.4.4. Recognition:

This work has been recognized as contributing to both the Air Force and Navy research objectives in ferroelectric devices for sonar and smart skin applications. Ginzburg has highlighted this work among his list a great accomplishments in physics in the past ten years and we have garnered more than four invited talks on this work.

### 3.4.5. Publication summary (to April 1, 1999):

1) Harish M. Manohara, Eizi Morikawa, Jaewu Choi and Phillip T. Sprunger, "Pattern Transfer by Direct Photo Etching of Poly(vinylidene fluoride) using X-rays", *IEEE Journal of Microelectromechanical Systems* 8 (1999) 417-423.

2) C.N. Borca, S. Adenwalla, Jaewu Choi, P.T. Sprunger, Stephen Ducharme, Lee Robertson, S. P. Palto, Jianglai Liu, Matt Poulsen, V. M. Fridkin, H. You, P. A. Dowben, "A Lattice Stiffening Transition in Copolymer Films of Vinylidene Fluoride (70%) with Trifluoroethylene (30%)", *Physical Review Letters*, **83** (1999) 4562-4565.

3) Jaewu Choi, C.N. Borca, P.A. Dowben, A. Bune, M. Poulsen, Shawn Pebley, S. Adenwalla, Stephen Ducharme, Lee Robertson, V.M. Fridkin, S.P. Palto, N. Petukhova, S.G. Yudin, "The Phase Transition of the Surface Structure in Copolymer Films of Vinylidene Fluoride (70%) with Trifluoroethylene (30%)", *Physical Review* **B 61** (2000), 5760

4) Jaewu Choi, H.M. Manohara, E. Morikawa, P.T. Sprunger, P.A. Dowben, and S.P. Palto, "Thin Crystalline Functional Group Copolymer(vinylidene fluoride -

trifluoroethylene) Film Patterning Using Synchrotron Radiation", *Appl. Physics Letters* **76** (2000) 381-383

5) Eizi Morikawa, Jaewu Choi, Harish M. Manohara, Hisao Ishii, Kazuhiko Seki, Koji K. Okudaira and Nobuo Ueno, "Photoemission study of direct photo-micromachining in poly(vinylidene fluoride)", *Journal of Applied Physics*, **87** (2000) 4010-4016

6) Jaewu Choi, S.-J. Tang, P.T. Sprunger, P.A. Dowben, V.M. Fridkin, A.V. Sorokin, S.P. Palto, N. Petukhova and S.G. Yudin , "Photoemission Band Symmetries and Dipole Active Modes of Crystalline Films of Vinylidene Fluoride (70%) with Trifluoroethylene (30%) Across the Ferroelectric Transition(s)", *J. Phys. Cond. Matter* **12** (2000) 4735-4745

7) C.N. Borca, S. Adenwalla, J. Choi, Lee Robertson, H. You, V.M. Fridkin, S.P. Palto, N. Petukhova, and P.A. Dowben, "Changes in Electron-Phonon Coupling across a bulk phase transition in copolymer films of vinylidene fluoride (70%) with trifluoroethylene (30%)", Applied Surface Science, sumitted

8) P.A. Dowben, Jaewu Choi, and Eizi Morikawa, "Band structure and molecular orientation of molecular overlayers using electron spectroscopies", THIN FILM HANDBOOK, Academic Press, H. S. Nalwa, Editor, in preparation

9) Jaewu Choi, E. Morikawa, P.A. Dowben, S.P. Palto, "Comparison of the Electronic and vibrational Structure of long chain vinylidene fluoride (70%) with trifluoroethylene (30%) with short chain poly(vinylidene fluoride), in preparation

Patents:

Harish M. Manohara, Phillip T. Sprunger, and Jaewu Choi, "X-ray Pattern Transfer in Poly (Vinylidene Fluoride), and Poly(Vinylidene Fluoride) X-ray Masks", US Patent Applied for, submitted on June 25, 1999

## 4.0. Conclusions

The progress made under this project over the period from May 1999 through September 2000 was substantial. Despite the fact that unexpected problems with protein efficiency resulted in a reevaluation of research effort priorities and direction, several key determinations were made. Among the successes are verification of the branched photocycle architecture, fabrication of improved memory materials, and construction of miniaturized prototypes. Perhaps the most valuable conclusion of this effort is that the technology is viable, and given the appropriate bacteriorhodopsin genetic variant there is the possibility of a commercially competitive technology—development of that genetic variant is the largest challenge that remains. Once that challenge is met, the technology necessary to integrate it into a fully functional memory device will fall into place. In fact, this very technology, including the computer interface, optics, and laser systems is being

developed in the form of several stand alone portable and fully functional prototypes as part of the parallel research effort.

## 4.1. Why Some Goals Were Not Met

The original statement of work for this contract had an ambitious set of tasks to be completed during the research effort. These tasks are listed below, followed by a brief discussion as to the extent to which each was addressed and completed.

1) Materials development, including an optical matrix characterized by reduced scattering and wavefront distortion of light propagation, long-term physical stability with respect to dehydration and shrinkage of the memory medium, and a compatible environment for the protein.

2) Protein optimization for efficient data storage, through genetic and chemical enhancement.

3) Implimentation of a Fourier-based optical system.

4) Implimentation of multiplexing techniques, including polarization and gray-scale.

5) Development of an electronic computer interface to facilitate invisible background operation of the volumetric memory device.

6) Build, deliver, test, and demonstrate a functional protein-based optical memory prototype.

The progress made on several of these tasks has already been described. Task number 1, Materials Development, is largely completed as described above (i.e., excluding protein optimization). The collaborative effort with Carleton University has proven to be very productive, with levels of light scattering in the memory gels being reduced substantially. And the aqueous-based polymer system lends itself to fascile modification of the milieu experienced by the protein in terms of pH, and chemical additives (for the purposes of optimization of protein efficiency). Large strides have been made in Task number 2 with enhancements in O-state production being increased by several orders of magnitude depending upon which mutant protein is being considered (see above). However, as of yet we have been unable to affect the quantum yeild of the O→P transition, which will be a necessary improvement for commercial viability. Tasks 3 and 4 were not completed for reasons that will be described below. However, the remaining two tasks, 5 and 6, are complete to the extent possible without tasks 3 and 4. A series of fully function small-scale prototypes has been fabricated in-house, with an advanced version developed at Critical Link, Inc. of Syracuse, NY (see above). Fully integrated Mac and IBM PC compatible interfaces have been developed for all of the prototypes. However, at this time, the interfaces are not what would be described as invisible to the end-user. Their primary function is to control the prototypes with the aid of parameter input from the user—a necessary feature for analyzing novel memory materials.

The primary reasons for not fulfilling tasks 3 and 4 can be found in the unexpected difficulties with the wild-type protein, which did not perform as originally predicted. In the absence of the needed efficiency, Fourier-based optical schemes and multiplexing techniques could not be realistically implemented at this point. The intensity needed to drive wild type bacteriorhodopsin into the branched photocycle is simply too great—multiplexing requires optical selection of select protein populations, determined either by polarization or the assignment of significance to the degree of photoconversion. The net result of each of these techniques is a decrease in actinic intensity—the amount of protein driven into the branched photocycle through the use of multiplexing schemes would effectively be below the limits of fascile detection. Ongoing experiments designed to reevaluate the basic properies of the branched photocycle are providing new insight into bacteriorhodopsin that will be integral to future optical and multiplexing systems. Tasks 3 and 4 will be revisited once more highly optimized bacteriorhodopsin mutant proteins are available.

The protein was only one impediment to progress. Several shifts in the direction of the research effort were unavoidable due to personnel changes and relocation of half of the group to the University of Connecticut. Changes such as these are inevitable in any long-term research project, and are better viewed as logistical, rather than technical impediments.

## 4.2. Future Directions

It is evident that the production of a commercially viable device hinges on the development of new more efficient mutant proteins. The routes to these new variants are three-fold, including genetic manipulation (directed evolution), chemical modification, and optimization of the chemical environment surrounding the protein. The most challenging, genetic manipulation *via* directed evolution, also has the possibility of the biggest reward—the ability to hone in on a mutant protein with a distinct set of predetermined properties. As part of the parallel research effort, a substantial amount of time has been put into directed evolution of bacteriorhodopsin—to date results have been mixed and the technique as applied to *H. salinarum* has not yet been perfected. However, none of the problems encountered thus far are viewed as insurmountable. *The technique of directed evolution is currently the best option by which the bacteriorhodopsin-based branched-photocycle three-dimensional optical memory can be made viable.* With respect to chemical modification, that route continues to be pursued and preliminary results are encouraging (results of both directed evolution and chemical modification will be reported in the final report for the parallel research effort, ending 10/29/01).

Improvements in the polymer matrix may be necessary as new BR mutants become available. The chemical environment plays a vast role in the response of the protein to light. Factors such as temperature, pH, and ionic strength all have a strong influence on the ability to access the branched photocycle. Results too recent to include here indicate that the polymer matrix also makes a difference in the magnitude of the O-state signal.

The miniature prototypes developed for this contract were primarily done for the purpose of materials evaluation and development. As detailed above, the branched photocycle architecture was verified for the first time in a miniaturized system—these systems employ diode lasers and are capable of single bit storage only. Prototype development is currently in the hands of Critical Link of Syracuse, NY. Advanced level prototypes are currently being developed that can be modified as more advanced memory materials become available.

Finally, it is important to point out that the ultimate goal of this research effort is the development of a commercially-viable technology, and the establishment of a start-up company based in Central New York. Although in many ways the branched-photocycle remains in the research domain, the progress made through this effort reaffirms the potential for eventual product development.

## 5.0. References

1.      Popp, A., M. Wolperdinger, N. Hampp, C. Bräuchle, and D. Oesterhelt, *Photochemical conversion of the O-intermediate to 9-cis-retinal-containing products in bacteriorhodopsin films.* Biophysical Journal, 1993. **65**(October): p. 1449-1459.

2.      Dancshazy, Z. and Z. Tokaji, *Blue light regeneration of bacteriorhodopsin bleached by continuous light.* FEBS Lett, 2000. **476**(3): p. 171-3.

3.      Dancsházy, Z., Z. Tokaji, and A. Dér, *Bleaching of bacteriorhodopsin by continuous light.* FEBS Letters, 1999. **450**: p. 154-157.

4.      Yang, D. and M.A. El-Sayed, *The $Ca^{2+}$ binding to deionized monomerized and to retinal removed bacteriorhodopsin.* Biophysical Journal, 1995. **69**(November): p. 2056-2059.

5.      Zhang, Y.N., L.L. Sweetman, E.S. Awad, and M.A. El-Sayed, *Nature of the individual $Ca^{2+}$ binding sites in $Ca^{2+}$-regenerated bacteriorhodopsin.* Biophys. J., 1992. **61**(May): p. 1201-1206.

## 6.0. Appendix 1: Annual Report: May 1998 – April 1999

# Annual Report
# May 1998 – April 1999
# F30602-98-C-0105

## PROTEIN-BASED THREE-DIMENSIONAL MEMORIES

Submitted To:
**AFRL/IFED Rome Research Site**
**32 Brooks Road, Room 321**
**Rome, NY 13441-4114**
**Attn: Bernard J. Clarke**

By

**Jeffrey A. Stuart**
**Research Assistant Professor**
**Director, Advanced Prototyping Laboratory**
**The W. M. Keck Center for Molecular Electronics**
**Syracuse University**
**111 College Place**
**Syracuse, New York 13244-4100**
**Email: jastuart@syr.edu**

**10 June 1999**

*Principal Investigators:*
**Robert R. Birge & Jeffrey A. Stuart**
W.M. Keck Center for Molecular Electronics
Department of Chemistry
Syracuse University
Syracuse, New York 13244-4100
315-443-1900 (FAX 315-443-4070)

90

# 6.1 Table of Contents

## 1.0 Abstract

The progress in the development of the bacteriorhodopsin-based three dimensional memory during the first year of Air Force Contract No. F30602-98-C-0105 is described. As the project currently stands, considerable progress has been made in nearly every phase of the effort. A modular prototype has been designed and constructed for evaluation of various optical components and configurations. Designs for a miniaturized prototype have been made and construction of the first computer-card sized unit will soon be underway. A fully functional molecular biology lab has been established and production of bacteriorhodopsin mutant proteins is routine. Considerable progress has been made in the development of high optical quality memory cuvettes, although a lot of work still needs to be done to complete this task. Quantitative studies on the origins of light scattering in the memory cuvettes are underway, with the goal of understanding the underlying principles involved: with understanding will come new directions of materials development. Protein modeling studies and computer simulations are shedding light on the nature of the bacteriorhodopsin P and Q states, the long term storage elements of the protein-based volumetric memory. The results of these studies are directing the development of new mutant proteins that are hoped to exhibit enhanced efficiency in the formation of P and Q.

Despite the progress outlined above, there is considerable room for improvement in several areas, specifically in materials development. Although several mutant and analog proteins have been isolated, we still do not have a protein with enhanced efficiency in the production of the P and Q states. It is hoped that with the incorporation of new techniques such as random mutagenesis, some of these materials problems will be solved during the next year. Development of a fast and efficient method of screening new mutant proteins is a definite priority. And although scattering in the memory medium itself has been reduced considerably, it still remains problematic, as does developing a successful way to seal the memory cuvettes. These issues are discussed in further detail below, and directions toward their resolution are outlined.

## 2.0 Introduction

Present computer memory architectures largely are confined to two dimensions, typically in the form of a disk. The storage density of such devices is ultimately constrained by the physical limitations of the materials, i. e., both the size of the actual bit and the ability to mechanically access that bit is limited by both the material used as a recording medium and the size of the device used to detect it. An approach to increasing storage density that holds a lot of promise is moving into three dimensions, in the form of volumetric optical molecular architectures. In their present form, conventional silicon-based technologies are incapable of making that transition. The need for new materials and architectures is becoming increasingly apparent.

Bacteriorhodopsin (BR) is a 26 kD photosynthetic protein isolated from the bacterium *Halobacterium halobium*, a common halophilic resident of salt marshes (**Figure 2.1**). The protein occurs in the membrane of the organism, arranged in a two-dimensional semi-crystalline array of trimers. When oxygen is scarce, the protein is used by the organism in a photosynthetic role, by functioning as a light to chemical energy transducer. The chromophore responsible for absorption of light by the protein is all-*trans* retinal, which is bound via a protonated Schiff base to Lys-216. Light induces an all-*trans* to 13-*cis* isomerization in the chromophore, followed by a series of thermal protein intermediates characterized by different absorption spectra, vectoral proton transport, and ultimately the reisomerization of the chromophore with consequent re-generation of the protein's resting state. The last of the thermal intermediates is the O-state, which absorbs maximally at 640 nm. Exposure of this state to 640 nm light results in a small segment of the protein population being driven into the branched portion of the photocycle, first characterized in 1993 [1], and containing two intermediates, P and its



**Figure 2.1:** Bacteriorhodopsin is a membrane-bound protein with seven alpha-helical segments. When it absorbs light, it pumps a proton, which the bacterium uses as a source of energy. We use the protein to store information by using light to induce a change in the geometry of the chromophore (orange atoms). The overall dimensions are roughly 40 Ångstroms x 40 Ångstroms x 50 Ångstroms, making it a nanoscale data storage device.

thermal product Q. The chromophore in both intermediates has a 9-cis configuration.
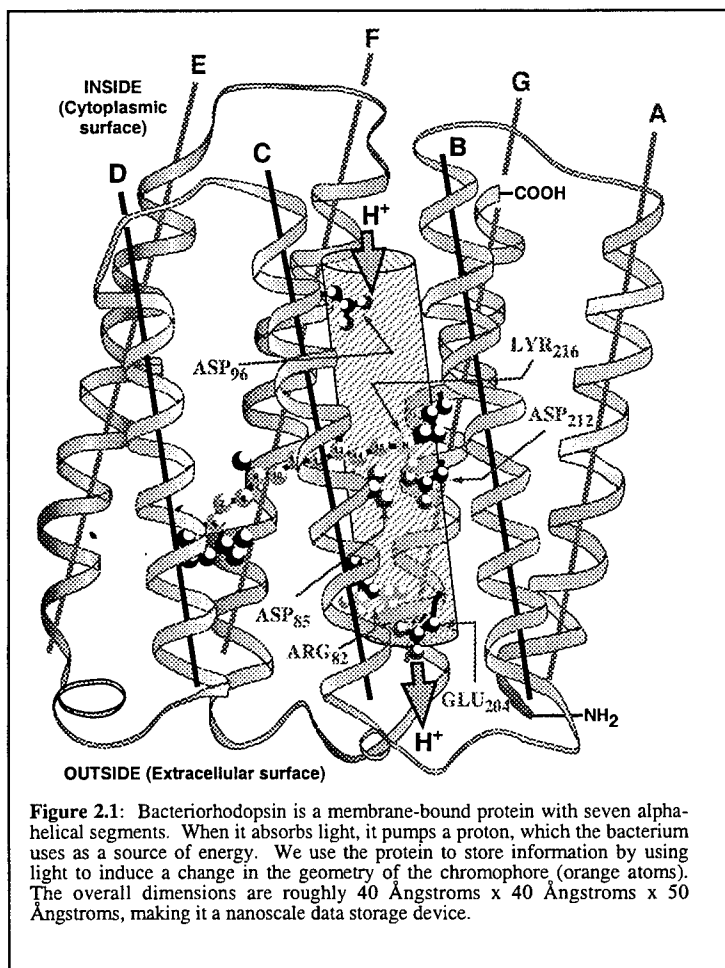
The Q-state is very long-lived, and is proving to be a promising candidate for long-term data storage.

The ultimate goal of this project is the creation of a new industry based on a novel product (the bacteriorhodopsin-based volumetric optical memory); therefore, the development and refinement of all aspects of this technology is of the utmost importance. A production strategy is necessary to create a new product capable of spawning an independent industry. Additionally, the industry should have the technical foundations and merit necessary to enable continuous research, development, and refinement, thereby securing its place as a competitive technological leader. The new opportunities presented by such an effort have the potential of bringing increased industry involvement, as well as employment. It is for these reasons that we plan to not only explore new architectures for our device, but also the different techniques necessary for the manufacture of a commercial product. In order to do this, it will be necessary to take into consideration the limitations imposed by the manufacturing process. It will therefore be necessary to explore component design and fabrication with an emphasis on mass production and the implementation of low cost solutions.

The current contract between Syracuse University and the United States Air Force, No. F30602-98-C-0105, is dedicated to the development of a volumetric optical memory based on the branched photocycle of the photosynthetic protein bacteriorhodopsin. The purpose of this engineering change proposal is to provide a research plan to justify the addition of two years of funding to this project. The proposal will be divided into four main areas, including an overview of the memory, a summary of the progress made to date in the current contract (section 4), a proposal describing the work to be accomplished with the additional time and funding, and a revised statement of work.

## 2.1. Overview of Bacteriorhodopsin-Based Volumetric Optical Memory.

The proposal for the original contract, Protein-based Three-dimensional Memories (No. F30602-98-C-0105) has a detailed description of both the theory behind the BR-based volumetric memory, and advantages over other volumetric optical architectures described in the literature (e.g., cyclicity, one-photon vs. two-photon issues, non-destructive writing and reading operations, etc.). The reader is referred to that document for further detail. However, a brief overview is included here for the sake of convenience.

In 1993, researchers in Germany described photoproducts that were produced upon illumination of the O-state[1]. Instead of converting to either BR or another main photocycle intermediate, a branching side reaction was found that contained two novel intermediates. These photoproducts, denoted as P and Q, were blue-shifted in absorbance with respect to most of the other photocycle intermediates, and were characterized as having a 9-*cis* chromophore. In addition, the Q-state displayed enhanced stability. The O-state acts as the entry point to the branched photocycle. Upon absorption of red light (~640 nm), an isomerization of the all-*trans* retinal chromophore occurs at the $C_9$-$C_{10}$ double bond, forming the P-state (490 nm). The resulting chromophore configuration is

not stable in the binding site, presumably due to steric interactions, ultimately breaking the bond between the chromophore and the protein. Concurrent with the cleavage of this bond is the formation of the Q-state (380 nm), which has a stability on the order of years. For the purposes of the branched-photocycle architecture, the bR state is assigned as a binary unit ZERO, and the P- and Q-states are collectively assigned as a binary unit ONE (**Figure 2.2**). Problems associated with previous architectures (two-photon-based systems) are easily circumvented by the unique nature of the branched-photocycle, in that it produces intermediates that are unaffected by the wavelengths of light used in write and read operations (i.e., unwanted photochemistry is rigorously avoided). Two photons are still required to write data, but they are absorbed by the protein sequentially, rather than simultaneously as in the two photon architecture.

The basis of the sequential one-photon branched photocycle architecture is illustrated in **Figures 2.2** and **2.3**. In order to access the branched portion of the photocycle, and thereby change a binary ZERO to a binary ONE, two conditions must be fulfilled: the bR photocycle must be initiated with a photon of green light, followed by a photon of red light at the appropriate time interval to drive O to the P-state. If, and only if, these two criteria are fulfilled, will data be written in the cube. The first process is referred to as paging, and involves initiating the BR photocycle with a photon of green light. The term "paging" refers to the process of using a green laser to select a slice within the cube where the protein is



**Figure 2.2:** The native photocycle includes the resting state (bR) and the intermediates K, L, M, N, and O. The last intermediate in the photocycle, O, will convert to a blue-shifted photoproduct, P, if it absorbs red light. The P state relaxes to form Q, a long-lived (>5 years) intermediate. Let bR represent bit 0 and P and Q represent bit 1. Data can be written into any location within a solid polymer matrix containing the protein by using a combination of paging (the green arrow) followed two milliseconds later by orthogonal writing (the red arrow). The protein operates like an optical AND gate— that is, data are written if, and only if, both of the input conditions are satisfied.

activated. The protein within this page starts to cycle through the photocycle intermediates, until the majority of the protein exists within the O-state after about 2 ms. At this time, the red data laser is fired, which drives the O-state into the branched photocycle, forming the P and Q intermediates. In this way, the protein acts as an optical AND gate: if only the green paging laser is fired, photochemistry is initiated and the net effect is that the protein cycles through the intermediates and returns to its resting state, resulting in the re-writing of a binary ZERO. If only the red data laser is fired, no action is stimulated in the protein because the wavelength of the data laser is not within the bR absorption band (net result = no change). However, if the green paging laser is fired, followed by the red data laser at the appropriate interval (after the paging laser has been turned off), protein that exists in the O-state is driven into the branched photocycle, the P-, and then Q-states are formed, and the formation of a binary ONE results. The combination of orthogonal laser excitation (enabling facile access to any volumetric element in three dimensions, as defined by the cross section of the two laser beams) and

95

the energetically and temporally separated states of the branched photocycle, provides a realistic basis for the storage of information in three dimensions.

**Figure 2.3:** The Paging, Writing, and Erasing operations correlated with the absorption spectra of each protein state. Paging activates the protein (outermost arrow), while Writing drives O to P and Erasing drives Q back to bR. The isomerization states of the chromophore and the absorption maximum of each state are also shown.

**Writing:** **Figure 2.4** illustrates both the parallel write and read operations for the sequential one-photon branched photocycle architecture. The process of orthogonal paging is shown in insert (a): volumetric elements within the cube are defined by the cross-sectional volume defined by the paging and data lasers. Note that these two lasers are not fired simultaneously, as illustrated in **Figure 2.4** (right- and left-hand columns). The vertical axis denotes time relative to the firing of the initial paging laser. To initiate the writing process, the paging lasers are fired to activate the protein. Photochemistry is initiated and after approximately 1 millisecond, the bulk of the protein excited during paging has cycled into the M-state. After an additional ms (2 ms relative to paging) the protein exists in the O-state, and the data laser is fired. The latter is modulated by some sort of spatial light modulator that defines exactly what volumetric elements will be irradiated in the paged region. Within these volumes, the branched photocycle is initiated photochemically by driving the O-state into the P-state. Finally, P decays to Q over several hours ($\tau_P$), completing the writing process. The full writing sequence (to the P-state) is complete in roughly 10 ms, the time necessary for the protein to complete the photocycle.

96

**Reading:** The reading process is unique in that it only examines those elements of data that exist as binary ZEROS. The operation starts out identically to that used to write data (**Figure 2.4**, right-hand column). The paging laser is used to select the page of interest, and after a few milliseconds, the majority of the protein excited by the paging operation exist in the O-state, just as in the writing process. Once again, the data laser is fired, but this time at a much lesser intensity. The amount of light allowed through the spatial light modulator is adjusted to be absorbed completely by the protein in the selected page (0.01% of full intensity). No appreciable photochemistry is stimulated by the low intensity laser light (the O $\rightarrow$ P transition is not very efficient), and those volumetric elements existing in the P- and/or Q-states are invisible to the wavelength used. Therefore, regions of the cube that exist as binary ones transmit the low-intensity light, because it can't be absorbed by P ($\lambda_{max}$=480 nm) or Q ($\lambda_{max}$=380 nm). The transmitted light is imaged onto a CCD or CID detector. If the page is imaged prior to, and then



**Figure 2.4:** The parallel write and read sequences (time progressing from bottom to top). The write sequence (left column) is as follows: (1) turn on the paging laser to activate the bR photocycle within selected page, (2) after ~2 ms, activate 690nm data Laser and select data elements with SLM to convert O to P. The read sequence (right column) is as follows: (1) page, (2) after ~2 ms, read entire page as an image on the CCD array detector. The basic optical architecture is shown in insert (a).

again during the firing of the data laser, a differential read can be done which has the added benefit of enhanced sensitivity. In this way, the read process essentially examines only the binary ZEROS, while leaving the ONES unperturbed, resulting in a reading operation that is totally nondestructive. Because the O-state has an absorptivity better than 1000 times larger than that of the remaining volume elements combined, a very weak read beam can generate a large differential signal. Erasing operations are currently implemented with a standard Xenon lamp to provide the blue light necessary to drive Q back to BR; because blue diode lasers do not yet commercially exist, at this time data can only be erased via a global operation. **Figure 2.5** shows a schematic of our current prototype performing routine operations.
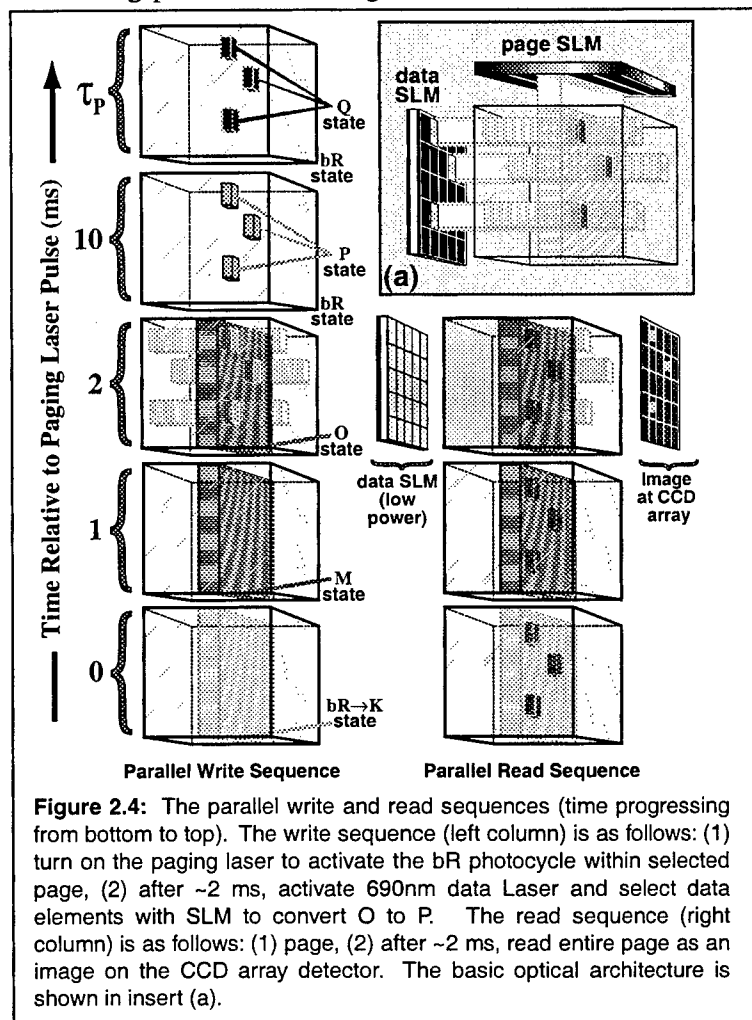
**Figure 2.5:** Schematic representation of the bacteriorhodopsin branched-photocycle 3D memory prototype, illustrating all routine data operations. See text for explanation. QHL = quartz halogen lamp, PA = page aperture, DBS = dichroic beam splitter, PBLN = prismatic beam line narrower, DC = data cuvette, BEO = beam expanding optics, SLM = spatial light modulator, BCO = beam condensing optics, DCKH = data cuvettet kinimatic holder, PTC = peltier temperature controler, CCD = charge coupled device (detector).
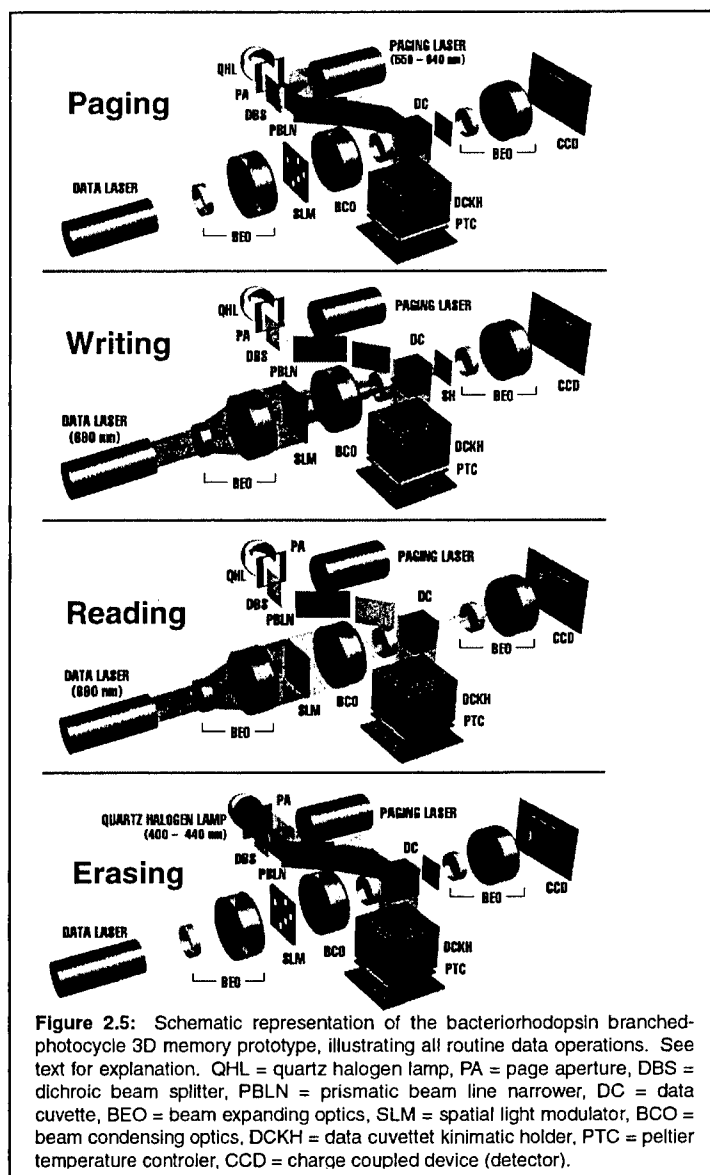
Before commercialization can be seriously considered, several issues must be addressed. Problems exist with both the materials used to manufacture the actual memory gels, and the overall reliability of the system. The memory gels consist of the protein encapsulated in polymer matrix, sealed in an optical cuvette. Long-term curing processes in both the polymer and the epoxy used to seal the cuvette cause the gel to contract and dehydrate, thereby compromising the ability of the gel to function adequately. The protein needs an aqueous environment in order to function properly. Contraction of the gel reduces optical quality, and shifts the relative locations of binary data. Several novel polymer host matrices are currently being investigated to address both issues. Improvements also need to be made in the overall efficiency and reliability of the system. One problem in this regard is with the reading operation; because intensity (as registered by the CCD detector) is used to distinguished a binary ZERO from a binary ONE, a range exists where the computer is unable to make a conclusive determination. Improvements in the optical system, and implementation of Fourier optical schemes, are expected to further improve the efficiency of the reading process. Another approach is to increase the efficiency of the formation of the P-state from O. As previously mentioned, this transition proceeds with very low efficiency, such that the yields of P (and Q) are relatively poor. There are two ways in which this efficiency can be increased: by optimization of O-state yield (i.e., a mass effect), and by optimization of the efficiency of the O to P transition. Both chemical and genetic methods (mutant proteins) are expected to help. A class of charged organic molecules called bolaforms has already been demonstrated to increase the yield of O—if more O is formed during the photocycle, more P will be formed during a write operation. And several mutant proteins have already been described in the literature that enhance the formation of the O-state.

Finally, methods by which the overall storage capacity of the memory gel can be increased are also being investigated. One that has been mentioned already is the implementation of Fourier optics. If information can be written in the Fourier plane, rather than the image plane, the optical system will be greatly simplified, the size of an individual page will decrease, as will the overall size of the prototype (a key requirement for ultimate commercialization). Other improvements include the implementation of polarization and gray-scale multiplexing techniques, which allow the storage of multiple sets of data in the same three-dimensional space. Polarization multiplexing utilizes the polarization of the laser light used for write and read operations to address individual populations of protein molecules. Different polarizations will address separate populations of bacteriorhodopsin molecules within the same volume. For any individual binary volumetric element, if two polarizations of laser radiation are used instead of one to write information, the storage capacity of that volumetric element is effectively doubled. The two polarizations should be orthogonal to minimize cross-talk. A 32-level gray scale can also be implemented, which has the modest effect of increasing storage density by a factor of five. With the implementation of just these techniques, the storage density is increased by an order of magnitude over the previous technology.

Over the past year, progress has been made in most of the areas described in the original Statement of Work for this contract. Although we are lagging behind in the materials work, in other areas we are ahead. However, this is not to diminish the importance of the materials research effort, and during the next year a considerable amount of additional time and resources will be dedicated toward resolving these issues (described in more detail below).

## 3.0. Progress by Task

In this section progress will be detailed in a format loosely based on the tasks described in the original Statement of Work. Included with each section is a Gantt chart detailing the real progress in each task, as determined by the people working in each respective area.

## 3.1. Materials

The materials research effort for this contract consists of two primary research efforts: development of an optimized bacteriorhodopsin protein for enhanced performance as the active element in the three-dimensional optical memory, and optimization of the polymer matrix that encapsulates the protein, especially with respect to optical quality and long-term stability. The latter effort is being done largely via subcontract to Dr. Wayne Wang and coworkers of Carleton University in Ottawa, and will be treated first.

### 3.1.1. Development and Optimization of the Polymer Matrix for the BR Memory Media

| ID | Task Name | Duration |
|---|---|---|
| 1 | BR Memory Cell Fabrication | 891 days |
| 2 | Analysis of Scattering an | 97 days |
| 3 | Evaluation of mutant BR n | 262 days |
| 4 | Cuvette Sealing | 544 days |
| 5 | Polymer Development | 891 days |
| 6 | Screening of BR-c | 66 days |
| 7 | BR-Compatible \ | 30 days |
| 8 | BR-Compatible \ | 36 days |
| 9 | Completion of BI | 0 days |
| 10 | Low light-scatterli | ######## |
| 11 | Effect of monon | 87 days |
| 12 | Effect of polyme | 50 days |
| 13 | Effect of Crossl | ######## |
| 14 | Effect of additiv | 131 days |
| 15 | Optimization of r | ######## |
| 16 | Obtain BR-poly( | 0 days |
| 17 | Provide improve | 0 days |
| 18 | Improvement of L | ######## |
| 19 | Study of gel shr | ######## |
| 20 | Photo-acids/Phc | 122 days |
| 21 | Optimization of j | 175 days |
| 22 | Fabricate memo | 0 days |
| 23 | Prepare suitablr | 0 days |
| 24 | Optimized formuli | 260 days |
| 25 | Design and test | 130 days |
| 26 | Analysis and te: | 130 days |
| 27 | Photo-curable Mel | 676 days |
| 28 | Evaluation of Ac | 44 days |
| 29 | Modification of / | 109 days |
| 30 | Synthesis of ph | 152 days |
| 31 | Preparations of | 131 days |
| 32 | Curing Study | 66 days |
| 33 | Analysis and O| | 174 days |
| 34 | Process Paramete | 128 days |
| 35 | Large-scale prc | 83 days |
| 36 | Pre-pilot produc | ######## |
| 37 | Obtain all proce | 0 days |
| 38 | Produce memor | 0 days |
| 39 | Final Technical I | 0 days |
| 40 | Invention disclo: | 0 days |

## 3.1.1.1. Screening of potential polymer systems for biocompatibilty & light scattering:

The basic requirements of such a matrix were defined from the start as follows; 1) the hydrogel must display low light scattering properties and 2) the hydrogel must be biocompatible with BR. Thus, we initially screened several potential hydrogel-forming polymers for both these characteristics. What this research defined was that several polymers were not suitable for use due to a failure in biocompatibility with BR or that some polymers had "good" biocompatibility but poor light scattering properties. One polymer in particular was found to display both the required properties however, it did not contain a crosslinking site and hence would not form a stable structure. We therefore turned our attention to a polymer that displayed poor light scattering and high biocompatibility in hopes of improving its overall light scattering properties.

100

### 3.1.1.2. Investigation of hydrogel variables and optimization of conditions:

Polyacrylamide (PAm) was chosen for the hydrogel matrix due to its abundant applications involving proteins, as well as the fact that it was readily available and economically favorable. Except for the drawbacks in light scattering, PAm was an ideal candidate for the project. In addition, PAm could be cross-linked with a variety of crosslinking agents which allowed for another variable to be easily investigated. After determining a suitable acrylamide concentration for polymerization and resultant light scattering, screening of the cross-linking agents was performed. From our research efforts, it was determined that methylene-bis-acrylamide (MBA) was a suitable cross-

**Figure 3.1.1:** PAM Gel Light Scattering vs Cross-linking Agent (MBA) Concentration
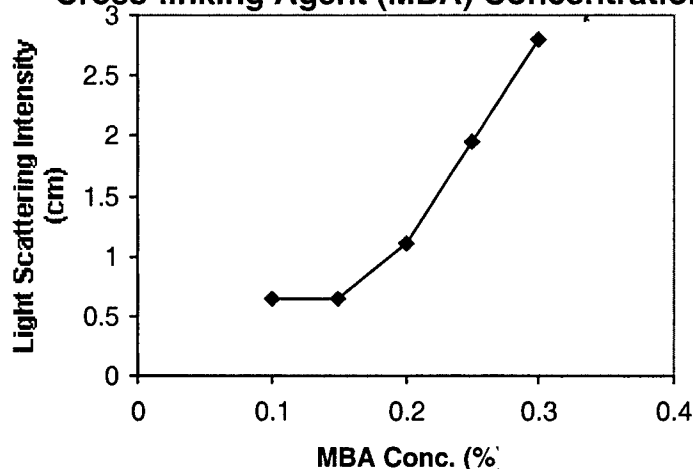
linking agent for the project so we investigated its concentration effects on light scattering of the PAm gel (Figure 1). The results defined a working range of cross-linking agent that compensated for both gel stability and light scattering properties of the gel (MBA Concentration of 0.18-0.30%).

After the basic variables were defined and optimized, our attention was turned to further improving the observed "poor" light scattering properties of PAm. From the mechanism of a cross-linking reaction during polymerization, it was known that the cross-linker brings two polymer chains together forming a four-chain joint. This increases the local polymer density at the cross-linking point. This increase in density causes the gel to have a more heterogeneous nature which then in turn, directly influences the refractive index in the gel. It was this change in matrix density which was believed to be directly related to the observed light scattering within the gel. Therefore, with this in mind we believed that the addition of a biocompatible compound to the gel solution that was not involved in the polymerization process could reduce the mass heterogeneity within the gel and hence the light scattering. Several compounds were screened for this purpose and one in particular was found to display very promising results.

101

### 3.1.1.3. Investigation of additive effects on PAm light scattering :

Sucrose was an additive which had a high solubility in water and that was biocompatible with BR. Investigations into its effects on light scattering of PAm gels revealed dramatic improvements over PAm itself. Several months were spent outlining and optimizing the conditions in which sucrose could be incorporated into the polymer system and the overall effects which it displayed. Additive concentrations of 10% sucrose up to 60% sucrose were investigated over this time. Light scattering intensity of the PAm gel was shown to decrease with increasing additive concentration. These studies were performed on series of gels each of which at a constant concentration of MBA (i.e. each series had a different concentration of MBA which was constant over that series) (Figure 2). As can be seen, the results showed that as additive concentration is increased, light scattering intensity of PAm is decreased.

**Figure 3.1.2:** Effects of increasing sucrose concentration over a range of MBA concentrations on the light scattering properties of PAm
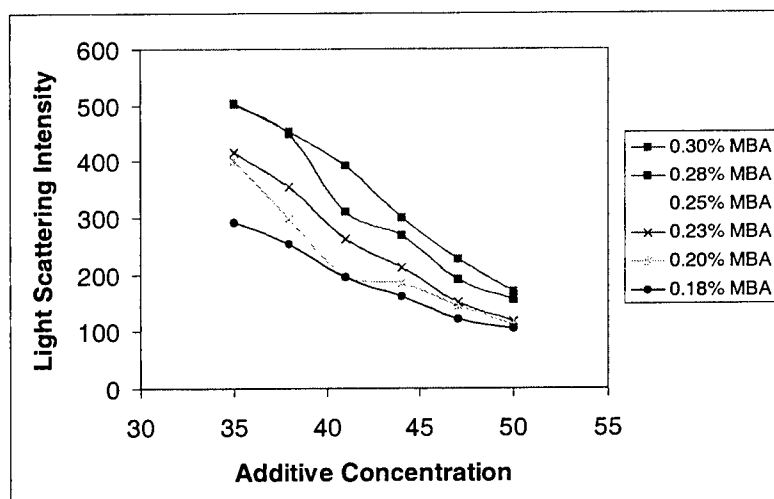


In the meantime, other potential hydrogel systems were investigated. Although we had successfully improved the light scattering properties of PAm there still remained one important problem, gel shrinkage. It was believed that since polymerization and cross-linking of PAm occur simultaneously, unreacted monomer, cross-linker, catalyst, etc., becomes trapped inside the gel framework. Over time these so called "leftovers" can polymerize and/or cross-link causing a tightening of the gel, leading to the observed shrinkage. For a 3D based memory system, this is a major downfall since it alters a given point in 3D space. Thus, the need to overcome this gel shrinkage was the driving force behind the investigation of other potential polymers. It was believed that by forming the polymer first, purification of this polymer from any unreacted species can be performed very easily. Once this is accomplished, if the polymer contained a photo-crosslinkable

site it could be crosslinked in the absence of any unreacted monomer, etc., leading to a stable gel that would not shrink over time.

### 3.1.1.4. Photo-crosslinkable Hydrogels; Monomer synthesis and copolymerization:

One of the first routes to alternative hydrogel systems was using the polymer Aquazol. This polymer was found to have both biocompatibility and low light scattering. However, it does not contain a cross-linking site so we attempted to partially hydrolyze the polymer such that we may add a photo-crosslinking site (i.e. cinnamoyl group). The polymer was successfully hydrolyzed, but once hydrolyzed it forms strong hydrogen bonding with other hydrolyzed chains in a sort of triple helix structure making it rather insoluble and unreactive towards the addition of the cinnamoyl group. This reaction may work under more extreme conditions such as in an industrial autoclave (i.e. high temperature, high pressure) but we have not pursued this approach any further as of yet.

Other approaches that have been investigated leading to alternative potential hydrogel systems include the synthesis of a cinnamyl acrylate monomer and a 2-cinnamyl oxazoline monomer (Figures 3 & 4 respectively). Each of these monomers could have been copolymerized with acrylamide and 2-ethyl oxazoline respectively to yield the desired photo-crosslinkable hydrogel once synthesized. The acrylate monomer was synthesized successfully, however, purification of the product became a problem. Thus, an alternative route to the copolymer was proposed (Figure 5). Copolymerization of acrylamide and 2-hydroxy-ethyl acrylate (HEA) was carried out first, then reaction of the polymer with cinnamoyl chloride was proposed to allow for a more easy isolation of the desired product. Copolymerization was successful, but unfortunately the polymer was not organo-soluble and hence could not be reacted successfully with the cinnamoyl chloride. In this case, slight modifications to the proposed route were made by using dimethyl acrylamide instead of acrylamide which made the end polymer more organo-soluble. Thus, a dimethyl acrylamide/ HEA copolymer (30% HEA) was synthesized successfully and reacted with excess cinnamoyl chloride. The desired modified copolymer was obtained and shown to contain the photo-crosslinking site. Further studies into molecular weights of synthesized copolymers, polymerization conditions, amount of cinnamoyl groups to incorporate, and photo-crosslinking studies are required to fully understand and optimize this approach.



Figure 3.1.3: Synthesis of photo-active acrylate monomer

Figure 3.1.4: Synthesis of photo-active oxazoline monomer
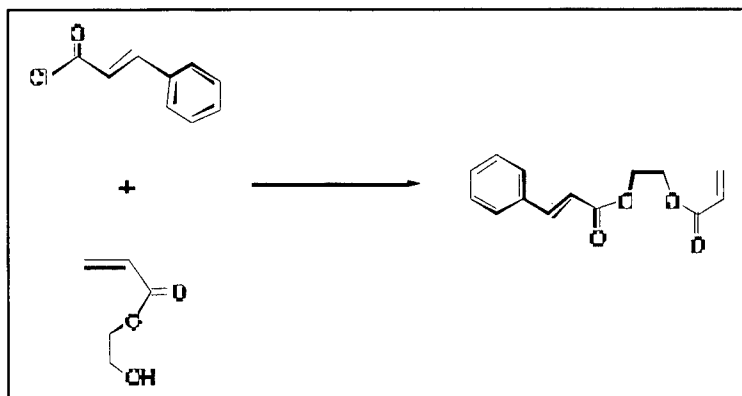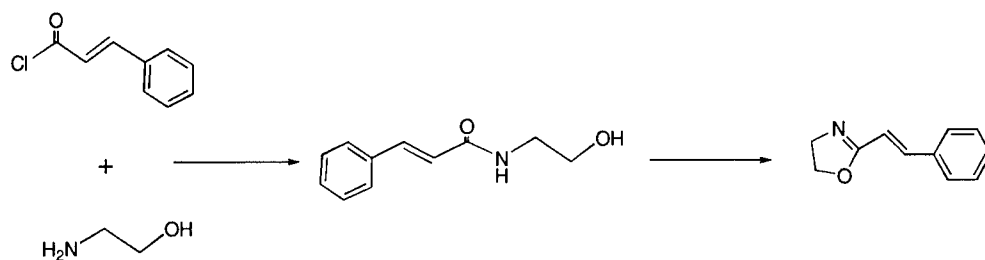
Figure 3.1.5: Alternative lab scale synthesis of a photo-curable acrylate hydrogel
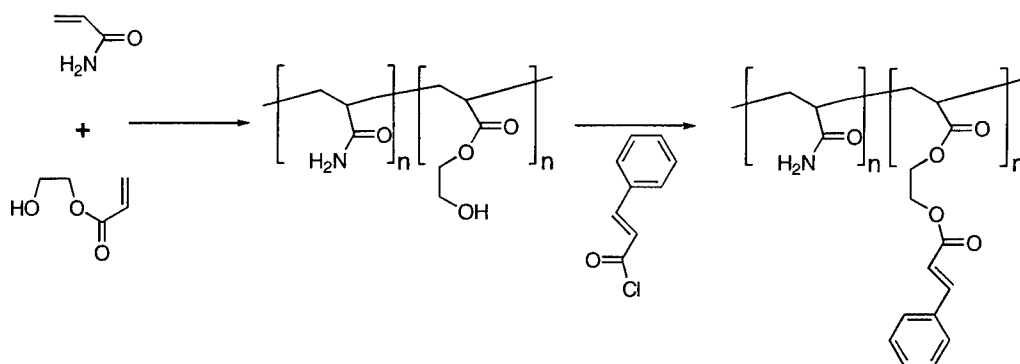


As for the synthesis of the proposed oxazoline monomer (Figure 4) , the first step has been completed successfully. The formation of this monomer has two reaction steps. The cyclodehydration in the second step is still required to finish the monomer synthesis. For all defined routes attempted and outlined above, several modifications to the reaction conditions were needed, as well as the characterization of all formed products. Therefore, several attempts were generally made in each case before getting acceptable results.

### 3.1.1.5. Additional developments and prospects :

In addition to the attempted development of alternative hydrogel systems, ongoing investigations into the current PAm system have occurred over the past year. Slight alterations to the polymerization conditions, alternative additives, and concentrations of BR to be added have all been performed in attempts to optimize the system. However, more recently incorporation of compounds to counteract shrinkage through swelling is being investigated. As well, pH effects on PAm are going to be

investigated since the swelling properties of this polymer are greatly affected by pH. Several alternative additives have been studied as well, some of which show great promise over that of the current additive, sucrose but more investigation is required.

### 3.1.1.6. Future Work:

The next year of research will be focused around the development of other possible hydrogel systems and their complete characterization, including photo-crosslinking studies and all the variables involved. As well, investigations into the PAm system will remain ongoing in hopes that the shrinkage problem may be overcome without having to change the entire hydrogel system. Means to maximize gel production will also be developed such that the complete optical cube may be produced in greater amounts in a minimal amount of time. Researchers at Syracuse University have been using the cube-fabrication protocol developed at Carleton (pAM formulation, use of refractive index matching agents, etc.) for the purpose of scattering and other spectroscopic studies.

## 3.1.2. Optimization of Bacteriorhodopsin for Efficient Data Storage



| ID | O | Task Name | Duration |
|---|---|---|---|
| 1 | | Site-Directed Mutagenesis | 718 days |
| 2 | ✓ | Establishment of Molecula | 133 days |
| 3 | ✓ | Perfection of SDM Procec | 153 days |
| 4 | | O-state Mutants from Lite | 263 days |
| 5 | | New O state mutants | 306 days |
| 6 | | O/P Mutants | 414 days |
| 7 | | 20 New Mutants | 0 days |
| 8 | | 40 New Mutants | 0 days |
| 9 | | 60 New Mutants | 0 days |
| 10 | | Development of Testing Appar | 85 days |
| 11 | | Development of Testing Appar | 90 days |
| 12 | | Spectroscopic Characterizatic | 500 days |
| 13 | | Characterize O in existing mut | 0 days |
| 14 | | Characterize O in new mutant | 0 days |
| 15 | | Random Mutagenesis | 650 days |
| 16 | | Research & Dvlpmt of Te: | 260 days |
| 17 | | Screening techniques | 262 days |
| 18 | | Finish Screening Apparat | 0 days |
| 19 | | Random Mutagenic Exper | 326 days |
| 20 | | Enhanced O-state Mutant | 0 days |
| 21 | | Enhanced P-state Mutant | 0 days |
| 22 | | Spectroscopic Character | 411 days |
| 23 | | Characterize O states | 0 days |
| 24 | | Finish screening of mutar | 0 days |
| 25 | | Fine Tune Existing Mutant | 478 days |
| 26 | | Evaluation in Memory cuv | 478 days |
| 27 | | Chemical Modification Stu | 807 days |
| 28 | | Bdatform synthesis and in | 393 days |
| 29 | | Spectroscopic Character | 414 days |

### 3.1.2.1. Establishment of a Functional Molecular Biology Laboratory

The first focus of the past year was to successfully establish a working molecular biology laboratory. The majority of the larger items were already in place at the beginning of the year (i.e. a shaking incubator, PCR/thermocycling apparatus, gel documentation system). However, in order to become completely ready to construct and characterize mutants in bacteriorhodopsin, many more items needed to be purchased. Glassware, pipettes, bottles, and storage containers had to be ordered and organized. Numerous reagents and enzymes needed to be obtained for the mutagenesis procedure. All of the enzymes needed for the synthesis of bacteriorhodopsin mutants are now on hand in the laboratory and have been used.

### 3.1.2.2. Mutant Construction - Making the DNA

There are three steps that are necessary for understanding the effects of altering the bacteriorhodopsin protein: construction of the bacteriorhodopsin gene containing a single amino acid substitution, reintroduction and expression of this DNA in *Halobacterium halobium*, and characterization of the mutant protein by spectroscopic methods.

After searching the literature, it was found that mutations of bacteriorhodopsin residues near the extracellular surface alter the lifetime of the O state. Since enhancement of the O state can lead to increased efficiency of entry into the branched P and Q photocycle intermediates, it was determined that the first mutants to be constructed would be of those residues shown to increase the O state lifetime. E194Q, and E204Q have both been shown to increase O state lifetime approximately ten-fold in relation to wild-type. Also, R82 has been shown to play an integral role in the proton movement from D85 to the proton release group (E194, E204 and bound water molecules). The first three mutations designed were based on previous experiments.

**1) E194Q** - glutamate residue 194 is changed to glutamine

**2) E204Q** - glutamate residue 204 is changed to glutamine

**3) R82A** - arginine residue 82 is changed to alanine

Since this was our first time using this mutagenesis procedure (Stratagene's QuikChange method) the first three mutants to be constructed were simply repetitions of known mutants in the literature. The purpose of this was two-fold. First, we insured the efficiency of our mutagenesis method. By selecting mutations already characterized in the literature, we reproduced and characterized mutants already constructed and made sure that these results corresponded to published data. Second, we wanted to have these mutants on hand for future studies, and for making multiple mutations.

The procedure for construction of bacteriorhodopsin mutants was carried out as described in the Stratagene protocol. The procedure involved designing mutant primers that introduce two things. First, they introduce a mutation that changes one amino acid to another. Second, they introduce a novel restriction site for quick analysis of the mutant. Initially, the three mutations mentioned above were constructed. All three of these mutants appeared to have the novel restriction site. They were then sequenced to verify

106

each nucleotide position, and to insure the presence of one and only one amino acid substitution. After verification, DNA containing these mutations was reintroduced into the bacteria.

### 3.1.2.3. Amino Acid Sequencing

In addition to the restriction site analysis performed in the laboratory here at Syracuse University, all three of the amino acid sequences were confirmed by DNA sequencing. The samples are sent out to Cornell University for prep and sequencing. This method ensures that each and every amino acid is correctly coded for. In addition, the presence (or absence) of the single amino acid mutation can be confirmed. All mutants are sent out to Cornell University before we become fully confident in the sequence. The insertion of the amino acid change and the silent restriction site can also be seen in the sequence.

We now have a standard purchase order with Cornell University, and sequencing of mutants is a routine practice for evaluating mutant sequences.

### 3.1.2.4. Bacteriorhodopsin Strain L33 (bop-)

The bop- strain (L33) has been received from Dr. Needleman, and cultures have been grown for use in the transformation procedure. The bop- strain is a *halobium* strain that contains an insertion element in the middle of the bacteriorhodopsin gene. This insertion element disrupts proper coding of the bacteriorhodopsin protein, and thus cannot produce the functional purple membrane. This strain produces white colonies when grown on basic salt medium agarose plates. Only reintroduction of a bacteriorhodopsin sequence (or one with an amino acid replacement) can restore production of the bacteriorhodopsin gene product. The gene is incorporated into the *halobium* genome by homologous recombination. Dr. Needleman has provided us with a protocol for transformation of the bop- strain, which has now proven successful on many occasions Supplies and reagents have been ordered and prepared for the transformation procedure.

Concomitant with the transformation of mutant DNA into wild-type cells is alteration in the shape and rigidity of the *Halobacterium halobium* cell membrane. In order for transformation to occur, a polyethylene glycol (PEG) solution mediates the structural change of the cell membrane from being rigid and DNA-impermeable to weakened and DNA permeable. An intermediate salt concentration of 2M is used (4M being the optimum in growth conditions and 0M resulting in lysis of the cells) in combination with PEG to allow uptake of the mutant DNA plasmid through the cell membrane.

Perhaps one of the most readily observed results of the PEG mediated transformation is the change in cell shape. The cell walls of *Halobacterium halobium*,

when transferred to spheroplasting solution (2M salt, PEG) undergo a geometric change from rod shaped to spherical.

This structural change can be witnessed with the aid of a microscope capable of 10 Ångstrom resolution. The rod shaped bacteria are approximately 10 X 2 Angstroms, while the spheroplasted cells have a spherical measurement of approximately 5 Angstroms in diameter.

### 3.1.2.5. Transformation of Bacteriorhodopsin Mutants into L33 Cells

Once the mutant sequences were verified, the DNA was reintroduced into the bacteria using a protocol supplied by Dr. Richard Needleman at Wayne State University in Detroit. Dr. Needleman also agreed to collaborate closely with us during the process and provided assistance or advice as needed.

Dr. Needleman supplied us with a bop- bacteriorhodopsin strain. This is a strain of the bacteria which lacks a functional bacteriorhodopsin gene. DNA containing a mutation(s) was then introduced into these cells. These cells will then produce the bacteriorhodopsin protein containing the desired mutation. After the DNA has been successfully reintroduced into the bacteria, freeze-downs and plates of *halobium* containing these mutations were made. After this, we can make as much of the mutant protein as desired in the 10 liter fermentor flasks in our laboratory.

Many early attempts to transform *E.coli* strain DH5α proved unsuccessful and/or inefficient at the step of ligating and re-introducing DNA containing the mutation. Very low transformation efficiencies were obtained and it appeared that another technique might be more useful. Dr. Needleman had reported that electroporation of the cell lines prior to transformation with mutant DNA would increase the efficiency of transformation 10-100X. An electroporator was ordered for this purpose.

Two methods of making cells competent are commonly cited in the literature. Electroporation involves permeabilizing the cell membrane with electric current. This is in contrast to the conventional and current method of imparting competency by using CaCl$_2$. A short (~5ms) pulse of current is applied to the cell membrane of *E.coli*, rendering it permeable to foreign DNA for a brief window in time. It has been reported in the literature that this method can increase the efficiency of large pieces of plasmid DNA. The expression vector that was originally used in our experiments was 15kb. This unusually large plasmid should transform more readily after a current has been applied to the cell membrane.

The most challenging aspect of dealing with such a large plasmid was the successful ligation of the mutant bacteriorhodopsin genes back into the large expression vector. No successful transformations had been completed for some time. After screening of approximately seventy colonies for the mutant R82A, it was found that one colony appeared to have the proper ligated products. The potential mutant protein was

isolated from this colony for restriction digest analysis. Agarose gel electrophoresis patterns indicated that the DNA band sizes corresponded to those expected for the mutant protein. This potential mutant was sent out for DNA sequencing and the results were positive; the protein had the proper sequence for the R82A mutation, and was transformed into *halobium* for expression.

The mutant R82A was the first mutant to be successfully cultivated. Freeze-downs were made of the samples, and the protein was isolated. The mutant protein was also stored on plates containing novobiocin. Spectroscopic properties of this mutant have been analyzed. UV-vis spectra of this mutant confer with known literature, and the $\lambda_{max}$ of this protein at pH 7 is ~580 nm. Titrations with HCl have been conducted, and absorbance changes in the protein have been measured. At pH 3 there is a shift toward 600 nm. At pH lower than 3, and down to 0, there is a shift back to 568 nm. Measurements at lower pH were generally unreliable due to aggregation of protein at low pH.

HCl titrations on wild-type bacteriorhodopsin were also conducted. Results of these experiments correlated nicely with the literature. At pH=3, the absorption maximum reaches 600 nm, and at lower pH the purple form is evident. As in R82A, the protein aggregates at lower pH (i.e. pH <=1.5).

After the construction of R82A using a 15 kilobase size plasmid, a new and revised technique was adopted to construct mutants. The mutagenesis procedure has been successfully refined to make the procedure easier and more time-efficient. The wild-type bop piece has been isolated and ligated into a different expression vector, pMR4. This vector was provided by Dr. Mark Braiman here at Syracuse, who has constructed bacteriorhodopsin mutants in the past. This ligation eliminated 3 steps from the mutagenesis procedure. One of the steps that was eliminated proved to be most troublesome, and circumventing this step provided the most efficient means for constructing mutants. The bacteriorhodopsin gene in this plasmid was sequenced and confirmed at every residue.

The new method utilizes a plasmid that has a size of 8 kilobases instead of 15 kilobases. This makes it unnecessary to ligate the bacteriorhodopsin gene to the plasmid before transfection; polymerases used in our current mutagenesis system have advanced enough to complete the thermocycling reaction with a plasmid of size 8kb. This bypasses the need to use the larger 15kb expression vector, and makes our procedure faster and more efficient than any currently existing one.

Using this new protocol, mutagenesis was attempted on the wild-type bop piece. E194Q and E204Q have been successfully transformed and expressed in *Halobacterium halobium*.

After the successful construction of these other two mutants, many more have been constructed. Below is a list of mutants which we currently using the new procedure. A total of 15 mutants have been constructed to date, and these proteins are now in the process of being isolated and analyzed.

D85N
R82A
R82C
R82K
R82Q
R82A/E194Q
R82A/E204Q
R82A/E194Q/E204Q

D96N
E194C
E194Q
E194Q/E204Q
E204Q
E204C
F208N

### 3.1.2.6. Collaboration Established

A collaboration with Dr. Needleman was established and dates were assigned for a visit that happened in early December. Mutagenesis procedures were refined and new mutants were supplied by Dr. Needleman and his technician. Since Dr. Needleman has constructed hundreds of mutations, gaining his advice and technical knowledge was critical in perfecting the mutagenesis technique. Dr. Needleman's support and advice have granted our laboratory with the capability to make site-directed mutants.

Approximately three days were spent at Wayne State University in Detroit, Michigan. Mutagenesis construction, transformation, and expression techniques were covered in detail and current protocols were advanced. Techniques were brought back and utilized at Syracuse, eventually replacing our current strategies. We learned how to overcome a few minor difficulties we had in constructing mutants.

### 3.1.2.7. Mutant F208N

Perhaps the most exciting and promising result of visiting Dr. Needleman was the procurement of a new mutant, Phenylalanine → Asparagine as position 208. A raw data spectrum was obtained from Dr. Needleman that showed marked enhancement of the O state. A long lifetime of the O state was evident in the sample spectrum; it appears to be greater than a second in length.

Although the exact mechanism by which F208N alters the photocycle remains elusive, it's position relative to the chromophore and other residues was modeled to determine it's spatial location. It was found that F208N was within 5 Ångstroms of R82, a key amino acid residue that is thought to be necessary for proper proton release to the extracellular surface. Preliminarily, it is thought that F208N may somehow interfere with the function of R82. More work needs to be conducted to determine the exact mechanism by which the O state is enhanced via alteration of F208.

In the meantime, Dr. Needleman provided us with a sample of *Halobacterium halobium* cells which express the F208N mutation. These cells have been used to inoculate 10L of broth and the protein was isolated. Spectroscopic analysis has shown

110

that the F208N mutant does indeed confer a greater O state lifetime to the protein. The sample provided by Dr. Needleman was grown and the protein containing the F208N mutant was isolated. As previously determined, the O state lifetime of this protein is increased to approximately 150-200ms. Although this length may be too long for this protein to be incorporated into the protein memory cube, it will be invaluable in further understanding the O state lifetime and the O→ P quantum efficiency. The goal now will be to understand how this mutant alters the O state, and how this mutant can be used in combination with other mutations to be useful for device applications. Other mutations may reduce the O state lifetime to a point where it will be reasonable to use in device applications.

### 3.1.2.8. Anticipated Progress

Since the site-directed mutagenesis technique has now been successfully refined and mastered, it is now our goal to examine other avenues to create and examine new mutations of bacteriorhodopsin for use in data storage. We are currently examining how to screen hundreds of random mutations quickly and easily. Once this is accomplished, we plan to use random mutagenesis and directed evolution to narrow in on a mutant which lengthens the O state, or increases the quantum efficiency by which O is driven to P and Q. A combination of site-directed and random mutagenesis techniques should lead us to the discovery of a mutant which will be optimal for use in data storage.

Also, we plan to do spectroscopic analysis of the mutant proteins already constructed, and those that will be constructed in the next year. Examination of photocycle state lifetimes and yields is necessary for understanding not only how the different mutant proteins function, but also how they can be used for improving data storage techniques. Understanding how the protein works is crucial for improving our knowledge of which residues to modify for using bacteriorhodopsin as a memory storage vehicle.

### 3.1.3. Protein Modeling and Simulations

| ID | ❶ | Task Name | Dur… | Gantt Chart |
|----|---|-----------|------|-------------|
| 1 | ✔ | Modeling Stu: | 282 d | |
| 2 | | Modeling Bi | 110 d | |
| 3 | ✔◇ | O-state M\. | 32 d | |
| 4 | ✔ | Solvate Mc | 4 d | |
| 5 | ◙◇ | Minimize st | 9 d | |
| 6 | ◙◇ | Dynamics | 66 d | |
| 7 | | Modeling Fi | 106 d | |
| 8 | ◙◇ | Input Struc | 35 d | |
| 9 | | Minimize St | 7 d | |
| 10 | ◙◇ | "Add to BR | 12 d | |
| 11 | ◙◇ | Dynamics | 52 d | |
| 12 | | Full QM/MM | 282 d | |
| 13 | ◙◇ | Set up 1BF | 55 d | |
| 14 | ◙ | Preliminary | 62 d | |
| 15 | ◙ | QM/MM cal | 56 d | |
| 16 | ◙ | O-state QA | 44 d | |
| 17 | | QM/MM on | 65 d | |
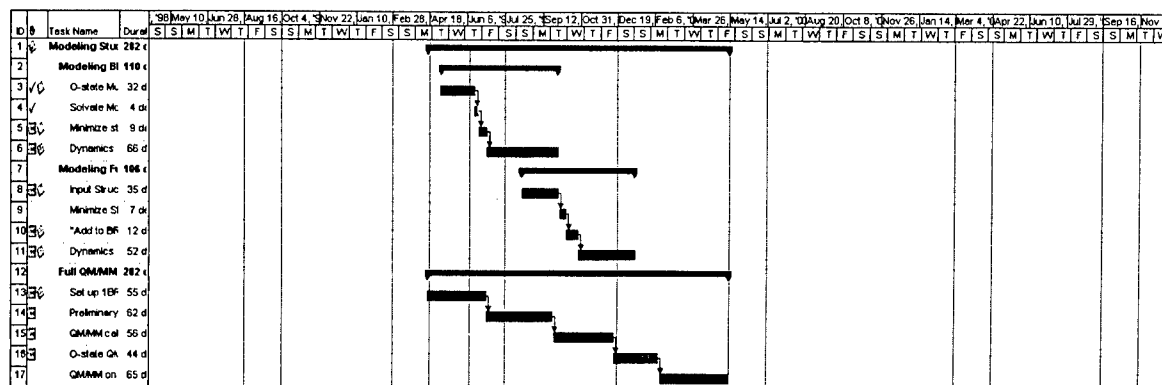
## 3.1.3.1. Progress

Any successful implementation of a branched-photocycle memory using bacteriorhodopsin requires the understanding of the branching photocycle from a structural and mechanistic standpoint. Molecular dynamics simulations and quantum mechanics are excellent tools which can be used to learn more about the O, P and Q states of the bacteriorhodopsin photocycle. The publication of several high-resolution structures of bacteriorhodopsin in the past year only added to complicate matters as these structures differed from one another in certain key areas. MNDO-PSDCI studies on the binding pockets of these structures were carried out. From our studies we concluded that the 2.3 Å structure of Leucke et al. (PDBID 1brx) was the most accurate structure and further work has been carried out primarily on this structure. This study also served in confirming the currently prevalent view that the Arg-82 sidechain is part of the chromophore-binding pocket.

The location of cation binding sites in bacteriorhodopsin is another area that has yet to be addressed satisfactorily. Knowledge of the location of these sites could be of key importance in protein modification. We carried out a series of studies based on the electrostatic properties of metal ions in proteins. These studies were backed up by quantum and molecular mechanical investigation into the feasibility of calculated binding sites. Our studies suggest that there is a high affinity binding site in the vicinity of Glu-204 and Glu-194. There are also high affinity sites on the extra cellular loops and in the chromophore-binding pocket. A manuscript for this study has been prepared for publication.

In an attempt to understand the properties of the branching reaction, molecular dynamics simulations on the O, P and Q states were carried out. The starting point for modeling the O, P and Q states of bacteriorhodopsin was the 2.3 Å crystal structure of bacteriorhodopsin ( 1brx). The chromophore and Lys-216 were combined into a single residue (LYR) for the purpose of these calculations. All minimization and dynamics simulations were carried out using the program CHARMM (c26a2) and revised all-atom CHARMM22 parameters Chromophore parameters were adapted from Hermone and Kuczera [1], who have used ab initio calculations to derive parameters for the

chromophore. All calculations were done *in vacuo*, i.e. any coordinates assigned to water in the crystal structure were ignored.

To set up our simulation, hydrogens were added to the protein, followed by 2000 steps of ABNR minimization using a non-bonded cutoff of 13 Å and a distance dependent dielectric (scaling as 1/r). These conditions were maintained throughout this study. This structure was then heated to 300 K in 50 ps employing the VERLET method, using a step size of 1 fs. Heating was followed by 50 ps of equilibration at 300 K. Through all the above calculations, the protein backbone and the chromophore were held constant. At this point the chromophore was unconstrained and the entire protein was again run through 50 ps of MD.

The structure of the O-state is a matter of debate. We used a simplified approximation, by setting the protonation states of the Schiff base and the neighboring Asp's. Asp-212 was kept unprotonated, whereas Asp-85 was protonated. The Schiff base protonation state was left unchanged, i.e. unprotonated. This was followed by 1000 steps of ABNR minimization and 100 ps of MD at 300 K. For the first 50 ps the chromophore was locked and for the last 50 the chromophore was free to move. The protein backbone was held stationary throughout the simulation.

The chromophore for this structure was converted from all-*trans* to 9-*cis* using CHARMM. Bad contacts were removed through 50 steps of Steepest Descent minimization, followed by 2000 steps of ABNR minimization. The structure was then equilibrated at 300 K for 50 ps.

After generation of the P-state, the chromophore was modified to break the Schiff base linkage, giving 9-*cis* retinal and lysine. This was achieved by creating a new residue, LYQ, and deleting the linkage between the chromophore and lysine using a patch. The Q-state was generated using the same procedure as for the P-state, i.e. 50 steps of SD minimization, followed by 2000 steps of ABNR minimization and 50 ps of molecular dynamics. All structures and trajectories were analyzed using QUANTA98 (Molecular Simulations, San Diego, CA). This analysis is still underway.

### 3.1.3.2. Future Goals

Several key processes in the bacteriorhodopsin photocycle involve the breaking and formation of bonds, including the P → Q transition. Processes involving bond changes and isomerization are poorly treated by molecular mechanics and require a quantum mechanical treatment. Unfortunately, proteins are very large and the computational resources required for a quantum mechanical treatment would be too large. Fortunately, hybrid quantum mechanical/molecular mechanical (QM/MM) methods have been devised wherein parts that undergo bond changes or isomerization can be treated quantum mechanically while the rest of the protein is treated using MM techniques. CHARMM includes a hybrid QM/MM Hamiltonian and is an ideal program to use to extend our studies to the QM/MM regime. All future calculations will also use an explicit solvent, as *in vacuo* calculations are not physically true. These calculations will

provide us with a more accurate picture of the structural and mechanistic properties of bR.

To begin this phase of the calculations, we are starting with the O and P structures generated as described in the above section. These structures will be fully solvated in 10 Å of TIP3P waters, arranged in layers around the residues. The structure and waters will be fully minimized by the standard method of alternately constraining either the protein/chromophore or the solvent, and allowing each to equilibrate. Constraints are slowly removed until a fully minimized structure is achieved. Following this, a full production run of molecular dynamics will be done, using the above-described methods, for a total of 500 ps. After this is completed, we will use the same method to study several mutant proteins, which are known to have extended O-state lifetimes. We have chosen to study E204Q, E194Q and F208N to begin this phase of our inquiry.

From the molecular dynamics trajectories, we expect to gain insight into the mechanistic properties of the different intermediates and their transitions. For example we will be able to compare and contrast the flexibility of the wild type and the mutants, as well as comparing the average structure of the O and P states. We are also interested in comparing the relative energies and the associated structures for each of these states.

1.      Hermone, A., and Kuczera, K. (1998) *Biochemistry 37*, 2843-2853.

### 3.1.4. Chemically Modified Bacteriorhodopsin Derivatives

Bolaform cations have been shown to modulate the photocycle of bacteriorhodopsin, specifically with respect to the generation of pronounced amounts of the O state during the photocycle. As such, the enhancement of the O state through the use of these organic cations has the potential to create analog BR proteins with an enhanced efficiency as a memory storage element. The reader is referred to the original proposal for this contract for details concerning the effect of bolaform cations on the O state, as well as the protocol for making the analog protein.

Fulgides represent a class photochromic organic compounds that have potential as analog chromophores in bacteriorhodopsin. These molecules are characterized by the ability to be photochromically switched between two states. However, the class as a whole suffers from low cyclicity, usually due to chemical degradation by free radical oxidation. If encapsulated in a protein matrix, the fulgides may very well be protected from such degradation. Modeling studies will soon be underway to examine the this possibility on a more formal basis. In addition, binding a fulgide into the protein binding site will pose some interesting challenges, especially from the synthetic organic point of view. This research effort will be started within the next few months.

Undergraduate honors student Bamdad Farhad has synthesized a number of the bolaform cations for incorporation into bacteriorhodopsin; he is currently in the process of confirming the identity of the compounds via NMR, etc. His synthetic routes are given below. Pending positive identification, the salts will be incorporated into the

protein using standard protocols, and evaluated for their use as an active memory element.

### 3.1.4.1. Synthesis of Bolaforms: (divalent quaternary amine salts)

Preparation of so-called 'bolaform" series of cations follows a standard method. A two-fold excess of the trialkylamine of choice was added to a methanolic solution of the dibromoalkane and refluxed for about three hours. The product, which was precipitated upon cooling the solution, was filtered off and washed three times with cold methanol. The supernatant was partially evaporated by using a rotary evaporator and few drops of ether was added before the solution was chilled to result in a second batch of product. The crude product was recrystallized three times from methanol to result in white-crystalline powder. Unfortunately, this method is not applicable to the preparation of $C_2Me_6$. The NMR spectrum reveals displacement of only one of the bromide of 1,2 dibromoethane by trimethyl ammonium. Thus, a different synthetic approach is used for $C_2Me_6$.

## Synthesis of C$_2$Me$_6$:
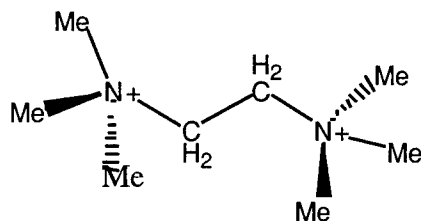


This compound was prepared by adding iodomethane dropwise into a methanolic solution of tetra methylethylenediamine. The mixture was left to stand for about an hour. The crude product which precipitated was filtered off, washed three times with cold methanol and recrystallized three times from methanol to give a white-crystalline product.

### Modern Synthesis of Bolaforms:

A six-fold excess of alkyl halide was added to the alkyl amine of choice dropwise at a rate of one drop a second. The reaction was carried out in THF and stirred while heating in order to speed up reaction. The mixture was allowed to reflux for at least 30 minutes to assure reaction completion and a water condenser was used in order to prevent reagent loss while heating. Without cooling while the mixture was still boiling, chilled diethyl ether was added and crystals were collected immediately by vacuum filtration.

The flask was cooled in dry-ice/Acetone mixture for further crystallization. The crude product was washed with cold ethyl ether at least three times and redissolved in THF/ethyl ether and recrystallized three times for purification. This method results higher purity and yield comparing to the classic synthesis discussed above and was used to synthesize the following bolaform salts.

C$_3$Me$_6$:
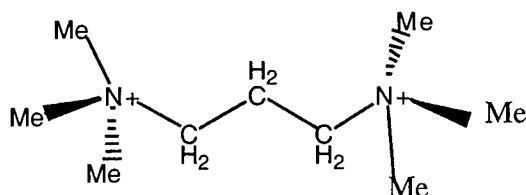
C$_4$Et$_6$:
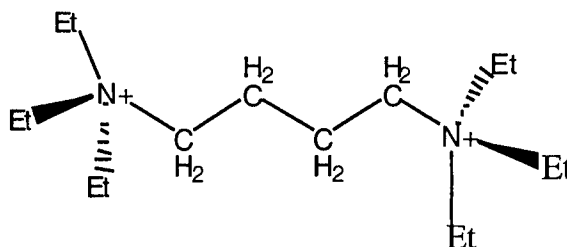
C$_4$Pr$_6$:
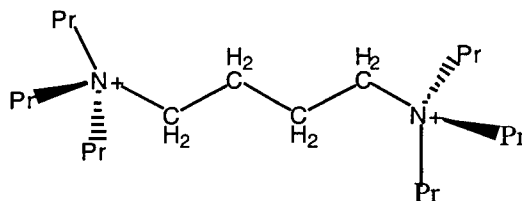
## 3.2. Prototype Development

In this section, all progress relevant to the actual construction of the prototype over the last year is described. Progress in optical layout development, fabrication of diffractive optics, electronic, and actual prototype construction will all be addressed. The work accomplished during the past 6 months (since Dr. Enrique Izaguirre joined the team in early October) can be categorized into the following areas:

A. Design and implementation of the memory prototype

B. Implementation of an experimental productions set-up for design and construction of miniaturized prototypes

C. Theoretical and experimental research in scattering

D. Examination of error correction techniques

The following sections discuss each of the above in detail, and a statement of future work is included as the end.

| ID | ❶ | Task Name | Duration | y | July | | January | July | | January | July | | January | July | |
|----|---|-----------|----------|----|------|------|---------|------|------|---------|------|------|---------|------|------|
| | | | | 3/15 | 6/14 | 9/13 | 12/13 | 3/14 | 6/13 | 9/12 | 12/12 | 3/12 | 6/11 | 9/10 | 12/10 | 3/11 | 6/10 | 9/9 |
| 1 | | Integrated Prototype Devel | 893 days | | | | | | | | | | | | | | | |
| 2 | | Modular Prototype Dev | 766 days | | | | | | | | | | | | | | | |
| 3 | | Modeling Studies | 766 days | | | | | | | | | | | | | | | |
| 4 | | Optical Layout | 523 days | | | | | | | | | | | | | | | |
| 5 | | Optical Modeling | 261 days | | | | | | | | | | | | | | | |
| 6 | | Design of Laser | 261 days | | | | | | | | | | | | | | | |
| 7 | | CCD Optics | 261 days | | | | | | | | | | | | | | | |
| 8 | | SHG Laser for | 261 days | | | | | | | | | | | | | | | |
| 9 | | Mechanical Des | 261 days | | | | | | | | | | | | | | | |
| 10 | | Optical Prototyp | 60 days | | | | | | | | | | | | | | | |
| 11 | | Optical Prototyp | 132 days | | | | | | | | | | | | | | | |
| 12 | | DSP/Motion Con | 262 days | | | | | | | | | | | | | | | |
| 13 | | Miniaturized Prototype | 893 days | | | | | | | | | | | | | | | |
| 14 | | Modeling Studies | 766 days | | | | | | | | | | | | | | | |
| 15 | | Optical Layout | 520 days | | | | | | | | | | | | | | | |
| 16 | | Optical Modeling | 261 days | | | | | | | | | | | | | | | |
| 17 | | Design of Laser | 261 days | | | | | | | | | | | | | | | |
| 18 | | CCD Optics | 261 days | | | | | | | | | | | | | | | |
| 19 | | SHG Laser for | 261 days | | | | | | | | | | | | | | | |
| 20 | | Mechanical Des | 261 days | | | | | | | | | | | | | | | |
| 21 | | Optical Prototyp | 60 days | | | | | | | | | | | | | | | |
| 22 | | Optical Prototyp | 132 days | | | | | | | | | | | | | | | |
| 23 | | DSP/Motion Con | 262 days | | | | | | | | | | | | | | | |
| 24 | | Component Fabric | 622 days | | | | | | | | | | | | | | | |
| 25 | | Establish Cap | 75 days | | | | | | | | | | | | | | | |
| 26 | | Diffractive | 75 days | | | | | | | | | | | | | | | |
| 27 | | Photoresist | 75 days | | | | | | | | | | | | | | | |
| 28 | | UV Source | 75 days | | | | | | | | | | | | | | | |
| 29 | | Diffractive Optic | 262 days | | | | | | | | | | | | | | | |
| 30 | | Higher Resolutic | 175 days | | | | | | | | | | | | | | | |
| 31 | | Further Lense D | 197 days | | | | | | | | | | | | | | | |
| 32 | | Optical encodin | 262 days | | | | | | | | | | | | | | | |
| 33 | | Miniaturization and A | 100 days | | | | | | | | | | | | | | | |
| 34 | | DSP/Motion Controlle | 262 days | | | | | | | | | | | | | | | |
| 35 | | Fabrication of Maste | 159 days | | | | | | | | | | | | | | | |
| 36 | | Optoelectronic Int | 787 days | | | | | | | | | | | | | | | |
| 37 | | First SCSI Interf | 262 days | | | | | | | | | | | | | | | |
| 38 | | Final SCSI Interf | 262 days | | | | | | | | | | | | | | | |
| 39 | | | | | | | | | | | | | | | | | | |
| 40 | | Multiplexing | 787 days | | | | | | | | | | | | | | | |
| 41 | | Modeling S | 416 days | | | | | | | | | | | | | | | |
| 42 | | Gray Scale | 152 days | | | | | | | | | | | | | | | |
| 43 | | Polarization | 108 days | | | | | | | | | | | | | | | |

### 3.2.1. Design and Implementation of the Memory Prototype

Our current prototype is a hybrid of commercially available optical mounts and those constructed in house. It represents the first generation of semi-miniaturized prototypes to be constructed, and has a modular design that enables exchange and evaluation of various components as the are designed and built. This facilitates the improvement of the prototype because it can be divided into sections avoiding excess complexity. The modular unit has been built and is being used to test improvements in the design of the optical layout, as well as for other related experiments. It consists of the following electro-optical and opto-mechanical components:

- Lasers for spatial light modulator illumination and paging

- Spatial light modulator with projection optics/controller and memory

- Bacteriorhodopsin memory cuvette mounted on a temperature controlled base

- Motorized translation stage for positioning then memory cuvette.

- CCD detector with a short focus lens system

- Soft UV lamps for global erasure of the BR memory cuvette

Our current prototype is shown in **Figure 3.2.1**.

The components of the prototype can be best described by illustrating their roles in the routine operations of writing, reading, and erasing. It is perhaps most convenient to describe these basic operations from the perspective of two orthogonal axes, with the memory cuvette placed at their intersection point. We will refer to the axis that crosses the prototype from the center of the spatial light modulator to the CCD camera as the principal optical axis. All the optical elements are aligned with this axis, with the exception of the paging lasers and their associated optics. These elements are aligned with an axis perpendicular to the principal axis (referred to as the paging axis).

**Writing:** A writing operation is initiated in the bacteriorhodopsin memory cuvette by a process referred to as paging. A thin slice of the cube is selected optically using lasers. The dimensions of the laser beam will determine the ultimate thickness of the page; two 635 nm lasers of 30mW nominal power are used to create the page (these are the shortest and highest power laser diodes available). The two lasers are positioned opposite one another with the cuvette in-between in order to obtain uniform illumination of the page through the protein-polymer gel. These lasers are stabilized in the emitted wavelength by controlling the case temperature using a Peltier cooler with a thermistor in a closed feedback loop. The power is also stabilized by driving the lasers with a constant power feedback loop. The paging beam (a vertical line of laser light) is created from the elliptical laser beam by collimating the beam through a micro lens, followed by a cylindrical lens with a long focal length (which generates the actual line). A long focal length is used to obtain a Rayleigh range larger than the cell dimensions to keep a thin page through the entire cell. This results in a collimated beam with a rectangular cross section of 0.5mm x 15mm.

After implementing a paging operation, which serves to prime the protein for receiving data, the data must be projected through the cell in the form of an image. This results in data being stored in the plane (the 'principal plane,' or page) of the memory gel previously selected in the paging operation. All of the optics is focused with respect to this plane, which is perpendicular to the principal axis, and generated along the paging axis. This plane is fixed in space. To project the data to the selected page, two 685 nm (data) lasers are employed as light sources with 30mW nominal power. Two lasers are used to meet power requirements and uniformity necessary to access the branched photocycle and drive the protein from the O-state to the P-state (a big fraction of this power is lost in the spatial light modulator). As with the paging lasers, these lasers are driven at constant temperature and power and the state if the laser (i.e., 'on' or 'off') can be controlled using TTL pulses (0.1 μsec transition time). The light from these lasers is projected through a holographic diffuser (10 degree diffuser) using micro lenses, resulting in the generation of a homogeneous rectangular light source capable of illuminating the spatial light modulator without hot spots.
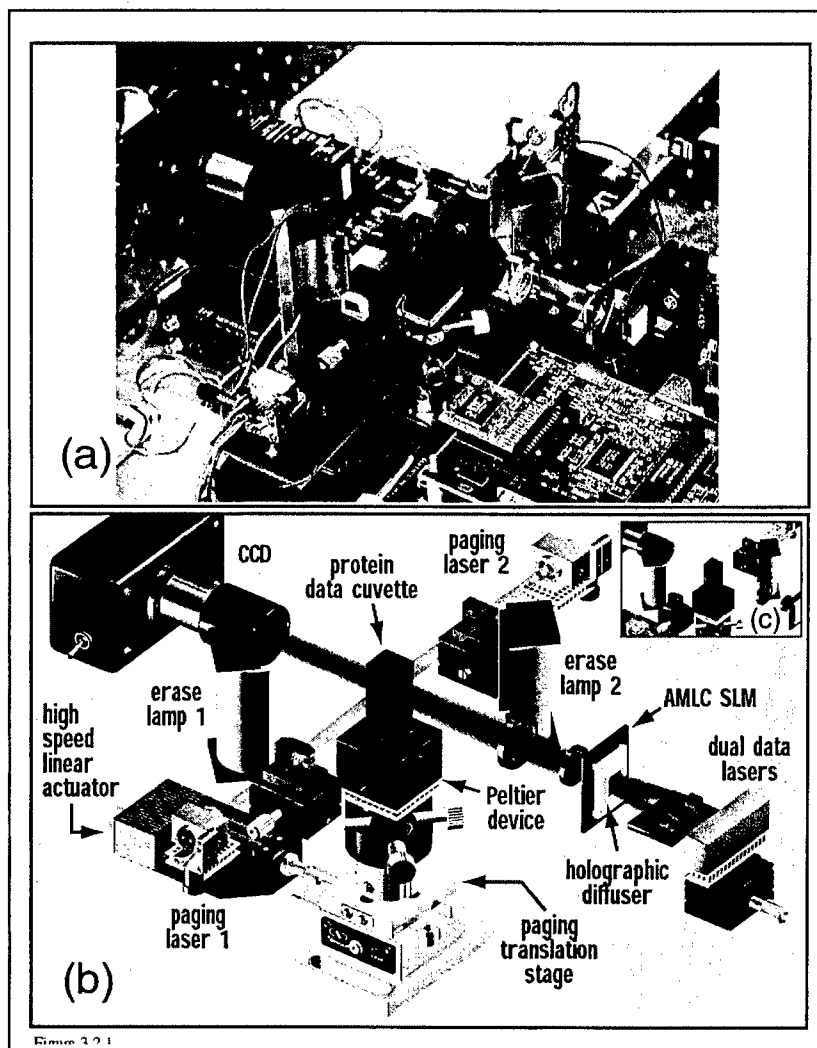


**Figure 3.2.1.** A close-up picture (a) and a schematic (b) of the current level II prototype of the branched-photocycle volumetric memory. Key components of the prototype are shown and labeled in the schematic (b). This prototype version uses a global erasure of the entire data cuvette via activation of a pair of cylindrical UV lamps which have outputs of 463 ± 40 nm. This soft uv light couples adequately to the absorption spectra of both P and Q, and sets all the bits within the entire memory cuvette to state zero (pure bR) in about ten minutes. The lamps are located at the focus of two cylindrical

hyperbolic mirrors and are collimated as shown in insert (c) so that the entire memory cuvette is irradiated when centrally located. Dual data lasers coupled to the active matrix liquid crystal spatial light modulator (AMLC SLM) via a holographic diffuser are used to generate noncoherent light so that the imaged data beam does not contain diffracted artifacts. The lower resolution of this system permits the use of a dual lens focussing system rather than a multicomponent prism system to generate the near-diffraction-limited paging beam. The other details of the memory design follow closely our basic prototype design (see discussion).

The Spatial Light Modulator, or SLM, is the component responsible for converting the electrical signal containing the information to a spatial beam profile in its spatial intensity distribution. The SLM used in this prototype is an array of liquid crystal cells with a polarizing film located behind the cells in close contact. The array's size is 320 x 240 pixels of 7.5μm x 7.5μm with a filling factor of 50% and a contrast ratio of 100:1. Its function can be described as follows: when a voltage is applied to a cell in the SLM, laser light passing through that cell will have its polarization rotated by an amount proportional to the applied voltage. After the beam crosses the polarizing film the intensity of the beam is going to be modulated according to the voltages applied to each individual cell, creating a pixelated beam where the intensity's spatial distribution is proportional to the voltage applied to the cells. In this way the light is encoded with spatial information—using a lens projection system located behind the spatial light modulator, the spatial profile of this beam is imaged on the previously selected page (at the position of the principal plane), where it is stored by the protein.

The result of the combined operations of paging followed by projection of information through the SLM is the writing of a page of data in the memory cuvette. This page will contain all the information processed by the spatial light modulator. Subsequent pages can be written after the cell is repositioned using a motorized translation stage. The new page will be located wherever the principal plane intersects the cell. The translational stage is controlled by a computer servo loop, and can be programmed to create a series of defined movements (e.g., going from one page to another). The motorized translational stage has the following mechanical characteristics: +/-1μm bi-directional repeatability, 0.59 μm resolution, and 6mm/sec maximum speed. Translational backlash is eliminated by software so that pages will not be accidentally misplaced. Bacteriorhodopsin, the active element of the memory medium, is housed inside a polished optical cuvette. The temperature of the memory cell is maintained by Peltier devices.

**Reading:** A reading operation is implemented in a manner very similar to writing, using a Charge Coupled Device (CCD) to digitize information read out of the optical memory. The CCD has the same resolution as the spatial light modulator (one to one correspondence) or higher (over sampling) and its exposure time can be controlled using TTL signals. In order to guarantee the acquisition of data with a high contrast ration, several requirements must be met: The CCD lens must have a short depth of focus with the focal plane located at the page in the principal plane (which is the same location of

the image created by the projector lens of the spatial light modulator). To read a page, the translation stage is moved along the principal axis until the page to be read is aligned in the principal plane. The paging lasers are turned on to activate the aligned page. The data lasers are fired and the spatial light modulator is used to create a low intensity and uniform beam, which (in effect) illuminates the page to be read. The stored information will act as a transparency, creating an object with the shape of the stored information. The CCD camera then starts its integration cycle until a clear image of the page is stored. With the data extraction from the CCD the reading of the page will be completed.

**Erasing:** An erase operation in the bacteriorhodopsin-based volumetric optical memory required blue light in the region of 380 – 480 nm. Lasers in this region of the visible spectrum are not yet commercially viable, which precludes their use in our memory architecture. For this reason, only a global erase is currently possible, i.e., the entire cube is erased at once with incoherent light. In its current implementation, two soft UV lamps are incorporated into the prototype to serve this function. These cylindrical UV lamps have their emission maximum centered at 463 nm with a FWHM of 40 nm (covering the absorption band of both the P and Q states). The lamps are located at the focus of two cylindrical hyperbolic mirrors. This geometry will generate a thick collimated beam that illuminates the entire BR memory cell. The lamps can be turned on and off by a TTL pulse which controls an inverter that ramps the low voltage source (12V) to the lamps' operating voltage (800 V).

The electro-optical elements described above require hardware in the form of control boards to make them function. All of the controllers will be synchronized in a host computer using the Lab View software package. The principal electronic components are detailed below (see Figure 3.2.2).

a). Constant power drivers for laser diodes with TTL control (four), to allow stabilization of the power and interface between the laser and the timing generator.

b). Temperature controllers for Peltier devices (five) for lasers and memory cell to regulate and stabilize temperature, as described above.

c). Programmable motion controller to drive the translation stage.

d). Image acquisition board and timing board for CCD camera to interface between the host computer and control the integration time of the camera.

e). Spatial light modulator controller with Flash memory to store test patterns; the controller converts a bit-mapped file to the SLM format, which can be stored in a flash memory for later use.

f). Timing generator to generate the reading, writing and erasing TTL sequences; the generator will create the TTL pulses needed to control the timing of the lasers, the camera, etc.

g). Analog acquisition board for power and temperature readings to facilitate analog to digital conversion of different control parameters during the prototype development, as well as for experimental uses.

The modular prototype is currently being evaluated and improved. The results of these evaluations will be valuable for design and construction of smaller prototypes, already underway.

## Figure 3.2.2. Block diagram of electronics
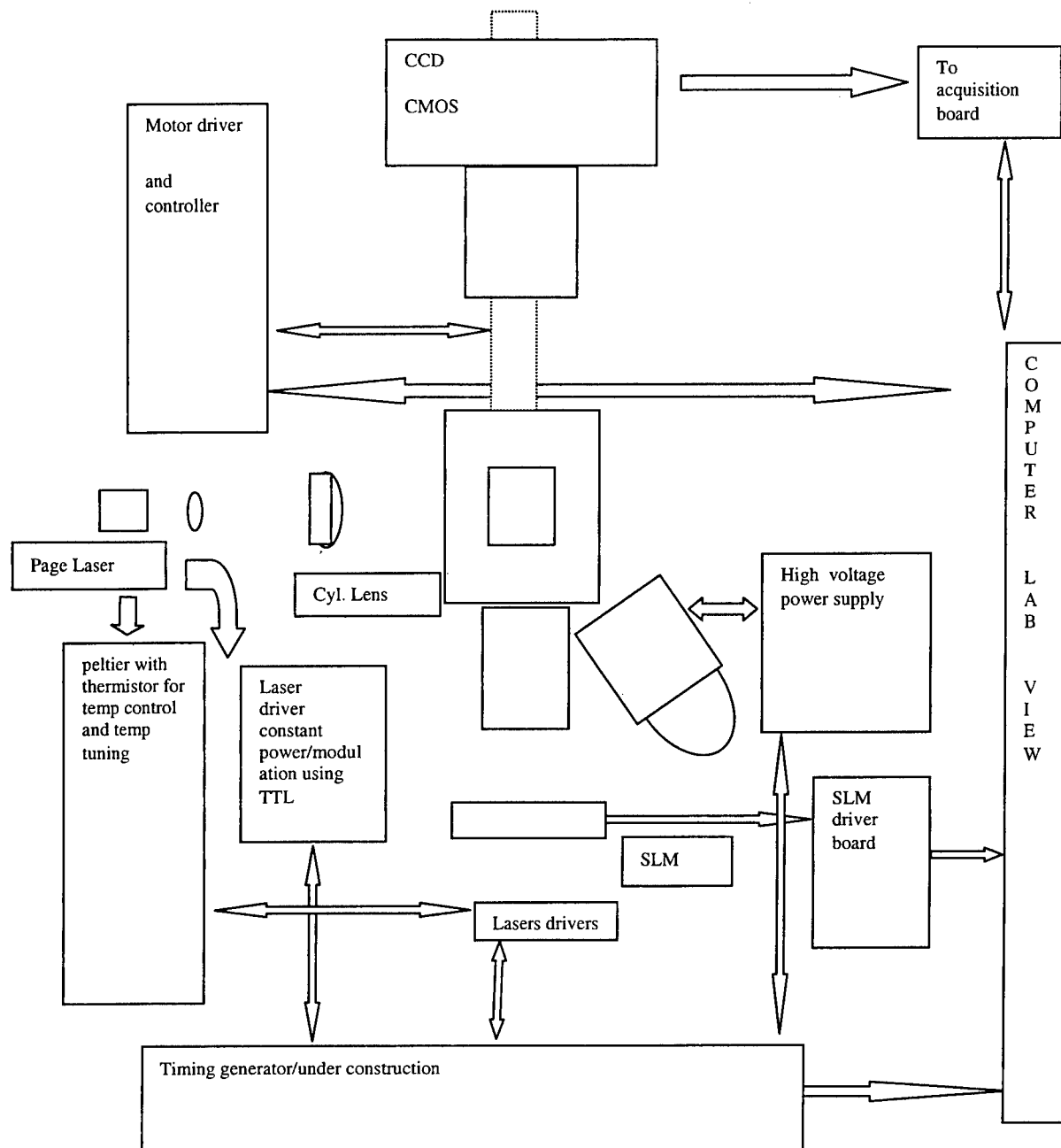
**Figure 3.2.3.** (a). Intensity profile of page through cube length. (b). Profile through cube width. (c). Three dimensional compilation of page showing both dimensions.
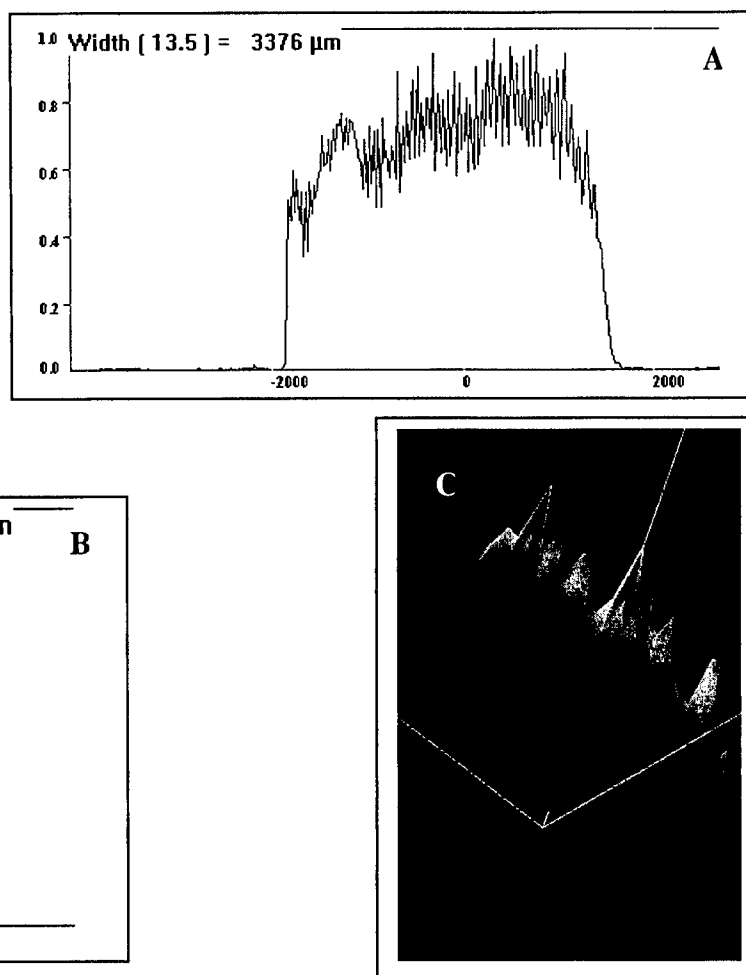


Experiments have been done evaluating the two dimensional beam profile and focussing the laser beam; the importance of these tests becomes obvious when considering the that these lasers are used either to illuminate the SLM (for the data lasers) or to define a page. The laser spatial profile for the paging lasers was measured in the actual set up. The sharpness of the image generated by the SLM was also measured. A typical measurement of the page thickness is in **Figure 3.2.3**. These measurements aid in fine-tuning the optical layout. With our current optics, the minimum page's thickness is 175 μm, but during the next month we plan to refine the optics to make it thinner. According to measurements of refractive distortion, the current pixel size for this prototype is 1 mm$^2$ (again, with the current materials and optical layout). Other improvements in our prototype are focused on the erasing process. For erasing individual pages, (rather than a global erase system as exists in the current prototype), a 355 nm source is needed. A Nd:YVO4 Q-switched and tripled diode pumped laser is currently being developed. In addition, the 635 nm lasers currently being used for paging will be exchanged for higher output lasers, and we will be testing (for paging) a 513 nm laser source (doubled Nd:YAG) that is currently under development.

### 3.2.2. Construction of Miniaturized Prototypes

During the past month, progress was made in several areas of the miniaturized prototype construction. The machines required for fabrication of the mechanical parts necessary to mount the optics and translational stages were installed. We also have the machinery and software to design and construct circuit boards using surface mount components. All of these machines are CNC operated, which will enable us to go from a CAD design to the final product. The software is working properly, and we are currently preparing to start fabricating the compact optical mounts and laser alignment systems all on a small board with a PCI-like format.

### 3.2.3. Theoretical and Experimental Research in Scattering

Lastly, a theoretical study is currently in progress on the scattering produced by the BR-gel memory medium. The study employs the theory of non-linear scattering (using transport theory to account for multiple scattering processes). A code capable of simulating the scattering problem is in development. This will provide a tool to gain insight into the fundamental issues causing the scattering, and to determine the best method by which they may be solved. This program will be used with our optics software to realistically simulate the operation of our prototypes.

As mentioned in previous reports, scattering is a primary concern for construction of our prototype, as it will affect the ultimate storage resolution of the memory. To analyze the extent of the problem, we have performed a simple experiment to quantify the small angle scattered energy. As is shown in **Figure 3.2.4. a**, the experimental set up consists of a cell mounted in a translation stage, from which the scattered light is projected onto a screen.



Figure 3.2.4a: Small Angle Scattering Apparatus
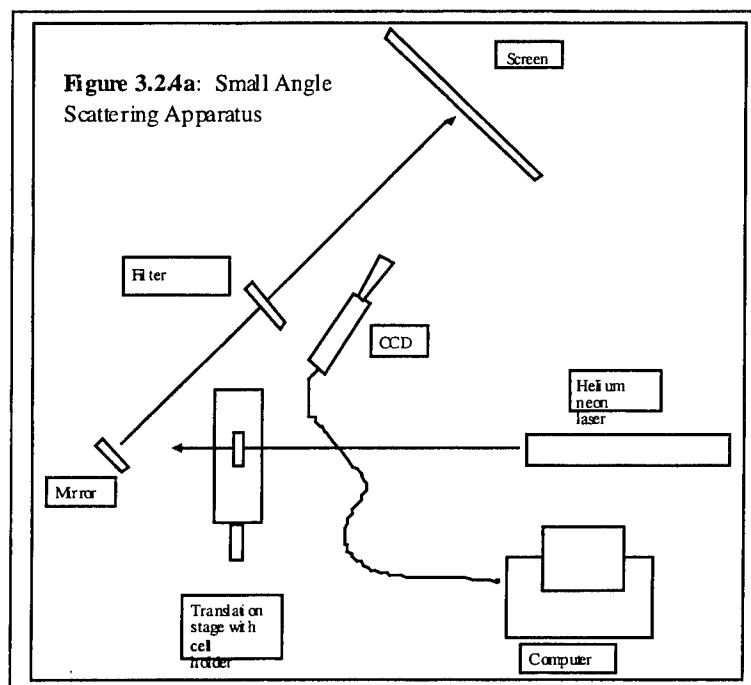
The collimated beam is filtered out and the resultant image is collected by a CCD camera for quantification. The integral of the image is calculated and the scattered energy can be compared/contrasted for different angles and samples. Using this experimental, set up we found that after a period of illumination the BR cell changes the index of refraction creating a self-modulation of the beam to a value of five wavelengths. This indicates that

we must consider this effect in future calculations of beam propagation inside of the cell, and we must also determine how to minimize this effect in order to avoid errors in reading data. We plan to continue in this direction in the following months. **Figures 3.2.4. b. and c.** show typical results.

**Figure 3.2.4b**: (Above Left) Small angle scattering for a 1cm BR cell. The image shows that most of the scattered energy is contained in angles smaller than 1 degree. This analysis will give us a clear indication of the improvements in image definition and resolution in the stored data.

**Figure 3.2.4c**: (Above Right) Self phase modulation originated by changes in the index of refraction in the BR cell. The image shows that the index of refraction is originating a change in phase of five wavelength in the observed area.

### 3.2.4. Examination of Error Correction Techniques

Several possible error correction algorithms are currently being considered, which will be executed by the DSP in order to increase the reliability of both read and write operations. An algorithm is also being considered to overcome the technical difficulties introduced by CCD technology.

The errors originated in the optics can be classified as standard aberrations and light gathering. The former is produced by optical components in the prototype, and can be minimized by using diffraction limited optics and a layout which is corrected for the principal aberrations. The latter will result in an uneven distribution of intensity across the page, which will lead to difficulties in discriminating between binary zeros and binary ones. In whatever way the errors are generated, it is important that the tools to reconstruct the data be part of the data itself, not a function of the prototype.

In our basic design the image of the spatial light modulator is projected by a two lens system to a plane inside the optical memory. Therefore, the spatial light modulator and the page of the memory are in conjugate planes. Reading is similar, except that now the page is the object and the CCD is at the image plane. If the spatial light modulator and the CCD have the same geometry (i.e., the same number of pixels, pixel size and pixel center location) the same optical system for writing can be used for reading. This, however, represents the ideal situation, and in reality this is not the case. Changes must be made in the optical system to resize the image to the proper format—the added complexity in the optical system will be considered below.

For the moment we will suppose that we have a perfectly symmetric system, with page being a mirror image of the CCD. Even for this ideal scenario, the intensity of illumination when reading the page cannot be constant. For a binary memory, however, the change in illumination through the image plane won't be serious, because the difference between the intensities that represent a binary zero vs. a binary one can be reconstructed using pixels that have a specific location and a constant value (i.e., pixels that exist for the sole purpose of calibrating the data on the page). But, the problem of page illumination will be a more serious issue when implementing a gray scale system. If each spatial location is to store more than two bits (i.e., a longer word length), it will become impossible to differentiate between pixels that vary in their gray level. There are several different solutions to this problem, all of which must meet the requirement that the solution must be independent of the prototype used to write or read information in the cube. We propose an algorithm to correct the errors originated by uneven intensity using fixed data points at the center of the memory and at the corners of the page to calibrate the light shining through the entire page and correct the overall change in the illumination in the CCD detector.



Figure 3.2.5a

An additional source of error is generated by imperfections in the CCD array, which are classified as either pixel defects or cluster defects. At this point we will focus on the former, which can be further described in terms of a total elimination of the pixel detectabillity or a partial elimination. In both cases we will assume that the corruption of the information is high enough that a defective element will not give the right reading in that location. Therefore, the same pixel is lost in every page of the memory. The following error correction method is proposed, where a structured memory is generated, as illustrated in **Figure 3.2.5**. It is assumed that there are no



Figure 3.2.5b
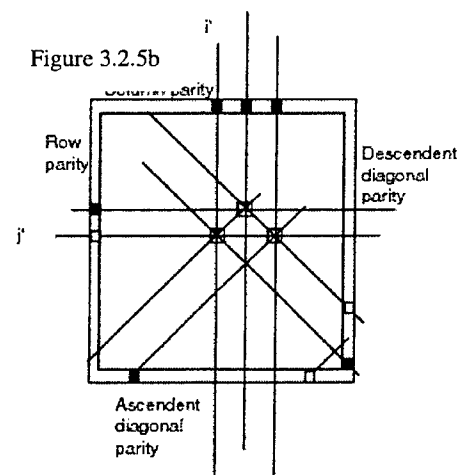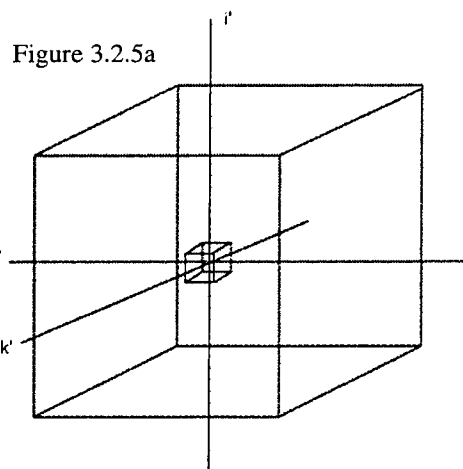
bad pixels in the perimeter of the CCD detector. In each location of the edge rows and columns, the parity of each respective row and column is recorded. At the vertices of the page the parity of the parity row or column is recorded. An example will serve to illustrate how this works. Suppose that the location Xi'j' is corrupted. Using the standard reading protocol, one page is read, after which the signal processor calculates the parity for each row and column and checks it by comparison to the values stored at the edges of the page. An error file is then generated where the parities that do not match are indicated. At this point, there are several resultant possibilities, the simplest of which is that a parity in column i' and row j' does not match. In this case, because there is a parity number for each bit, the complete word can be regenerated and kept in the error file to complete the page whenever necessary. Once this process has been completed, the location of the error can be used for other pages to avoid unnecessary repetitions during reading subsequent pages.

The possibility also exists that there will be two errors (pixel defects) in an individual row or column. For example, if there are two pixel defects in column i', then the parity of column i' will not indicate an error. Therefore, errors will be indicated in two rows, but not in the corresponding column., but the location of the errors will be indeterminate. However, the two edge lines (one row and one column) can be used to store a diagonal parity, as illustrated in **Figure 3.2.4b**. The parity of the diagonals can be used to solve the location of the pixel defects, as illustrated in the figure. Using this algorithm, cluster defects with a radius of 1 pixel element can be easily corrected. In light of the fact that most manufacturers reject units with clusters of this size, our method of data reconstruction for this kind of error will be effective in real devices.

### 3.2.5. Final Remarks

In conclusion, we have successfully constructed a modular prototype of the bacteriorhodopsin-based three-dimensional optical memory. The modules can be tested and modified to improve our design, with the ultimate goal of a more economic and reliable device. The following months will bring continued experiments on the prototype and evaluations of new designs. Additionally, new laser sources, CCDs, and spatial light modulators will be examined. The research effort on scattering continues towards a fuller understanding of the underlying processes and causes, with the goal of creating memory cells of higher optical quality. The infrastructure needed to fabricate micro opto-mechanical assemblies and electronic circuits has been established, and in the following months these will be employed to construct a single board miniaturized prototype.

### 3.3. Electronics Development

Progress in the development of the necessary electronic support for the prototype falls largely into two categories: interface development and digital circuitry to control the routine prototype operations. The progress made in both of these areas is detailed below.

### 3.3.1. Digital Timing Circuitry

Electronics technician Mike Brandt has designed two types of timing circuitry that will enable automatic control of the paging and data lasers in the prototype. The first of the two designs will consist of a programmable, free-standing unit that uses thumb-wheels to enter the values necessary for timing the lasers during routine write and read operations. The second design, which has been constructed, is an integrated ISA bus unit where all values are entered through software. All timing signals are generated by a 20MHz on board microcontroller, with the host PC used only to set the desired timing values and modes. Host software was written in Visual Basic to allow for control and display of the timing values. In order to achieve communication with the timing circuit through the ISA bus, a small Dynamic Link Library was created in 'c'. This DLL can be accessed from the Visual Basic program. The user interface appears as follows:



The prototype ISA bus card was first tested with an oscilloscope. With some minor adjustments to the microcode, the desired signal outputs were obtained. Both software triggered and externally triggered modes were tested, while in continuous mode one cycle currently starts as soon as the previous one ends. More microcode must be written to generate cycles continually at a desired frequency.

The timing generator's laser control outputs were connected to the diode laser modules, and visually appeared to work properly. Output amplifiers were added to all signal paths coming from the timing generator, providing sufficient current to drive any TTL compatible input, even over relatively long cables. The amplifiers invert the signals, so that an output bit with the value '1' results in a 0 volt (grounded) signal, which triggers the 'on' state of the lasers currently in use.

In order to test the frame grabber, the timing generator was connected to the read laser (aimed at the CCD camera) and to the frame grabber's external trigger. Full frames were captured with the trigger set to the minimum delay time.

The timing generator's output signals were observed and stored on a digitizing oscilloscope. The following graph shows actual signals for the following settings:

Page delay = $100\mu s$.    Page duration = $150\mu s$.

Read delay = $200\mu s$.    Read duration = $250\mu s$.

Frame grabber delay = 5 $\mu$s. Frame grabber duration = 5 $\mu$s.
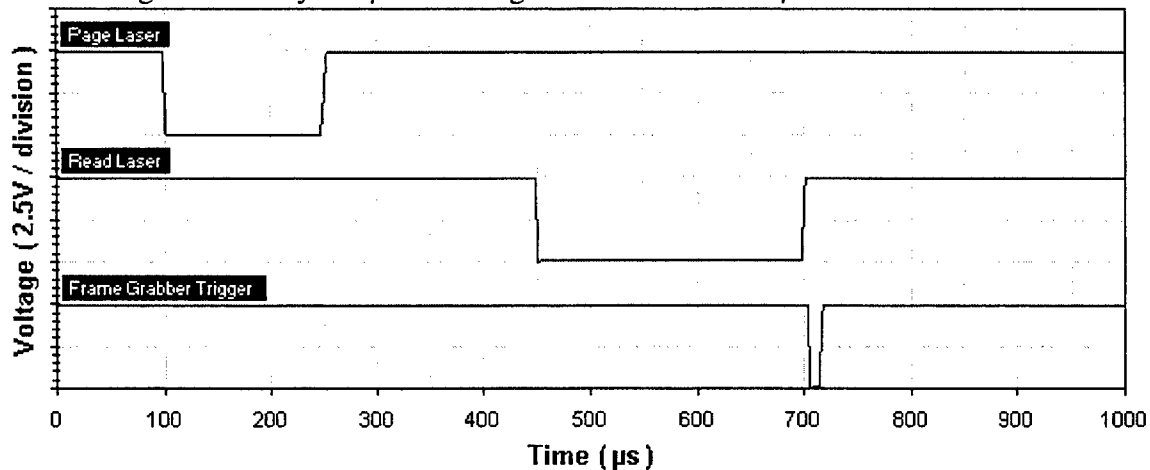


A new software package from Mental Automation, Inc. has been acquired, which includes two programs. The first, SuperCAD, is used for circuit design and analysis. The results from SuperCAD can be fed to the second program, SuperPCB, which creates printed circuit board patterns..

A circuit has been designed to be used in the stand-alone timing pulse generator, which serves as the interface between the main microcontroller chip and up to 32 thumbwheel switches which will be used to set the timing values.
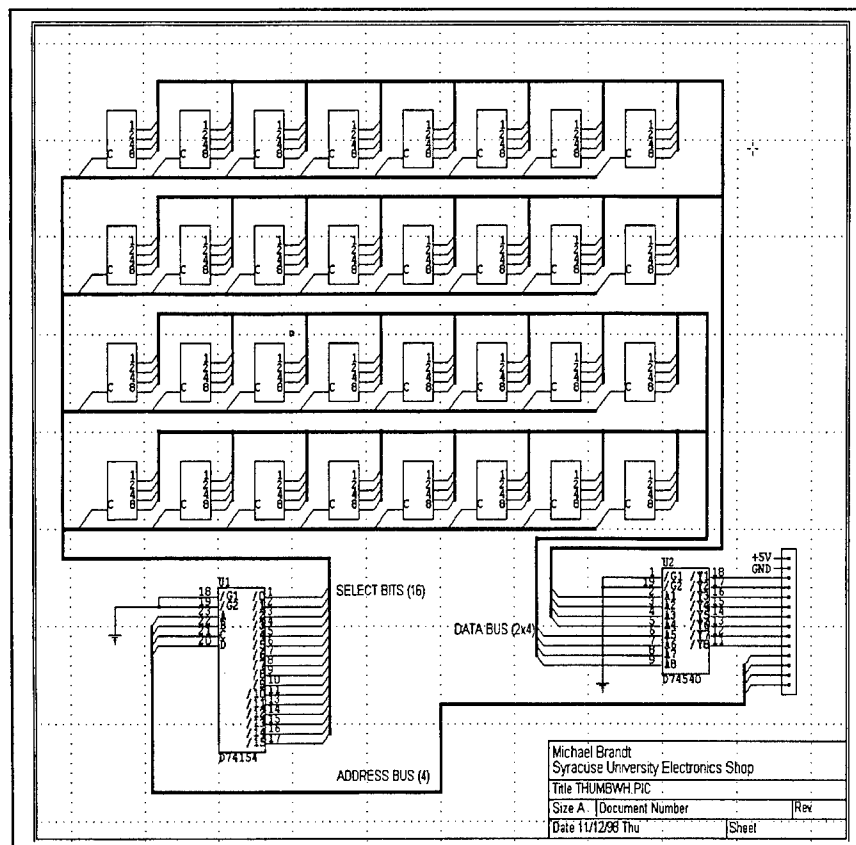
Within the project's new prototype development in early 1999, an embedded microcontroller will be interfaced to motors (for both translation of the sample as well as for adjustment of the focussing optics), to encoders for positional feedback, to the paging and read/write lasers, and to the spatial light modulator.

A number of microcontroller chips were evaluated, resulting in the decision to use Motorola's 68HC11E9. This particular chip offers the necessary ports for interfacing, including an analog-to-digital converter which may be useful for increasing the precision of the position encoders. The 68HC11 also includes EEPROM which can retain values even when the chip is unpowered. An evaluation board for the 68HC11 has been obtained; this includes a computer interface for programming the chip. Work on both the programming and the interfacing of this microcontroller has begun.
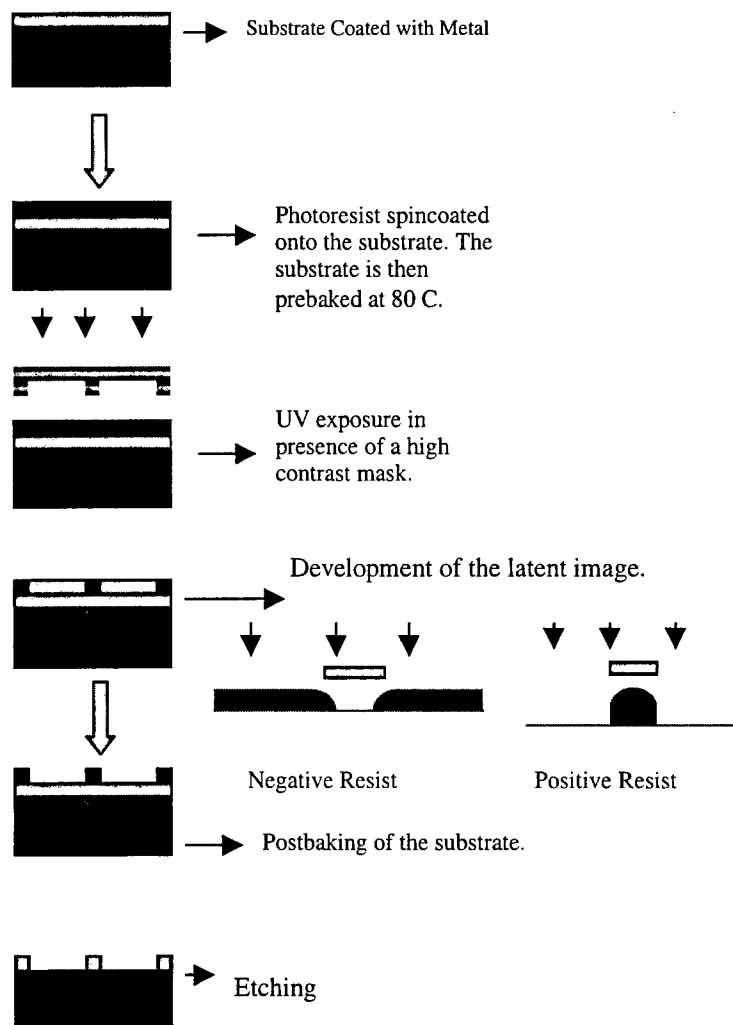
### 3.3.2. Computer Interface Development

Work in this area has started only recently. Technician Josh Weissman has been evaluating potential methods by which the interface can be developed, and has decided on the type of interface to start with (SCSI-2-A). Hardware design and construction of the interface is also underway. This portion of the project is still in its infancy, and a report on the progress made over the last few months is not currently available. A summary of the progress made to date will be reported in the next monthly progress report.

### 3.4. Development of Diffractive Optics

Of primary importance to the process of designing a commercial device is its cost and the possibility of mass production. With respect to the optical memory, the optical components constitute one of the largest factors in ultimate cost of the device. Diffractive optics provide a way by which the cost can be lowered. We are therefore actively establishing the capability to fabricate diffractive optics in house. This will make is possible to fabricate a high volume of micro optical elements for a fraction of the cost of traditional optics. Our objective is to design and fabricate diffractive optical elements (DOEs) by generating binary masks for simple structures and gray scale masks for multiple level structures or 'kinoforms'. Ordinary desktop publishing hardware and commercially available software, in conjunction with photo-reduction techniques, is being used to produce binary and gray masks for DOEs. Postdoctoral researcher Sukeerthi Seetharaman, in addition to her materials work in making protein-based memory cells and thin films, has made this effort her primary focus. Her work over the last few months is summarized below (Dr. Seetharaman joined the team in January 1999). The process is illustrated schematically below.

## Microfabrication Process

**Substrate Coated with Metal**

**Photoresist spincoated onto the substrate. The substrate is then prebaked at 80 C.**

**UV exposure in presence of a high contrast mask.**

Development of the latent image.

Negative Resist          Positive Resist

Postbaking of the substrate.

Etching

### 3.4.1. Mask generation

Simple patterns were generated using Adobe Illustrator 7.0. These patterns were transferred and photoreduced on to a transparency sheet. This was then used as a mask for lithography. Such masks were made for detector arrays and metal molds and optical encoder masks. Various mask patterns are shown below.
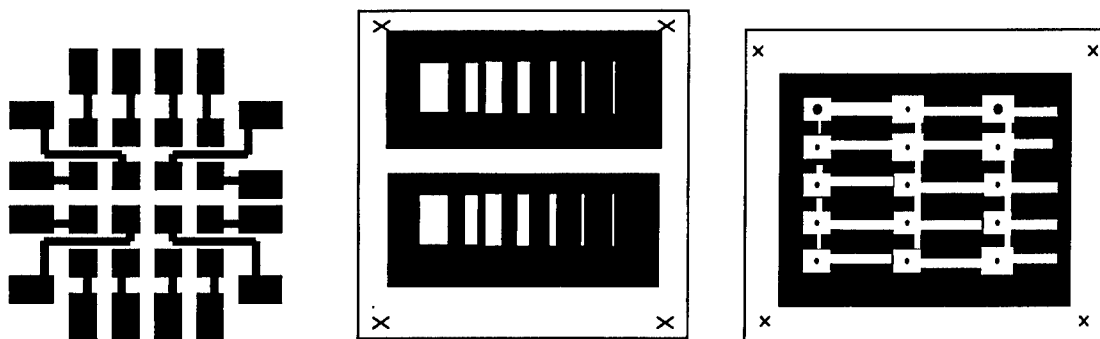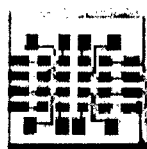
## 3.4.2. Pattern Transfer

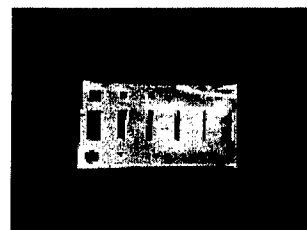### 3.4.2.1. Pattern Transfer Using Positive Photoresist (PPR)

The substrates used for pattern transfer to make metal molds were Brass sheets of (0.05 mm and 0.1 mm thickness). In addition circuit patterns onto Cu clad boards were carried out and a photodetector array was generated. AZ 1500, deep UV positive photoresist (PPR) was used. 0.5 ml of photoresist was dispensed on to the substrate and was spin coated at 5000 rpm for 30 sec. The PPR coated substrate was then prebaked at 90 °C for 30 sec to remove excessive solvent . This was followed by UV exposure. A high contrast mask was placed in contact with the substrate and was exposed to UV (435 nm) for 30 sec. The pattern was then developed in AZ 400K (1:1) developer for 30 sec to develop the latent image. The substrate was then etched in freshly prepared FeCl$_3$ solution in a Etchomatic bath with constant agitation. The substrate was then copiously rinsed in de-ionized water. The PPR from the pattern was removed by washing in acetone.
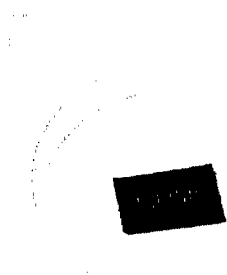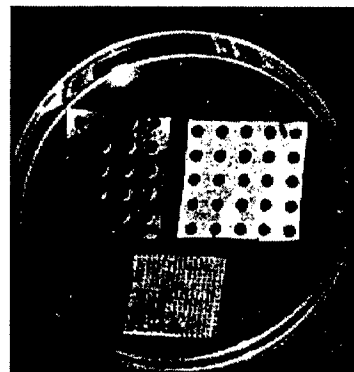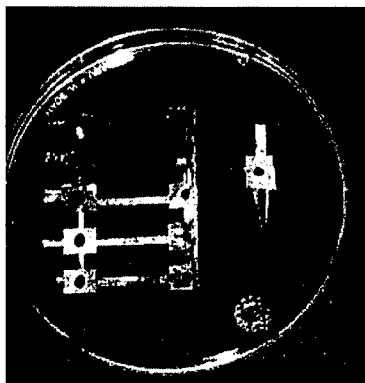


| **Circuits** | **Photodetector array** | **Metal Mold** |

### 3.4.2.2. Pattern Transfer Using Negative Photoresist (NPR): Brass sheets

The substrates used for pattern transfer to make metal molds were Brass sheets of (0.05 mm and 0.1 mm thickness). KPR111(Kodak photoresists), negative photoresist (NPR) was used. Brass sheets were dip coated with NPR. The NPR coated substrate was then prebaked at 90 °C for 30 sec to remove excessive solvent . This was followed by UV exposure. A high contrast mask was placed in contact with the substrate and was exposed to UV (435 nm) for 30 sec. The pattern was then developed KPR developer. The sheet was then etched in Kepro FeCl₃ solution in an Etchomatic bath with constant agitation. The substrate was then copiously rinsed in de-ionized water. The NPR from the pattern was removed by washing in acetone. The metal molds are shown in the photographs below.



## Metal Molds for optical encoders

### 3.4.2.3. Pattern Transfer Using Negative Photoresist: Stainless Steel Sheets

The substrates used for pattern transfer to make metal molds were Stainless Steel of (0.04 mm and 0.1 mm thickness). KTFR(Kodak photoresists), negative photoresist (NPR) was used. Stainless steel sheets were dip coated with NPR. The NPR coated substrate was then prebaked at 90 °C for 30 sec to remove excessive solvent . This was followed by UV exposure. A high contrast mask was placed in contact with the substrate and was exposed to UV (435 nm) for 30 sec. The pattern was then developed KPR developer. The sheet was then etched in Kepro FeCl₃ solution in an Etchomatic bath with constant agitation. The substrate was then copiously rinsed in de-ionized water. The NPR from the pattern was removed by washing in acetone. The metal molds are shown in the adjacent photograph.
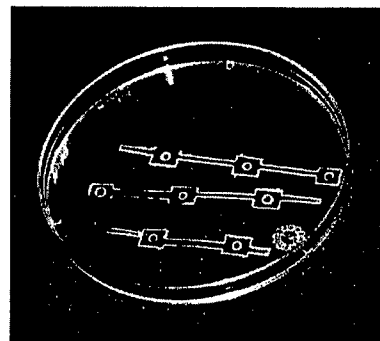
### 3.4.3. Evaporation

Vacuum evaporation techniques were used to make optical coatings like ITO (indium tin oxide), aluminum, silver, copper, quartz, zinc sulfide, and magnesium flouride, for eventual use in fabrication of DOEs.

## 3.5. Refractive Index and Paging Issues

### 3.5.1. Light Propagation in the Memory Medium and the Refractive Index

#### 3.5.1.1. Summary Of Previous Work

**Significance of Refractive Index:** Writing a bit to memory entails a change in the index of refraction. In current implementations of our BR memory a bit is written into a rectangular prism $3\mu \times 3\mu \times 15\mu$, with the long dimension along the direction of the activation beam. Given that a zero bit is in the **bR** state and the one bit is in the **Q** state, one bits would represent regions of inhomogeneity in the optical properties of the medium. Writing the change of index of refraction as $\Delta n$, then the gradient in the index is comparable to the quantity $\Delta n/l$, where l is the minimum distance from the center of the prism to a boundary. This may create a problem, because light passing through an inhomogeneous region is bent in the direction of the gradient. We may apply some fundamental formulas of geometric optics to estimate the degree of bending.

$$n\mathbf{K} = \text{grad}(n) - \frac{dn}{ds}\mathbf{s},$$

$$\mathbf{K} = \frac{1}{\rho}\mathbf{v}. \tag{1}$$

In these formulas, $\mathbf{K}$ and $\mathbf{v}$ are normal to the direction of propagation, $\mathbf{v}$ is the unit normal, $\mathbf{s}$ is the direction of propagation, $n$ is the index of refraction $s$ is the arc length parameter and • is the radius of curvature of the bending of the ray. We can assume that the index of the medium in the ground state is about 1.4, and that the change in index is about 7%. Using the formula $\Delta n/l$ for the gradient, and assuming that the light is propagating perpendicularly to the gradient, we obtain a radius of curvature of about 40 wavelengths, assuming we are using laser light with wavelength $\lambda \cong 500\text{nm}$. Memory dimensions, on the other hand, may be as large as two or three centimeters. Therefore it is possible that refraction could lead to focussing and interference within the activation, read and write beams used to access the bits written within the memory.

**Computer Model of Memory:** In order to gauge the significance of changes of index we have developed a computer model of beam propagation in a memory page. Information gained from this model can be used to evaluate the relative importance of index changes when compared with other noise sources such as random inhomogenieties from the fabrication process and noise in the laser beams. This model will also aid in evaluating limits imposed by the material properties of the memory medium, specifically,

the fundamental limitations imposed by index changes. Given that index changes are significant, our model can be extended by addition of modules which model the read and write processes. Our computer model is based on standard ray tracing techniques, which we outline below.

Geometrically, our model is divided into memory planes, each 15μ deep. The number of planes ($y$ dimension) and the other two dimensions ($x$ and $z$ dimensions; in multiples of 3μ) may be specified in advance. Each bit is confined to a volume 3μ × 15μ × 3μ. In the present code we assume the activation and write beams are gaussian, so the actual physical form of the area written to is a fuzzy ellipsoidal solid. Along any cross section, the index profile is gaussian, and the index change falls to less than one part in 1000 at the boundaries of the prism. The actual formula for the index used in our code is

$$n = n_0 + (n_1 - n_0)\exp\{-2.0[(x - x_0)^2 + (z - z_0)^2] + 0.07111(y - y_0)^2\}, \qquad (2)$$

where $n_0$ and $n_1$ are the indices of refraction for the **bR** and **Q** state regions, and $x_0$, $y_0$ and $z_0$ are the centers of the prism. This formula may be changed to accommodate changes in the activation and write beam wavelengths or intensities, or the material properties of the BR medium. Structural changes in the BR molecule make a range of maximum index changes possible. At present we assume that the distribution of one and zero bits is random. Accordingly, we can specify in advance a random pattern of bits in a given a rectangular segment of the memory. The proportion of one bits can be any number between 0 and 100%. This pattern is saved in a disk file for different runs of our computer model.

Our computer code computes the intensity profile of a planar laser beam 15μ•wide with its long dimension aligned with the x-axis. The direction of propagation is parallel to the z-axis. For purposes of computation the beam is divided into several thousand rays. The spacing between the initial positions of the rays can be specified in advance; generally, the initial spacing between rays is between 0.1 and 0.25 wavelengths in the $x$ and $y$ directions.

The propagation equation for a given ray is derived from the eikonal equation

$$[\text{grad}(S)]^2 = n^2, \qquad (3)$$

where $S$ is a real scalar function of position. Rays are normal to the surfaces $S(x, y, z)=constant$, (the wavefronts) and satisfy the equation

$$\frac{d}{ds}\left(n\frac{d\mathbf{r}}{ds}\right) = grad(n), \qquad (4)$$

where s is the arc length parameter (as in Eq. 1), and $\mathbf{r}$ is the position vector. In our computer code we employ a simple linear approximation for the derivatives in the above

equation, with small spatial steps ($\Delta s = 0.2\lambda$). The gradient is computed to the accuracy of floating point arithmetic on the computer on which the code is run.

The function $S$ is computed by tracing rays from the $z=0$ face of the memory segment to the opposite face (the $z$-boundary). During the course of tracing the ray we sum the optical path. This gives the phase of the electric field vector at the $z$-boundary. Transport of the electric field vector along a ray is given by

$$n\frac{d\mathbf{u}}{ds} = \mathbf{u} \cdot grad(n)\frac{d\mathbf{r}}{ds},$$ (5)

where $\mathbf{u}$ is the unit vector in the direction of the electric field vector. As with the ray tracing we employ a simple linear approximation for the derivatives to solve Eq. 5. Initially we take this vector to be the unit vector in the $y$ direction. Because we sum the optical path during the course of tracing a ray, a phase and E-field vector are assigned to the point of intersection of the ray with the $z$-boundary. Typically, in order to compute an interference pattern we divide the $z$-boundary into small squares 0.2 wavelength on a side and sum the complex E-field vectors associated with the rays passing through each square.
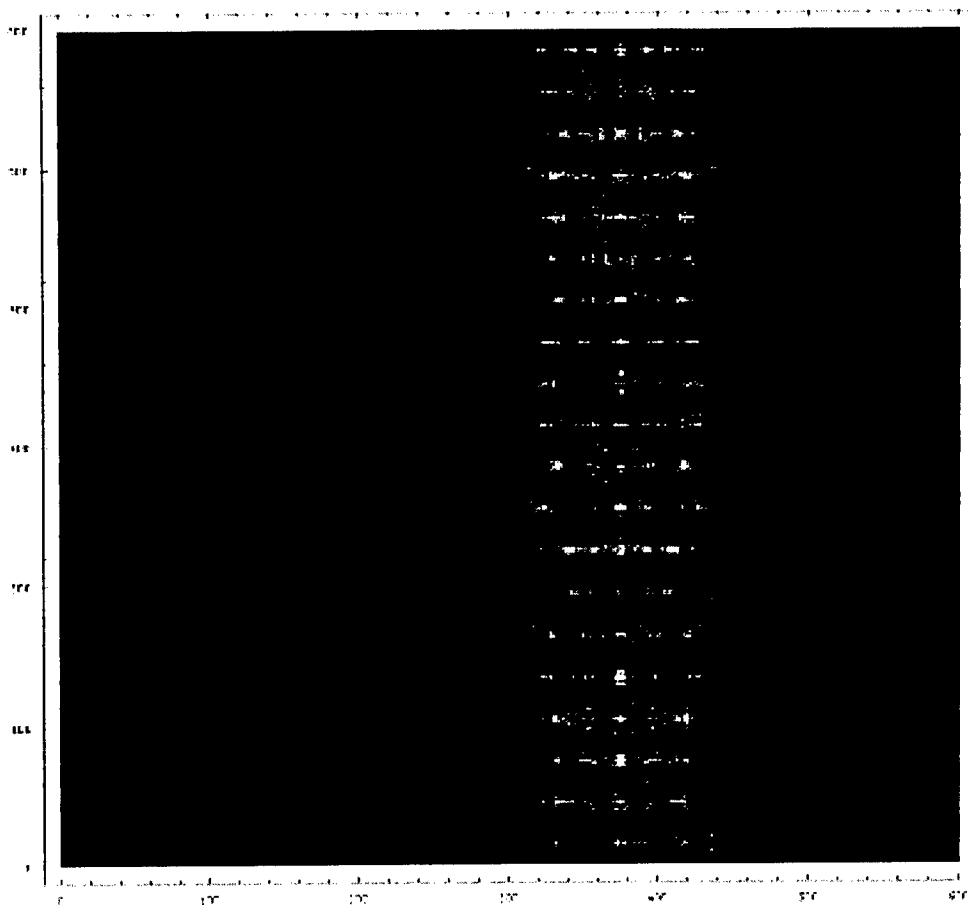
**Figure 3.5.1.** (Previous page) Interference pattern in path of activation beam after passing the 500th row of random bits (bit proportion 50% '0' 50% '1'. Nominal index of medium (and '0' bit) is 1.475. Nominal index of '1' bit is 1.5. Wavelength of light is 500nm. Scale of plot: 100 = 50 micrometers. Black = no light.

**Figure 3.5.1.** shows the interference pattern generated by an entrant beam with 15$\mu$ wide at a depth of 1.5 mm (500th row of bits, or 1.5 mm into the medium). Note that strong diffraction effects are already present at that depth. **Figure 3.5.2.** shows the interference pattern generated at a depth of 1.5 cm. The illuminated area should correspond precisely to the area illuminated in **Fig. 3.5.1.**. At this depth, diffraction effects have scattered most of the activation beam away from the nominal plane of illumination. The bright spots represent rays which pass through the centers of the ellipsoids or chance focal points. We can conclude that diffraction due to index changes can become a serious problem in three-dimensional optical memories if the index change is larger than a fraction of a percent.
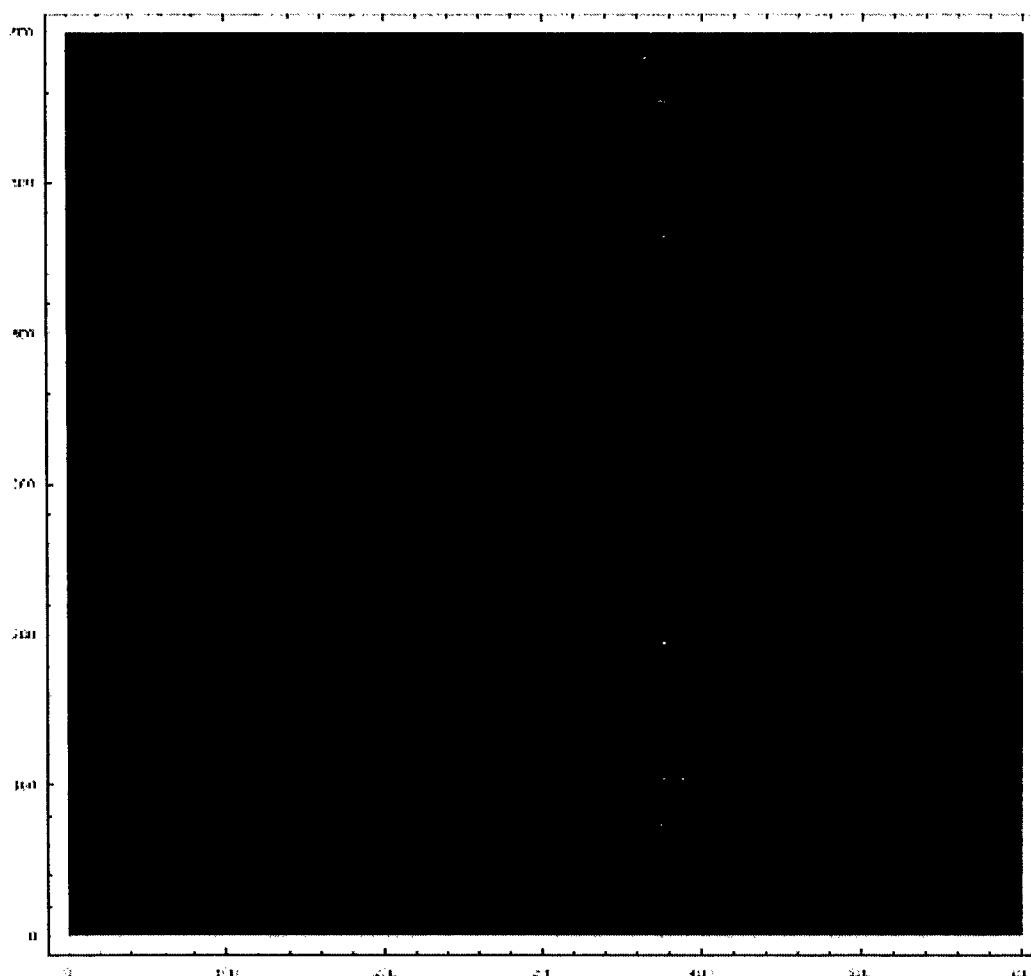
**Figure 3.5.2.** (Previous page) Interference pattern in path of activation beam after passing the 5000th row of random bits (bit proportion 50% '0' 50% '1'. Nominal index of medium (and '0' bit) is 1.475. Nominal index of '1' bit is 1.5. Wavelength of light is 500nm. Scale of plot: 100 = 50 micrometers.

One problem that we have observed in our computer models is that for distances between 2 mm and 1.0 cm, our present scheme does not trace enough rays to generate a continuous diffraction pattern. Installing code which would refine the grid of starting points should improve this situation.

### 3.5.1.2. Improvements In The Propagation Scheme

In our present code we start single rays from positions on a predetermined grid. This scheme may be used to calculate interference patterns a millimeter or so within the memory, but does not allow for such problems as the large divergences between adjacent rays which occur after the rays have gone through a focal point or caustic and the paths are traced several tens of millimeters further. In order to handle such problems, we will trace several adjacent rays rather than starting with a single ray and tracing it to the end point. A scheme in which rays starting from four adjacent grid points permits the detection of singularities and large divergences. When necessary, such as when the rays diverge, the grid may be refined by subdividing the grid within the original rectangle, and additional rays may be propagated. This will require a more sophisticated iteration scheme and the use of more complex data structures, such as linked lists and quad-trees to handle the grid refinements.

Another source of error in our code is through the reduction of Maxwell's equations to the eikonal equation. This equation is derived from Maxwell's equations under the assumption that the wavelength of light is small in comparison to other spatial scales. As noted above, the gradient of the index of refraction can be comparable to the wavelength. In order to see the significance of this, we substitute the general expression for the electric field, $E_0 = \exp(ik_0 S(\mathbf{r})/e(\mathbf{r})$, into the equation $div(\varepsilon E_0) = 0$ to obtain

$$\mathbf{e} \cdot grad(S) = \frac{1}{ik_0}[\mathbf{e} \cdot \mathrm{grad}(\log(\varepsilon)) + \mathrm{div}(\mathbf{e})].$$ 
(1)

Note that the gradient term in the field transport equation

$$n\frac{d\mathbf{u}}{ds} = \mathbf{u} \cdot grad(n)\frac{d\mathbf{r}}{ds},$$ 
(2)

can be significant under the conditions encountered in our optical memory.

One method for obtaining a more accurate approximation is to develop the field vectors into asymptotic series, for example

$$\mathbf{E}_0 = \exp(ik_0 S)\sum_{m \geq 0}\frac{\mathbf{e}^{(m)}}{(ik_0)^m},$$ 
(3)

for the electric field vector. This series can be substituted into the field equation:

$$\nabla^2 \mathbf{E} - \frac{\varepsilon\mu}{c^2} \ddot{\mathbf{E}} - grad(div(\mathbf{E})) = 0 \qquad\qquad (4)$$

(we can assume the magnetic permeability is constant). This gives a series in $ik_0$. If we collect terms of the same degree and equate to zero, we obtain the following series of coupled equations:

$$[grad(S)]^2 = n^2$$

$$\nabla^2 S e^{(0)} + 2[e^{(0)} \cdot grad(\log(n))]grad(S) + 2[grad(S) \cdot grad]e^{(0)} = 0$$

$$\nabla^2 e^{(i)} + grad[e^{(i)} \cdot grad(\log(\varepsilon))] + \nabla^2 S e^{(i+1)} + 2[e^{(i+1)} \cdot grad(\log(n))]grad(S) + 2[grad(S) \cdot grad]e^{(i+1)} = 0,$$

$$i = 0,1,...$$

$$(5)$$

We note that the first two equations are equivalent to the ray tracing and transport equations. We will incorporate corrections provided by higher terms of this series wherever necessary.

### 3.5.2. Refining the Paging Accuracy

Working in collaboration with Rick Lawrence, Bob Birge has been analyzing the issue of refractive index gradients causing problems in paging accuracy. Preliminary results suggest that we can avoid problems by mixing the number of 1 and 0 bits so that there is a nearly random population, but a fool-proof algorithm has not been found. Dr. Lawrence is working on an algorithm that does a whole page transformation based on a bit population analysis. The entire data set on the page would then be rotated by 90 degree increments to randomize the bit populations. This is a very simple method that would require almost no computational overhead.

For this approach to work, an outer edge pattern needs to be maintained that would serve as an optical alignment guide, as well as provide a fixed set of other data that would allow the read software and/or firmware to assign unambiguously the following information:

1. page number (10 bits; allows for a total of 1024 pages in a single volume)
2. volume number (10 bits; allows for a total of 1024 volumes, each containing 1024 pages)
3. gray scale assignment (16 bits of varying density to calibrate the array detector for that page)
4. page transformation (12 bits; 4 bits of polarization; 8 bits of transformation data)
5. polarized gray scale read test (a gray scale readout at the orthogonal polarization).

An assignment along the top rows might look something like the following:
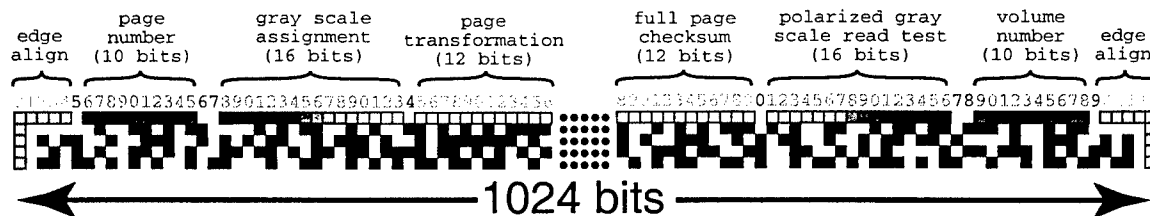
The above approach will certainly require modification as the prototype development continues. Thus, it represents a starting point, rather than a final model. Key to this approach is the recognition that polarization and gray scale multiplexing will require that each page have a separate gray scale calibration, and this is accomplished by using the 16 bit field shown above. Our preliminary goals of gray scale multiplexing is much more modest that 16 bits, but by including a larger range in the assignment, a higher reliability can be achieved. The following figure provides a perspective on the use of redundancy to enhance reliability.
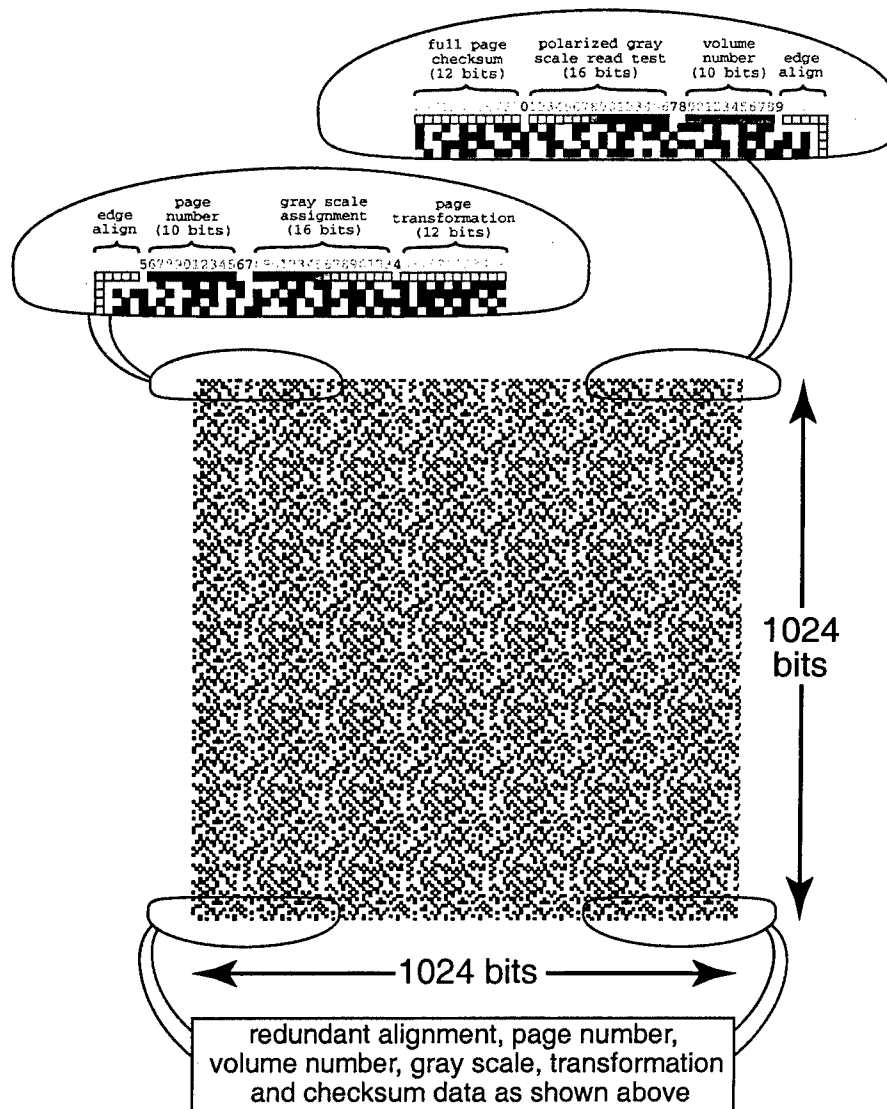
## 3.6. Multiplexing Techniques

As the modular prototype has only recently reached the stage where formal testing is possible, we have not done any actual experimental multiplexing studies yet. However, Dr. Q. Wang Song of the Syracuse University Department of Electrical Engineering has recently agreed to work on multiplexing techniques. Dr. Song has extensive experience in optical materials and holography. In addition, an effort to mathematically model multiplexing techniques is underway. Because these simulations are ongoing, no concrete results are yet available.

## 3.7. Progress at the W. M. Keck Center for Molecular Electronics Beamline Facility Report

Researchers Peter Dowben and Phil Sprunger have been working on the production of gratings and masks for potential eventual use in the protein-based three-dimensional optical memory as spatial light modulators (AFOSR contract #F30602-98-C-0105/ subcontract SU #3531141). They report the following progress for the first year. For more detail the reader is referred to previous monthly progress reports.

The major scientific accomplishments fall into two categories. First there is grating development. We have fabricated a ferromagnetic grating of cobalt. There is an excellent aspect ratio off this grating and good diffraction. We have also fabricated a grating from a ferroelectric polymer system poly-vinylidene fluoride (PVDF), and have provided this deliverable. This latter work is sufficiently novel to merit publication. One paper is written [1] and another is in preparation [2]. We have fabricated a variety of gratings and lithographically patterned a number complex features, some suitable for device applications in this molecular (polymer) ferroelectric. We have developed some insight into the photochemistry of the single step synchrotron based lithography of this molecular ferroelectric system [1].

In addition we have developed some understanding of the switching mechanism of the ferroelectric copolymer poly(vinylidene fluoride-trifluoroethylene) [3]. The ultimate goal here is to pattern ferroelectric memory elements directly onto an IC to add molecular electronics functionality to integrated circuit electronics.

There has also been substantial instrumentation development. We have ordered new gratings for the monochromator which will lead to better resolution and have also purchased new manipulators for better sample control. This instrumentation continue to be put into place. We have the 3 meter TGM beamline up and running with light though the beamline (with the old gratings).

This is a substantial level of progress given the brief amount of time spent thus far on this project. The work has already helped to generate two invited talks.

**Publications:**

[1] Jaewu Choi, H.M. Manohara, E. Morikawa, P.T. Sprunger P.A. Dowben and S.P. Palto, "Very Thin Crystalline Functional Group Copolymer (vinylidene fluoride - trifluoroethylene) Film Patterning Using Synchrotron Radiation", submitted to Appl. Phys. Lett.

[2] H.M. Manohara, J. Choi and P.T. Sprunger, in preparation

[3] Jaewu Choi, C.N. Borca, P.A. Dowben, A. Bune, M. Poulsen, Shawn Pebley, S. Adenwalla, Stephen Ducharme, Lee Robertson, V.M. Fridkin, S.P. Palto, N. Petukhova, S.G. Yudin, "The Phase Transition of the Surface Structure in Copolymer Films of Vinylidene Fluoride (70%) with Trifluoroethylene (30%)", submitted to Phys. Rev. B

**Invited Talks:**

"Changes in Metallicity and Electronic Structure Across the Surface Ferroelectric Transition of Crystalline Poly(vinylidene Fluoride-trifluoroethylene)" 1999 Centennial March Meeting of the APS, Atlanta GA, March 22, 1999; published abstract FC03-1, P.A. Dowben , Bulletin of the American Physican Society, 44, 278 (1999)

"The First Surface Ferroelectric Transition", CAMD User's Meeting, Baton Rouge, LA, May 7, 1999

## 4. Research Plan for 1999-2000

The Gantt charts included throughout this report also serve to illustrate the direction planned for the contract over the next few years. Plans for future research are included in the task progress sections detailed above. However, it is worth noting a few of the more prominent goals that we seek to accomplish over the next year.

- Construction of the fully miniaturized prototype. This unit has already been designed, and most of the parts have already arrived. Dr. Izaguirre plans to begin work on this within the next two months. Unfortunately, a figure illustrating the design was not ready at the time of submitting this report. In addition, we will soon have established the techniques required to produce diffractive optical elements, which will be extremely valuable in miniaturization and cost reduction.

- Random mutagenic techniques will be used to create BR mutants optimized for memory storage. These techniques can be used for "Directed Evolution" of proteins, and have proven to be incredibly powerful for producing proteins with desirable properties. The key to making this work, however, is the development of an efficient screening technique. This unit has already been designed (as illustrated in the recent reengineering proposal), and parts for its construction have been ordered. In

combination with the ongoing protein modeling studies, the possibility of generating optimized and efficient protein analogs is strong.

- The use of photocurable polymers, as proposed by Dr. Wayne Wang and his coworkers at Carleton University in Ottawa, has the potential to solve the problems we have had with gel contraction and stability. Work on this effort is proceeding and we hope to see the first cuvettes made by this technique by Fall. With the completion of our scattering spectrometer, the underlying causes of the optical problems should become apparent, as well as potential solutions.

- On a more practical level, we now have all of the equipment in house to design and construct specialized parts for the prototype. Despite the fact that this capability has taken over 6 months to establish, the easy access and automation will make prototyping much more efficient. In addition, an analogous device has been delivered to automate the production of circuit boards, which otherwise would have been contracted out at huge expense. We are in the process of hiring a technician to handle all routine fabrication of components.

## 5. Comments and Conclusions

It took the first half of the past year before the development effort for the bacteriorhodopsin-based three-dimensional optical memory was fully up and running with the necessary support and personnel. This is the single largest determining factor responsible for holding up progress on several of the tasks. Since then, significant progress has been made in nearly all areas of the contract. However, we recognize that deficiencies still exist in several areas, the most prominent being in materials development. We are approaching these deficiencies by redoubling our efforts where needed, and monitorring the progress in these areas closely. Because part of the current problem is a shortage of personnel, we are planning on hiring 2-3 new personnel during the next three months to aid in both the molecular biology effort and component fabrication (as discussed above). All things considered, we feel that the contract is still in good standing, and estimate our overall progress to be in the range of 35-40%.

## MISSION
## OF
## AFRL/INFORMATION DIRECTORATE (IF)

*The advancement and application of Information Systems Science*

*and Technology to meet Air Force unique requirements for*

*Information Dominance and its transition to aerospace systems to*

*meet Air Force needs.*